

EUROPEAN ORGANISATION FOR NUCLEAR RESEARCH (CERN)



Submitted to: JHEP



CERN-EP-2024-290
7th November 2024

Search for a heavy charged Higgs boson decaying into a W boson and a Higgs boson in final states with leptons and b -jets in $\sqrt{s} = 13$ TeV pp collisions with the ATLAS detector

The ATLAS Collaboration

This article presents a search for a heavy charged Higgs boson produced in association with a top quark and a bottom quark, and decaying into a W boson and a 125 GeV Higgs boson h . The search is performed in final states with one charged lepton, missing transverse momentum, and jets using proton–proton collision data at $\sqrt{s} = 13$ TeV recorded with the ATLAS detector during Run 2 of the LHC at CERN. This data set corresponds to a total integrated luminosity of 140 fb^{-1} . The search is conducted by examining the reconstructed invariant mass distribution of the Wh candidates for evidence of a localised excess in the charged Higgs boson mass range from 250 GeV to 3 TeV. No significant excess is observed and 95% confidence-level upper limits between 2.8 pb and 1.2 fb are placed on the production cross-section times branching ratio for charged Higgs bosons decaying into Wh .

© 2024 CERN for the benefit of the ATLAS Collaboration.

Reproduction of this article or parts of it is allowed as specified in the CC-BY-4.0 license.

arXiv:2411.03969v1 [hep-ex] 6 Nov 2024

Contents

1	Introduction	2
2	ATLAS detector	4
3	Data and simulated event samples	5
4	Event reconstruction	7
5	Analysis strategy and event selection	10
5.1	Reconstruction and classification of resolved charged Higgs boson decays	11
5.2	Reconstruction and classification of merged charged Higgs boson decays	13
5.3	Definition of signal and control regions	15
6	Background modelling	19
7	Systematic uncertainties	20
7.1	Experimental systematic uncertainties	20
7.2	Modelling systematic uncertainties	21
8	Results	24
9	Conclusion	38

1 Introduction

The Higgs boson discovery at the Large Hadron Collider (LHC) was a great success of the ATLAS and CMS collaborations [1, 2]. Following its discovery, numerous studies have been performed to establish whether it is a Standard Model (SM) particle or rather the first observed physical state of an extended scalar sector.

Searches for an extended scalar sector are crucial as numerous models of new physics beyond the SM require additional scalar states. For example, two Higgs doublets [3, 4] are required in the minimal supersymmetric extension of the SM, while Higgs triplets [5–9] are required in models with a type-II seesaw mechanism. In addition, an extended scalar sector can modify the electroweak phase transition and facilitate baryogenesis, enhance vacuum stability, provide a dark matter candidate or provide a solution to the strong CP problem (i.e. predict axions). In short, extending the scalar sector provides solutions to some of the open questions in the SM.

Various theories predicting an extended scalar sector postulate also the existence of at least one set of charged Higgs bosons in addition to the discovered neutral one, such as models that add a second doublet or one or more triplets to the scalar sector. The main production and decay modes of these new particles are strongly model dependent. For example, in the alignment limit of the two-Higgs-doublet model (2HDM) [10], the dominant production mode, for charged Higgs boson masses larger than the sum of the top and the bottom quark masses, is expected to be in association with a top quark and a bottom quark

(tbH^\pm) ,¹ while the dominant charged Higgs boson decay modes are via $H^\pm \rightarrow tb$ or $H^\pm \rightarrow \tau^\pm \nu$. However, there are also several models such as the next-to-minimal two-Higgs-doublet model (N2HDM) [11, 12], the three-Higgs-doublet Model (3HDM) [13] or the Georgi-Machacek model [14] in which other decay and production modes become important. The studies presented in this article search for charged Higgs bosons decaying via $H^\pm \rightarrow W^\pm h$, where h is a Higgs boson with mass $m_h = 125$ GeV. This decay mode is predicted to have significant branching ratios by various extended scalar sector models [15–18].

The ATLAS and CMS collaborations searched for charged Higgs bosons in proton–proton (pp) collisions at $\sqrt{s} = 7, 8$ and 13 TeV with data samples corresponding to integrated luminosities ranging from 2.9 up to 140 fb⁻¹, probing the mass range below the top-quark mass in the $\tau^\pm \nu$ [19–24], cs [25, 26], and cb [27, 28] decay modes, as well as above the top-quark mass in the $\tau^\pm \nu$ [29] and tb [30–32] decay modes. Searches for $H^\pm \rightarrow W^\pm Z$ decays have been performed in the vector-boson-fusion (VBF) production mode [33–35]. Searches for doubly-charged Higgs bosons have also been performed [35–38]. Charged Higgs boson decays via $H^\pm \rightarrow W^\pm h$ have been so far not yet searched for by either the ATLAS or CMS collaborations.

This article describes a first search for a charged Higgs boson produced in association with a top quark and a bottom quark with subsequent decays of the charged Higgs boson via $H^\pm \rightarrow W^\pm h \rightarrow \ell^\pm \nu b \bar{b}$ or $H^\pm \rightarrow W^\pm h \rightarrow q \bar{q} b \bar{b}$. The search is performed in events that are consistent with the final state $\ell^\pm \nu b \bar{b} b \bar{b} q \bar{q}$ (with $\ell = e, \mu$), where the charged lepton can originate either from the decay chain of the charged Higgs boson or of the associated top quark. Representative lowest-order Feynman diagrams of these processes are shown in Figure 1.

To ensure high sensitivity to both low- and high-mass resonances, two different analysis techniques are used. At low charged Higgs boson masses, when the final state particles have a relatively low Lorentz-boost, the decay products of neutral Higgs boson and hadronically decaying W boson are reconstructed via individual small-radius jets (such decays are referred to as ‘resolved’). At high charged Higgs boson masses, when the final state particles have a relatively large Lorentz-boost, the neutral Higgs boson and the hadronically decaying W boson are reconstructed as single large-radius jets (such decays are referred to as ‘merged’).

The search for charged Higgs bosons is performed by probing for a localised excess in the invariant mass distribution of the reconstructed $\ell^\pm \nu b \bar{b}$ and $q \bar{q} b \bar{b}$ systems. This is achieved through a simultaneous profile likelihood fit on the invariant mass distribution obtained in selected signal and control regions. The signal and control regions are defined based on requirements on kinematic properties of the final-state particles and event-level quantities. Multivariate analysis techniques are used to improve the background rejection and to reconstruct the decays of the charged Higgs boson candidates. The major backgrounds are modelled using simulation and their normalisations are determined by a profile-likelihood fit to data. The results are presented as upper limits at 95% confidence level (CL) on the production cross-section times branching ratio $\sigma(pp \rightarrow tbH^\pm) \times \mathcal{B}(H^\pm \rightarrow W^\pm h) \times \mathcal{B}(h \rightarrow b \bar{b})$ of the signal process. In this article, charged Higgs boson mass hypotheses are probed in a range from 250 GeV to 3 TeV.

¹ The notation tbH^\pm is used to represent the $\bar{t}bH^+$ and $t\bar{b}H^-$ processes. In general, the difference between particles and antiparticles is to be understood from the context.

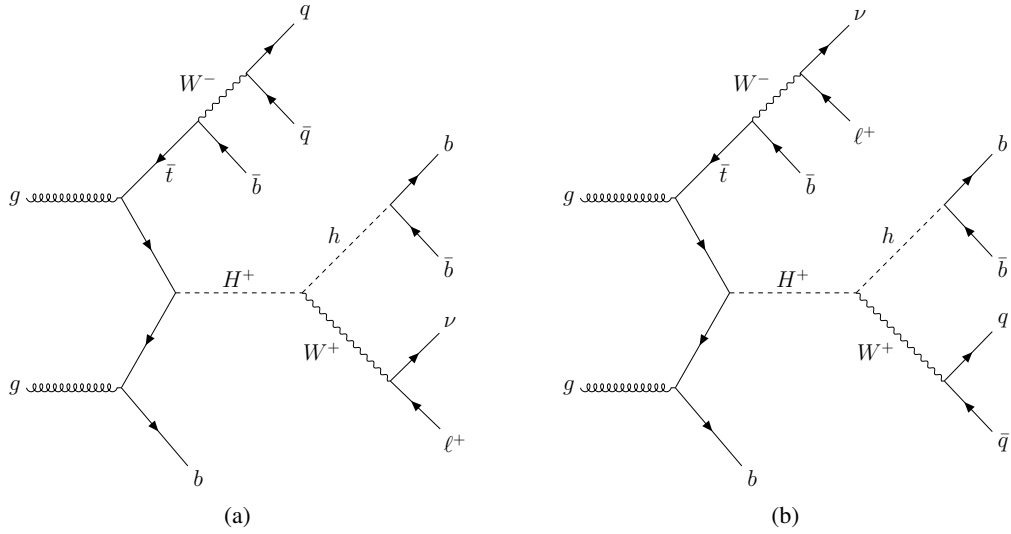


Figure 1: Representative lowest-order Feynman diagrams of $pp \rightarrow \bar{t}bH^+$ production and subsequent decays via (a) $H^+ \rightarrow W^+h \rightarrow \ell^+\nu b\bar{b}$ and (b) $H^+ \rightarrow W^+h \rightarrow q\bar{q}b\bar{b}$.

2 ATLAS detector

The ATLAS detector [39] at the LHC covers nearly the entire solid angle around the collision point.² It consists of an inner tracking detector surrounded by a thin superconducting solenoid, electromagnetic and hadronic calorimeters, and a muon spectrometer incorporating three large superconducting air-core toroidal magnets.

The inner-detector system (ID) is immersed in a 2 T axial magnetic field and provides charged-particle tracking in the range $|\eta| < 2.5$. The high-granularity silicon pixel detector typically provides four measurements per track, the first hit generally being in the insertable B-layer (IBL) installed before Run 2 [40, 41]. It is followed by the SemiConductor Tracker (SCT), which usually provides eight measurements per track. These silicon detectors are complemented by the transition radiation tracker (TRT), which enables radially extended track reconstruction up to $|\eta| = 2.0$. The TRT also provides electron identification information based on the fraction of hits (typically 30 in total) above a higher energy-deposit threshold corresponding to transition radiation.

The calorimeter system covers the pseudorapidity range $|\eta| < 4.9$. Within the region $|\eta| < 3.2$, electromagnetic calorimetry is provided by barrel and endcap high-granularity lead/liquid-argon (LAr) calorimeters, with an additional thin LAr presampler covering $|\eta| < 1.8$ to correct for energy loss in material upstream of the calorimeters. Hadronic calorimetry is provided by the steel/scintillator-tile calorimeter, segmented into three barrel structures within $|\eta| < 1.7$, and two copper/LAr hadronic endcap calorimeters. The solid angle coverage is completed with forward copper/LAr and tungsten/LAr calorimeter modules optimised for electromagnetic and hadronic energy measurements respectively.

² ATLAS uses a right-handed coordinate system with its origin at the nominal interaction point (IP) in the centre of the detector and the z -axis along the beam pipe. The x -axis points from the IP to the centre of the LHC ring, and the y -axis points upwards. Polar coordinates (r, ϕ) are used in the transverse plane, ϕ being the azimuthal angle around the z -axis. The pseudorapidity is defined in terms of the polar angle θ as $\eta = -\ln \tan(\theta/2)$ and is equal to the rapidity $y = \frac{1}{2} \ln \left(\frac{E+p_z}{E-p_z} \right)$ in the relativistic limit. Angular distance is measured in units of $\Delta R \equiv \sqrt{(\Delta y)^2 + (\Delta \phi)^2}$.

The muon spectrometer (MS) comprises separate trigger and high-precision tracking chambers measuring the deflection of muons in a magnetic field generated by the superconducting air-core toroidal magnets. The field integral of the toroids ranges between 2.0 and 6.0 T m across most of the detector. Three layers of precision chambers, each consisting of layers of monitored drift tubes, cover the region $|\eta| < 2.7$, complemented by cathode-strip chambers in the forward region, where the background is highest. The muon trigger system covers the range $|\eta| < 2.4$ with resistive-plate chambers in the barrel, and thin-gap chambers in the endcap regions.

The luminosity is measured mainly by the LUCID-2 [42] detector that records Cherenkov light produced in the quartz windows of photomultipliers located close to the beam pipe.

Events are selected by the first-level trigger system implemented in custom hardware, followed by selections made by algorithms implemented in software in the high-level trigger [43]. The first-level trigger accepts events from the 40 MHz bunch crossings at a rate below 100 kHz, which the high-level trigger further reduces in order to record complete events to disk at about 1 kHz.

A software suite [44] is used in data simulation, in the reconstruction and analysis of real and simulated data, in detector operations, and in the trigger and data acquisition systems of the experiment.

3 Data and simulated event samples

The pp collision data at $\sqrt{s} = 13$ TeV used in the analysis were recorded with the ATLAS detector between 2015 and 2018, and correspond to a total integrated luminosity of $140.0 \pm 1.2 \text{ fb}^{-1}$ [45]. The data are required to satisfy criteria that ensure that the detector was in good operating condition [46]. Monte Carlo (MC) simulation samples were used to model the background and signal processes, as well as to derive modelling uncertainties. The MC simulation samples were processed using either the GEANT4-based simulation of the ATLAS detector geometry and response [47, 48] or fast simulation [49], where the GEANT4 simulation of the calorimeter response is replaced by a detailed parameterisation of shower shapes. The simulated events were reconstructed using the same algorithms as were used for the data events.

The signal process, i.e. the associated production of a charged Higgs boson, a bottom quark and a top quark, was simulated using the matrix element (ME) generator MADGRAPH5_AMC@NLO 2.7.3 [50] in the 4-flavour scheme (4FS) at next-to-leading-order (NLO) accuracy in QCD and the NNPDF3.0NLO [51] set of parton distribution functions (PDFs). PYTHIA 8.244 [52] with the A14 set [53] of tuned parameters is used to decay the charged Higgs boson and to model the parton shower (PS), hadronisation, and underlying event. The renormalisation and factorisation scales μ_R and μ_F were set to $\frac{1}{3} \sum_i \sqrt{m_i^2 + p_{T,i}^2}$, where i runs over all final state particles used in the matrix element calculation. The signal process is simulated using the FeynRules [54] model 2HDMtypeII [55] using a narrow-width approximation. The choice of model is expected to have only small impact on the results of this search as long as the narrow-width approximation is valid. While specific models may alter the cross-section times branching ratio values, they typically do not affect the event kinematics of the tbH^\pm process. Seventeen signal samples were generated covering a mass range between 250 GeV and 3 TeV.³ Fast detector simulation was employed for mass points below

³ In the mass range between 250 GeV and 400 GeV, the signal samples are produced in 50 GeV steps, while in the ranges from 400 GeV to 1000 GeV and 1000 GeV to 2000 GeV step sizes of 100 GeV and 200 GeV were chosen. In addition, signal masses of 2500 GeV and 3000 GeV are considered.

500 GeV and the GEANT4-based simulation of the ATLAS detector was used otherwise.⁴ In the simulation of the signal processes, only the H^+ decay into W^+h and Higgs boson decaying to pairs of b -quarks were considered assuming a Higgs boson mass of $m_h = 125$ GeV. Other decay modes of the 125 GeV Higgs boson were neglected, as their contributions to the signal and control regions (cf. Section 5) were an order of magnitude lower than those for the $h \rightarrow b\bar{b}$ decay.

The production of top-quark pair ($t\bar{t}$) events was modelled using the POWHEG BOX v2 [56–59] generator in the five-flavour scheme (5FS) to calculate the ME at NLO accuracy in QCD, and the NNPDF3.0_{NLO} PDF set. The h_{damp} parameter⁵ was set to $1.5 m_t$ [60], where m_t is the top-quark mass. The top-quark decays are modelled using MADSPIN [61, 62]. The PS, hadronisation, and underlying event were modelled with the PYTHIA 8.230 generator using the A14 set of tuned parameters and the NNPDF2.3_{LO} [63] PDF set. The top-quark pair events are normalised to the state-of-the-art cross-section prediction calculated with TOP++ 2.0 [64–70] at next-to-next-to-leading order (NNLO) in QCD, including the resummation of next-to-next-to-leading logarithmic (NNLL) soft-gluon terms.

The $t\bar{t} + h$ sample was generated at NLO accuracy in QCD using the POWHEG BOX v2 generator in the 5FS, and the NNPDF3.0_{NLO} PDF set. The h_{damp} parameter was set to $\frac{3}{4} \cdot (2m_t + m_h) = 352.5$ GeV and the events were showered with PYTHIA 8.230, which used the A14 set of tuned parameters and the NNPDF2.3_{LO} PDF set. The $t\bar{t} + h$ production cross-section is calculated at NLO accuracy in both QCD and electroweak (EW) using MADGRAPH5_AMC@NLO, as reported in Ref. [71]. The production of $t\bar{t} + V$ (with $V = W^\pm$ or Z) events was modelled using the MADGRAPH5_AMC@NLO 2.3.3 generator, which provides MEs at NLO in QCD with the NNPDF3.0_{NLO} PDF set. The events were interfaced to PYTHIA 8.210 using the A14 set of tuned parameters and the NNPDF2.3_{LO} PDF set.

The associated production of a top quark and W boson (Wt), and the s - and t -channel single-top-quark production were modelled with the POWHEG BOX v2 generator at NLO in QCD using the 5FS and the NNPDF3.0_{NLO} set of PDFs. The diagram-removal (DR) scheme [72] was used to remove interference and overlap with the production of top-quark pairs. The events were interfaced to PYTHIA 8.230, which used the A14 set of tuned parameters and the NNPDF2.3_{LO} set of PDFs.

Rare processes including top-quarks, such as tZq , tWZ , $thjb$, tWh , and $t\bar{t}\bar{t}$, were also simulated and accounted for, even though their contribution to any analysis region is lower than 1% of the total background yields. The MADGRAPH5_AMC@NLO generator and the NNPDF PDF set were used to calculate the MEs for these processes. The events were interfaced to PYTHIA 8.2 using the A14 set of tuned parameters and the NNPDF2.3_{LO} set of PDFs. The MEs of the tZq process was calculated at leading-order (LO) accuracy in QCD, while the MEs of the other four processes were calculated at NLO accuracy in QCD.

A sample of V +jets events was simulated using SHERPA 2.2.11 [73] with the NNPDF3.0_{NNLO} [51] PDF set. The ME was calculated based on the COMIX [74] and OPENLOOPS [75–77] libraries at NLO accuracy in QCD for diagrams with up to two additional parton emissions, and LO accuracy in QCD for diagrams with three, four or five additional parton emissions. The MEPS@NLO prescription [78–81] was used to merge the ME and the SHERPA PS [82], which is based on a set of tuned parameters developed by the SHERPA authors. The V +jets event sample was normalised to match cross-section predictions at NNLO accuracy in QCD calculated with FEWZ [83].

⁴ The decision to employ GEANT4-based simulation for masses above 500 GeV was motivated by the onset of the merged analysis at this mass point and the limitations of the fast detector simulation to accurately describe the properties of large-radius jets, which are essential to the merged analysis.

⁵ The h_{damp} parameter is a resummation damping factor and one of the parameters that control the matching of POWHEG MEs to the parton shower, effectively regulating the high- p_T radiation against which the $t\bar{t}$ system recoils.

Diboson (VV) events with decays into semileptonic final states were simulated using SHERPA 2.2.1, while events with decays into fully leptonic final states were simulated using SHERPA 2.2.2. Both samples include off-shell effects and Higgs boson contributions where appropriate. Diagrams with up to one additional emission were calculated at NLO accuracy in QCD, while diagrams with two or three parton emissions were described at LO accuracy. The ME calculations were matched and merged with the SHERPA PS using the MEPS@NLO prescription. Virtual QCD corrections for the ME at NLO accuracy were provided by the OPENLOOPS library. Loop-induced diboson processes initiated via the gg production mode were simulated at LO in QCD for diagrams with up to one additional parton emission in the ME using OPENLOOPS in SHERPA 2.2.2. For electroweak $VVjj$ production, the calculation of the ME was performed in the G_μ -scheme [84] to describe the pure electroweak interactions at the electroweak scale. All diboson events were generated using the NNPDF3.0_{NNLO} PDF set, along with the SHERPA PS.

Finally, the production of a SM Higgs boson in association with a vector boson (Vh) was simulated using POWHEG BOX v2, interfaced with PYTHIA 8.212 for PS and non-perturbative effects. The POWHEG prediction is accurate to NLO in QCD for the production of Vh plus one jet. The loop-induced $gg \rightarrow Zh$ process was generated separately at LO. The PDF4LHC15 PDF set [85] and the AZNLO set of tuned parameters [86] of PYTHIA 8.212 were used. The $gg \rightarrow Zh$ production cross-section was calculated at NLO accuracy in QCD, including the resummation of next-to-leading logarithmic (NLL) soft-gluon terms [87]. For the generation of Vh events, the Higgs boson mass was set to 125 GeV.

All simulated event samples include the effect of multiple pp interactions in the same and neighbouring bunch crossings (pile-up) by overlaying simulated minimum-bias events on each generated signal and background event. The minimum-bias events were simulated with the single-, double- and non-diffractive pp processes of PYTHIA 8.186 using the A3 set of tuned parameters [88] and the NNPDF2.3_{LO} PDF set. GEANT4-based simulations of the ATLAS detector were used for the production of the background samples (unless otherwise stated). For all samples produced with MADGRAPH and POWHEG BOX, the EVTGEN 1.6.0 programme [89] was used to model the decays of bottom and charm hadrons. Simulated events were corrected to compensate for differences between data and simulations regarding the energy (or momentum) scale and resolution of leptons and jets, the efficiencies for the reconstruction, identification, isolation and triggering of leptons, and the tagging efficiency for heavy-flavour jets.

A summary of MC generators and programs used to model the signal and background processes is provided in Table 1.

4 Event reconstruction

Charged-particle tracks are reconstructed in the ID. They are required to have a transverse momentum (p_T) larger than 500 MeV, $|\eta| < 2.5$, and at least seven hits in the pixel and SCT detectors. A maximum of one (two) of the expected hits may be missing from the pixel (SCT) detector sensors, and no more than one hit may be shared with other tracks [90]. Collision vertices are reconstructed from at least two ID tracks [91]. Among all vertices, the one with the highest p_T^2 sum of associated tracks is chosen to be the primary vertex (PV) of the event. The properties of ID tracks are calculated relative to the PV.

Electrons are reconstructed from ID tracks originating from the PV that are matched to clusters of energy deposits in the electromagnetic calorimeter [92]. The compatibility of the track and the PV is satisfied by a requirement on the transverse impact parameter significance $|d_0|/\sigma_{d_0} < 5$, and on the longitudinal impact parameter $|z_0 \sin \theta| < 0.5$ mm. Electron candidates must satisfy requirements on the electromagnetic

Table 1: Overview of the simulation tools used to generate signal and background processes, and to model the underlying event and parton shower (UEPS). The PDF sets are also summarised. The perturbative accuracy (in QCD and if relevant in EW corrections) of the total cross-section is stated for each process. Alternative event generators and configurations used to estimate systematic uncertainties are discussed in Section 7.

Process	Matrix element	UEPS	PDF set	Perturbative accuracy of total cross-section
$tbH^\pm(\rightarrow W^\pm h \rightarrow \ell^\pm \nu b\bar{b}, q\bar{q}b\bar{b})$	MADGRAPH5_AMC@NLO 2.7.3	PYTHIA 8.244	NNPDF3.0NLO	NLO (QCD)
$t\bar{t}$ + jets	POWHEG Box v2	PYTHIA 8.230	NNPDF3.0NLO	NNLO+NNLL (QCD)
$t\bar{t} + W^\pm$	MADGRAPH5_AMC@NLO 2.3.3	PYTHIA 8.210	NNPDF3.0NLO	NNLO (QCD) and NLO (EW)
$t\bar{t} + Z$	MADGRAPH5_AMC@NLO 2.3.3	PYTHIA 8.210	NNPDF3.0NLO	NLO+NNLL (QCD)
$t\bar{t} + h$	POWHEG Box v2	PYTHIA 8.230	NNPDF3.0NLO	NLO (QCD) and NLO (EW)
single top quark (s - and t -channels)	POWHEG Box v2	PYTHIA 8.230	NNPDF3.0NLO	NLO (QCD)
single top quark (Wt -channel)	POWHEG Box v2	PYTHIA 8.230	NNPDF3.0NLO	approx. NNLO (QCD)
tZq	MADGRAPH5_AMC@NLO 2.3.3	PYTHIA 8.210	NNPDF3.0LO	NLO (QCD)
tWZ	MADGRAPH5_AMC@NLO 2.3.3	PYTHIA 8.212	NNPDF3.0NLO	NLO (QCD)
$t\bar{t}t\bar{t}$	MADGRAPH5_AMC@NLO 2.6.2	PYTHIA 8.230	NNPDF3.1NLO	NLO (QCD)
$thj\bar{b}$	MADGRAPH5_AMC@NLO 2.6.2	PYTHIA 8.230	NNPDF3.0NLO	NLO (QCD)
tWh	MADGRAPH5_AMC@NLO 2.6.2	PYTHIA 8.235	NNPDF3.0NLO	NLO (QCD)
$q\bar{q} \rightarrow Wh$	POWHEG Box v2	PYTHIA 8.212	PDF4LHC15	NNLO (QCD) and NLO (EW)
$q\bar{q} \rightarrow Zh$	POWHEG Box v2	PYTHIA 8.212	PDF4LHC15	NNLO (QCD) and NLO (EW)
$gg \rightarrow Zh$	POWHEG Box v2	PYTHIA 8.212	PDF4LHC15	NLO + NLL (QCD)
$W^\pm \rightarrow \ell^\pm \nu, Z \rightarrow \ell^\pm \ell^\mp$	SHERPA 2.2.11		NNPDF3.0NNLO	NNLO (QCD)
$qg/q\bar{q} \rightarrow VV \rightarrow \ell^\pm \ell^\mp / \ell^\pm \nu / \nu \nu + q\bar{q}$	SHERPA 2.2.1		NNPDF3.0NNLO	NLO (QCD)
$qg/q\bar{q} \rightarrow VV \rightarrow \ell^\pm \ell^\mp \ell^\pm \ell^\mp / \ell^\pm \nu \ell^\pm \ell^\mp / \ell^\pm \ell^\mp \nu \nu / \ell^\pm \nu \nu$	SHERPA 2.2.2		NNPDF3.0NNLO	NLO (QCD)
$gg \rightarrow VV$	SHERPA 2.2.2		NNPDF3.0NNLO	NLO (QCD)
$VVjj$	SHERPA 2.2.2		NNPDF3.0NNLO	LO (QCD)

shower shapes, track quality, and track-cluster matching, using a likelihood-based approach [92], where the *Tight* operating point is used for this study. Electrons are also required to have a p_T larger than 27 GeV and $|\eta| < 2.47$, with the transition region between the barrel and endcap electromagnetic calorimeters, $1.37 < |\eta| < 1.52$, being excluded. Finally, to reduce contributions from hadrons mimicking electron signatures or non-prompt electrons from heavy-flavour decays or photon conversions, a multivariate classifier is used. This classifier considers the energy deposits and charged-particle tracks in a cone around the electron direction and information from secondary vertices [93].

Muon reconstruction [94] is based on matching MS tracks to ID tracks. A combined fit is then performed incorporating the information from the ID, MS and the energy deposits in the calorimeter system. Similar to electrons, muon candidates have to satisfy selection requirements on the impact parameters: $|d_0|/\sigma_{d_0} < 3$ and $|z_0| < 0.5$ mm. Muon candidates are required to have a minimum p_T of 27 GeV and lie within $|\eta| < 2.5$. Furthermore, they are required to satisfy the *Medium* identification operating point. However, candidates with $p_T > 300$ GeV must satisfy tighter identification requirements in the MS to improve the p_T resolution [94]. To reduce contributions from non-prompt muons from heavy-flavour decays, muon candidates are required to be isolated in the ID system using the *TightTrackOnly* operating point [94]. A muon is considered to be isolated if the p_T sum within a cone around the combined track is smaller than 0.06 times the muon's transverse momentum, p_T^μ . The size of the isolation cone is $\Delta R = \min(0.3, 10 \text{ GeV}/p_T^\mu)$ for $p_T^\mu < 50$ GeV, and remains constant at $\Delta R = 0.2$ for $p_T^\mu > 50$ GeV.

Three jet types are reconstructed, using the anti- k_t [95] algorithm as implemented in the FASTJET package [96]: small-radius (denoted small- R) jets, large-radius (denoted large- R) jets, and variable-radius jets. The small- R jets are built using a radius parameter of $R = 0.4$ and particle-flow objects as input [97]. They are required to have $p_T > 25$ GeV and $|\eta| < 2.5$. To reduce the contamination from jets originating from pile-up interactions, a selection requirement on a multivariate classifier is applied to the selected jets. This classifier is based on calorimeter and tracking information and is applied to jets with $p_T < 60$ GeV

and $|\eta| < 2.4$ [98]. Large- R jets are used to reconstruct high-momentum Higgs or W -boson candidates, for which the hadronic decay products are emitted with small angular separation. These jets are built using a radius parameter of $R = 1.0$ and topological calorimeter clusters with noise suppression as input [99]. The clusters are locally calibrated [100] before being combined into jets. Trimming [101] is used to minimise contributions from initial-state radiation, pile-up interactions or the underlying event. This is done by reclustering the constituents of the initial jet, using the k_t algorithm [102, 103], into subjets with a radius parameter of $R^{\text{sub}} = 0.2$ and then removing any subjet with a p_T less than 5% of the p_T of the parent jet [104]. The trimmed large- R jets are required to have $p_T > 250$ GeV and $|\eta| < 2.0$. The momenta of both the small- R and large- R jets are corrected for energy losses in passive material and for the non-compensating response of the calorimeter. Small- R jets are also corrected for the average additional energy due to pile-up interactions [105, 106]. A third type of jets is clustered from ID tracks using a variable radius (VR) parameter that shrinks with increasing p_T of the studied proto-jet [107]. VR track-jets are used in this analysis to identify decays of boosted Higgs bosons into a pair of bottom quarks. The VR track-jets must contain at least two ID tracks compatible with the PV and must have $p_T > 7$ GeV as well as $|\eta| < 2.5$.

Small- R jets containing b -hadrons are identified (b -tagged) using the DL1r b -tagging algorithm [108] based on a deep neural network that combines information from displaced tracks and reconstructed secondary and tertiary vertices inside jets. A jet is b -tagged if the response value of the DL1r algorithm exceeds a predefined threshold. Four operating points are defined with efficiencies of 60%, 70%, 77%, and 85% for b -jets, as measured in simulated $t\bar{t}$ events. These operating points divide the DL1r response score distribution into five intervals. The lower edge of the lowest interval corresponds to a b -tagging efficiency of 100%, and the upper edge of the highest interval corresponds to an efficiency of 0%. These intervals are referred to as pseudo-continuous operating points. The number of b -tagged jets per event is evaluated at a fixed b -tagging efficiency of 77%. Applying the b -tagging algorithm at this operating point reduces the number of light-flavour and gluon jets, and jets containing c -hadrons, by a factor of 192 and 5.6, respectively [108]. The pseudo-continuous operating points are used as input to the machine learning algorithms that are designed to reconstruct the charged Higgs boson's decay chain. For this purpose, a score, w_{DL1r} , is defined for each jet as the number of pseudo-continuous operating points the jet satisfies, where zero corresponds to failing and four to satisfying all operating points.

Boosted $h \rightarrow b\bar{b}$ decays are identified exploiting the kinematics of the large- R jet as well as the flavour-tagging information of up to three VR track-jets that are spatially matched via ghost-association [109] to the reconstructed large- R jet [110]. The identification algorithm is based on a feed-forward neural network which is trained using the probabilities of the b -, c - and light-flavour hypotheses of the three leading VR track-jets⁶ and the p_T and η of the large- R jet. The neural network is trained to separate boosted $h \rightarrow b\bar{b}$ jets from boosted top-quark jets and jets arising from multijet processes. The network maps the input vector to a three-dimensional output layer. The three output nodes quantify the probabilities for a large- R jet to correspond to the signal class, and to either of the two background classes. The three output nodes of the neural network are combined into a single discriminant:

$$D_{\text{Xbb}} = \ln \frac{p_{\text{Higgs}}}{f_{\text{top}} \cdot p_{\text{top}} + (1 - f_{\text{top}}) \cdot p_{\text{multijet}}},$$

where f_{top} determines the fraction of top-quark jets, which is set to $f_{\text{top}} = 0.25$. Furthermore, p_{Higgs} , p_{top} , and p_{multijet} are the probabilities for the Higgs boson jet, top-quark jet, and multijet hypotheses. An

⁶ If there are fewer than three associated track-jets with $p_T > 7$ GeV, the inputs corresponding to any missing subjets are replaced with the mean input values.

operating point that corresponds to a selection efficiency of 60% for large- R jets containing $h \rightarrow b\bar{b}$ decays is chosen for this analysis. The $h \rightarrow b\bar{b}$ tagging algorithm reduces contributions from QCD jets and boosted top-quark jets by a factor of 92 and 31, respectively [110], as measured in simulated $t\bar{t}$ events.

Electrons, muons, and jets are reconstructed and identified independently. This can lead to ambiguous identifications when these objects are spatially close to each other. Therefore, an overlap removal procedure is applied to uniquely identify these objects. First, the closest small- R jet within a cone of size $\Delta R = 0.2$ around an electron is removed. Furthermore, a small- R jet with fewer than three associated tracks is removed if the jet is within a cone of $\Delta R = 0.2$ around a selected muon. Finally, electrons and muons are discarded if they are within a cone of size $\Delta R = \min(0.4, 0.04 + 10 \text{ GeV}/p_T^\ell)$ around the axis of any surviving jet, where p_T^ℓ is the transverse momentum of the electron or muon. The latter requirement reduces the background contribution from semileptonic decays of heavy-flavour hadrons.

The missing transverse momentum (with magnitude E_T^{miss}) is computed as the negative vector sum of the p_T of selected electrons, muons and jets, plus a track-based soft term, i.e. all tracks compatible with the PV and not associated with any lepton or jet used in the E_T^{miss} calculation [111].

5 Analysis strategy and event selection

This analysis selects events consistent with the $\ell^\pm \nu b\bar{b} b\bar{b} q\bar{q}$ final state. The pp collision events are retained for further analysis using single-lepton triggers [112, 113]. The transverse momentum thresholds range from 24 GeV to 26 GeV for single-electron triggers and from 20 GeV to 26 GeV for single-muon triggers, depending on the data-taking period. The trigger-level lepton is required to match within $\Delta R = 0.07$ (0.1) a reconstructed electron (muon) with $p_T > 27$ GeV.

Two different analysis strategies are applied to ensure high sensitivity to both low- and high-mass resonances. One analysis strategy targets the ‘resolved’ event topology, in which the final state objects are well separated from each other. The second analysis strategy targets the ‘merged’ event topology, in particular events containing hadronic decays of strongly boosted Higgs and W bosons. These decays are reconstructed using large- R jets.

Events are required to contain exactly one prompt electron or muon and a missing transverse momentum of $E_T^{\text{miss}} > 30$ GeV. In addition, events for the resolved categories are required to contain at least five small- R jets of which at least two have to be b -tagged. For the merged categories, events are required to contain at least one large- R jet. Among all large- R jets in the event, exactly one has to be identified as a $h \rightarrow b\bar{b}$ candidate using the boosted $h \rightarrow b\bar{b}$ identification technique described previously.

This analysis targets two charged Higgs boson decay channels: $H^\pm \rightarrow W^\pm h \rightarrow \ell^\pm \nu b\bar{b}$ (referred to as the $\ell^\pm \nu b\bar{b}$ channel) and $H^\pm \rightarrow W^\pm h \rightarrow q\bar{q} b\bar{b}$ (referred to as the $q\bar{q} b\bar{b}$ channel). Leptons from charged Higgs boson decays generally tend to have higher momenta and are more centrally located in the detector compared with those from top-quark decays. This allows to exploit the differences in the event kinematics to separate the two decay channels. The $\ell^\pm \nu b\bar{b}$ and $q\bar{q} b\bar{b}$ channels are created to be mutually exclusive using distinct selection criteria. Dedicated analysis techniques including machine learning are employed to reconstruct the targeted charged Higgs boson decay modes. These techniques are detailed in Sections 5.1 and 5.2 for the resolved and merged analyses, respectively.

To fully reconstruct the $H^\pm \rightarrow W^\pm h \rightarrow \ell^\pm \nu b\bar{b}$ decay chain, the four-vector of the neutrino has to be determined. The p_x and p_y components of the neutrino momentum are directly obtained by the p_x^{miss} and

p_y^{miss} , while the longitudinal component of the neutrino momentum is calculated by applying an on-shell W -boson mass constraint to the charged lepton plus neutrino system. This approach leads to a quadratic equation, which provides either two, one, or zero real solutions. If it does not have an existing real solution, the missing momentum vector \vec{p}_T^{miss} is rotated until a real solution is found. If this procedure leads to ambiguities, the rotation which provides the minimal change in the \vec{p}_T^{miss} is chosen. If two real solutions are obtained, the solution with the smallest $|p_z^{\nu}|$ is used [114].

Both the resolved and merged analyses are applied to all events, and the same events can be selected by either analysis. Hence, the final search result is reported using the analysis that is most sensitive to the specific mass hypothesis being tested (cf. Section 8).

5.1 Reconstruction and classification of resolved charged Higgs boson decays

For low charged Higgs boson masses, the $\ell^\pm \nu b \bar{b}$ and $q \bar{q} b \bar{b}$ decay channels produce identical detector signatures, as indicated in Figure 1. To differentiate between them, events are classified based on a requirement on the reconstructed leptonic top-quark mass, $m_{\text{top}}^{\text{lep}}$. This observable is calculated from the four-vector sum of a selected b -tagged jet, the charged lepton, and the neutrino candidate. Since several b -tagged jets are present in the event, the selected b -tagged jet is chosen to minimise $|m_{\ell \nu j} - 172.5 \text{ GeV}|$, where $m_{\ell \nu j}$ is the invariant mass of the combined b -tagged jet, charged lepton, and neutrino system. While $m_{\text{top}}^{\text{lep}}$ is distributed around the top-quark pole mass for events containing a leptonically decaying top quark (as in the $q \bar{q} b \bar{b}$ channel), it exhibits broader distributions at higher values for true $\ell^\pm \nu b \bar{b}$ events. Consequently, events with $m_{\text{top}}^{\text{lep}} > 225 \text{ GeV}$ are classified into the $\ell^\pm \nu b \bar{b}$ analysis channel, while those with $m_{\text{top}}^{\text{lep}} \leq 225 \text{ GeV}$ are classified as $q \bar{q} b \bar{b}$ candidates. Distributions of the $m_{\text{top}}^{\text{lep}}$ observable are presented in Figure 2 for a representative charged Higgs boson mass.

The accuracy of the classification requirement on $m_{\text{top}}^{\text{lep}}$ varies as a function of the charged Higgs boson mass. For a mass of 250 GeV, around 40% (45%) of the signal events are correctly classified into the $q \bar{q} b \bar{b}$ ($\ell^\pm \nu b \bar{b}$) analysis channel. The success rates increase with increasing charged Higgs boson mass, reaching values around 75% (90%) for the $q \bar{q} b \bar{b}$ ($\ell^\pm \nu b \bar{b}$) analysis channel.

The charged Higgs boson decays are reconstructed either via a charged lepton, a neutrino candidate, and two small- R jets (for the $\ell^\pm \nu b \bar{b}$ decay mode) or via four small- R jets (for the $q \bar{q} b \bar{b}$ decay mode). Reconstructing the decay of the charged Higgs boson is challenging due to the large number of objects produced in association with it. To address this challenge, sets of boosted decision trees (BDTs) are used to identify the correct decay products of the charged Higgs boson. This allows the four-momentum, and thus the invariant mass, of the heavy scalar to be reconstructed. One set of BDTs is applied to events in the $\ell^\pm \nu b \bar{b}$ category, and another set of BDTs is applied to events in the $q \bar{q} b \bar{b}$ category. The BDTs are trained to distinguish between the correct pairings of the final state objects, i.e. leptons and jets, labelled as signal, and the incorrect pairings labelled as background.⁷ All available signal samples are used to train the BDTs. However, the BDT performance remains stable when adding or removing individual mass points.

⁷ To determine whether a pairing is correct, generator-level particles (i.e. the decay products of the Higgs and W bosons) are spatially matched to the reconstructed objects. A dijet system is considered correctly associated with the generator-level Higgs or W boson if its angular distance to the combined four-vectors of the decay products of the Higgs or W boson is smaller than 0.3. The matching between the charged lepton + neutrino system and the corresponding generator-level particles is based on the same criteria.

The BDTs are implemented into the analysis using the TMVA package [115]. Both sets of BDTs contain a total of 400 decision trees, using the Gradient Boost algorithm with a learning rate of 0.1 and a maximum depth of five.

The BDTs dedicated to reconstruct the charged Higgs boson in the resolved $\ell^\pm \nu b \bar{b}$ category are trained on seven input features built from the four-vectors of the charged lepton, the neutrino candidate and the two jets used to construct the W and Higgs boson candidates. These features are the invariant mass of the Higgs boson candidate ($m_{j_1 j_2}$), the azimuthal angular difference and the pseudorapidity difference between the Higgs boson candidate and the W -boson candidate ($\Delta\Phi(\ell\nu, j_1 j_2)$ and $|\Delta\eta(\ell\nu, j_1 j_2)|$), the ratio of the Higgs boson transverse momentum to the invariant mass of the reconstructed charged Higgs boson candidate ($p_T^{j_1 j_2}/m_{\ell\nu j_1 j_2}$), the ratio of the W -boson transverse momentum to the invariant mass of the reconstructed charged Higgs boson candidate ($p_T^{\ell\nu}/m_{\ell\nu j_1 j_2}$), and the pseudo-continuous b -tagging intervals of the two jets used to build the Higgs boson candidate ($w_{DL1r}^{j_1}$ and $w_{DL1r}^{j_2}$).

These BDTs are iteratively applied to all possible lepton, neutrino, and dijet pairings of events in the resolved $\ell^\pm \nu b \bar{b}$ category. The pairing with the largest BDT score, $w_{\text{BDT}}^{\text{max}}$, is used to construct the four-momentum vector (and hence the invariant mass) of the charged Higgs boson candidate. Furthermore, the $w_{\text{BDT}}^{\text{max}}$ distribution is used to define signal and control regions, motivated by the fact that the dominant backgrounds tend to have lower $w_{\text{BDT}}^{\text{max}}$ values than the signal process.

The BDTs dedicated to the resolved $H^\pm \rightarrow W^\pm h \rightarrow q\bar{q}b\bar{b}$ decay are trained on ten input features built from the four-vectors of the four jets used to construct the W and Higgs boson candidates. These features are the invariant mass of the Higgs boson and W -boson candidates ($m_{j_1 j_2}$ and $m_{j_3 j_4}$), the azimuthal angular difference and the pseudorapidity difference between the Higgs boson candidate and the W -boson candidate ($\Delta\Phi(j_1 j_2, j_3 j_4)$ and $|\Delta\eta(j_1 j_2, j_3 j_4)|$), the ratio of the Higgs boson candidate's transverse momentum to the invariant mass of the reconstructed charged Higgs boson candidate ($p_T^{j_1 j_2}/m_{j_1 j_2 j_3 j_4}$), the ratio of the W -boson transverse momentum to the invariant mass of the reconstructed charged Higgs boson candidate ($p_T^{j_3 j_4}/m_{j_1 j_2 j_3 j_4}$), and the pseudo-continuous b -tagging intervals of the four jets ($w_{DL1r}^{j_1}$, $w_{DL1r}^{j_2}$, $w_{DL1r}^{j_3}$, and $w_{DL1r}^{j_4}$).

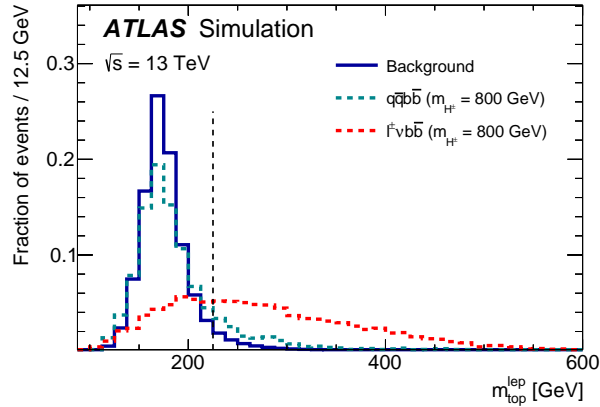


Figure 2: Distributions of the $m_{\text{top}}^{\text{lep}}$ observable for $H^\pm \rightarrow W^\pm h \rightarrow \ell^\pm \nu b \bar{b}$ and $H^\pm \rightarrow W^\pm h \rightarrow q\bar{q}b\bar{b}$ decays as well as the sum of backgrounds after the preselection requirements of the resolved analysis. The distributions are presented for a representative charged Higgs boson mass of $m_{H^\pm} = 800$ GeV. All distributions are normalised to unit area. The dashed vertical line indicates the threshold of the selection requirement on $m_{\text{top}}^{\text{lep}}$ used to define the $\ell^\pm \nu b \bar{b}$ and $q\bar{q}b\bar{b}$ analysis regions.

These BDTs are iteratively applied to all possible four-jet pairings of events in the resolved $q\bar{q}b\bar{b}$ category. The pairing with the largest $w_{\text{BDT}}^{\text{max}}$ value is used to construct the four-momentum vector and the invariant mass of the charged Higgs boson candidate. Again, selection requirements on the $w_{\text{BDT}}^{\text{max}}$ observable are used to define signal and control regions.

To protect against potential biases due to overtraining, a two-fold cross-validation is employed. Events are randomly divided into two equal-sized subsamples, A and B . Two independent boosted decision trees are trained on the two subsamples. The BDTs trained on sample A are evaluated with sample B and vice versa. Half of the data are analysed with the BDTs trained on sample A , and the other half with the BDTs trained on sample B . Finally, the output distributions from both BDTs are merged for both simulated and collision data. This approach results in four sets of BDTs: two for the $\ell^\pm\nu b\bar{b}$ channel and two for the $q\bar{q}b\bar{b}$ channel.

The sets of BDTs perform well in reconstructing the targeted final states. At a charged Higgs boson pole mass of 500 GeV, the final state is reconstructed correctly in about 55% (45%) of the time for the $H^\pm \rightarrow W^\pm h \rightarrow \ell^\pm\nu b\bar{b}$ ($H^\pm \rightarrow W^\pm h \rightarrow q\bar{q}b\bar{b}$) decay mode⁸. The success rates increase with increasing charged Higgs boson mass values, reaching around 90% for both decay modes at masses above 1 TeV. The reconstruction efficiency drops to around 12% for the lowest considered Higgs boson masses, as the decay products tend to fail the kinematic selection requirements and the charged Higgs boson decay cannot be fully reconstructed.

The invariant masses of the reconstructed charged Higgs bosons are determined with a resolution⁹ below 10% for both decay chains and all event categories. The corresponding invariant mass distributions of the reconstructed final states are shown in Figure 3, separated by decay mode and for different signal mass hypotheses.

Finally, events are further categorised according to the overall number of jets (j), and the number of b -tagged jets (b) in the event. In this context, four exclusive categories are defined: $5j3b$, $5j \geq 4b$, $\geq 6j3b$, and $\geq 6j \geq 4b$.

5.2 Reconstruction and classification of merged charged Higgs boson decays

For sufficiently high charged Higgs boson masses, the ambiguities between the $\ell^\pm\nu b\bar{b}$ and $q\bar{q}b\bar{b}$ decay channels are largely reduced due to their distinct detector signatures. Thus, the events in the merged analysis are classified based on the number and properties of selected large- R jets. The $q\bar{q}b\bar{b}$ category requires one large- R jet tagged as a $h \rightarrow b\bar{b}$ candidate and another large- R jet with a mass m_J within the W -boson mass window, $50 \text{ GeV} < m_J < 110 \text{ GeV}$ ($N^{W\text{-tags}} = 1$). Events lacking a second large- R jet with mass around the W boson pole mass ($N^{W\text{-tags}} = 0$) are classified as $\ell^\pm\nu b\bar{b}$. Consequently, the charged Higgs boson decays are reconstructed using a charged lepton, a neutrino candidate, and one large- R jet (for the $\ell^\pm\nu b\bar{b}$ channel) or two large- R jets (for the $q\bar{q}b\bar{b}$ channel). Events are further categorised based on the number of additional b -tagged jets (b), considering only small- R jets that are spatially separated from any

⁸ This reconstruction efficiency is defined as the ratio of the number of correctly reconstructed $\ell^\pm\nu b\bar{b}$ ($q\bar{q}b\bar{b}$) decays to the number of true $\ell^\pm\nu b\bar{b}$ ($q\bar{q}b\bar{b}$) events satisfying the preselection and classification requirements.

⁹ The mass resolution is determined by fitting the convolution of a Gaussian and an exponential function (i.e. a Bukin function) through the distributions of $(m_{W^\pm h} - m_{W^\pm h}^{\text{truth}})/m_{W^\pm h}^{\text{truth}}$, where $m_{W^\pm h}$ and $m_{W^\pm h}^{\text{truth}}$ represent the reconstructed and generator-level invariant masses of the $W^\pm h$ system, respectively. The extracted mass resolution values are given by one standard deviation of the Gaussian component.

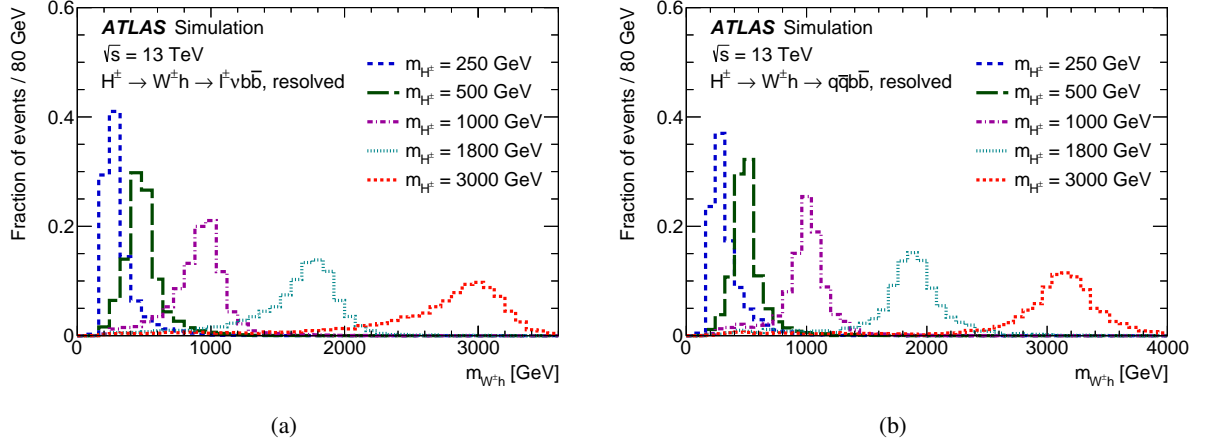


Figure 3: Distributions of the invariant mass of the (a) $H^\pm \rightarrow W^\pm h \rightarrow \ell^\pm \nu b \bar{\ell}$ and (b) $H^\pm \rightarrow W^\pm h \rightarrow q \bar{q} b \bar{b}$ signal hypotheses presented for a selection of different charged Higgs boson pole masses. The final states are reconstructed by applying boosted decision trees to events satisfying the resolved preselection requirements. All distributions are normalised to unit area.

large- R jet used in the analysis. Two exclusive categories are defined, $0b$ and $\geq 1b$, based on the number of b -tagged small- R jets.

A neural network (NN) algorithm is used to further distinguish between the signal and background processes. Its architecture is sequential with three (two) fully connected dense layers of 128 nodes for the merged $\ell^\pm \nu b \bar{\ell}$ ($q \bar{q} b \bar{b}$) category. The NNs are implemented with the PYTHON-based deep learning library, KERAS [116]. The networks are trained and optimised separately for the $\ell^\pm \nu b \bar{\ell}$ and $q \bar{q} b \bar{b}$ decay modes, due to differences in the event kinematics. Both networks use the ADAM optimiser [117] to minimise a Binary Cross Entropy loss function and seven input features. All signal samples with charged Higgs boson masses greater than or equal to 1200 GeV are used to train the NNs. Lower mass hypotheses were excluded from the training to optimise the NN performance for the high-mass hypotheses. Consequently, the NNs tend to assign lower scores to lower mass hypotheses due to their inherent mass dependence.

The NN for the merged $\ell^\pm \nu b \bar{\ell}$ category is trained on input features built from the leptonically decaying W boson (W^{lep}) obtained from the four-vector sum of the charged lepton and the neutrino candidates and the large- R jet used to construct the boosted Higgs boson candidate. These features are the angular separation between the charged lepton and the Higgs boson candidate ($\Delta R(\ell, h)$), the azimuthal angular difference and the pseudorapidity difference between the Higgs boson candidate and the reconstructed W boson ($\Delta\phi(W^{\text{lep}}, h)$ and $|\Delta\eta(W^{\text{lep}}, h)|$), the ratio of the Higgs boson transverse momentum to the invariant mass of the reconstructed charged Higgs boson candidate ($p_{T,h}/m_{W_h}$), the ratio of the W -boson transverse momentum to the invariant mass of the reconstructed charged Higgs boson candidate ($p_{T,W^{\text{lep}}}/m_{W_h}$), the reconstructed leptonic top-quark mass ($m_{\text{top}}^{\text{lep}}$), which is calculated in the same way as for the resolved analysis, and the ratio of the W -boson transverse momentum to the transverse momentum sum of all the decay products of the charged Higgs boson candidate ($p_{T,W^{\text{lep}}}/(p_{T,W^{\text{lep}}} + p_{T,h})$).

The NN for the merged $q \bar{q} b \bar{b}$ category is trained on input features built from the charged lepton and neutrino candidates and the two large- R jets used to reconstruct the hadronically decaying W -boson (W^{had}) and the Higgs boson candidates. Similar to the NN trained for the merged $\ell^\pm \nu b \bar{\ell}$ category, the $\Delta R(\ell, h)$, $\Delta\phi(W^{\text{had}}, h)$, $|\Delta\eta(W^{\text{had}}, h)|$, $p_{T,h}/m_{W_h}$, and $p_{T,W}/m_{W_h}$ observables are used in the training. In addition,

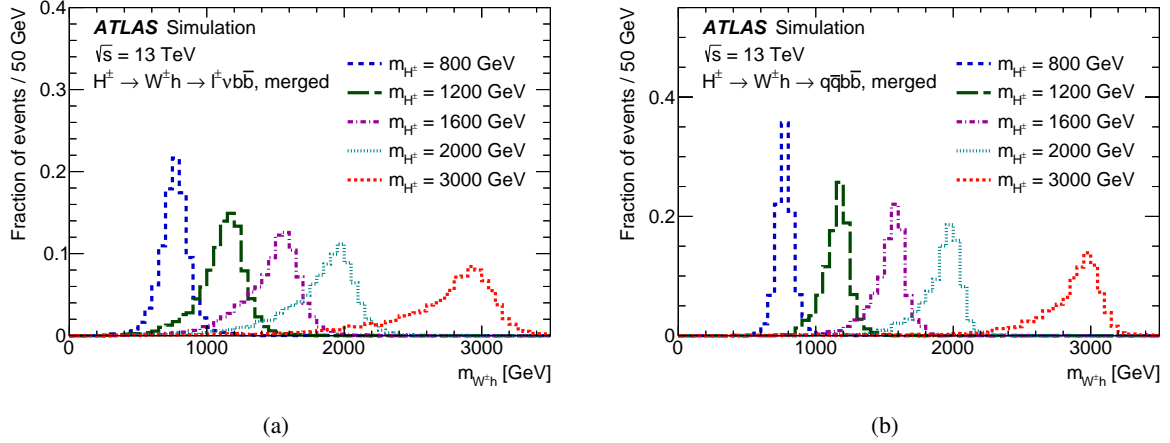


Figure 4: Distributions of the invariant mass of the (a) $H^\pm \rightarrow W^\pm h \rightarrow \ell^\pm \nu b\bar{b}$ and (b) $H^\pm \rightarrow W^\pm h \rightarrow q\bar{q}b\bar{b}$ signal hypotheses presented for a selection of different charged Higgs boson pole masses. The final states are reconstructed using either a charged lepton, a neutrino candidate, and one large- R jet (for the $\ell^\pm \nu b\bar{b}$ channel) or via two large- R jets (for the $q\bar{q}b\bar{b}$ channel) for events entering the merged analysis regions. All distributions are normalised to unit area.

the angular separation between the charged lepton and the hadronically decaying W -boson candidate ($\Delta R(\ell, W^{\text{had}})$), and the ratio of the transverse momentum of the leptonically decaying W -boson candidate to the transverse momentum sum of the leptonically decaying W -boson candidate, the hadronically decaying W -boson candidate and the Higgs boson candidate ($p_{T,W^{\text{lep}}} / (p_{T,W^{\text{lep}}} + p_{T,W^{\text{had}}} + p_{T,h})$), are used as input features.

The same two-folded cross-validation approach as used in the BDT training is employed in the NN training to mitigate any bias due to overtraining.

The invariant mass of the charged Higgs boson candidates is reconstructed in all event categories with a resolution below 9% for the $\ell^\pm \nu b\bar{b}$ category and below 6% for the $q\bar{q}b\bar{b}$ category. The corresponding charged Higgs boson invariant mass distributions are shown in Figure 4, separated by decay mode and for various signal mass hypotheses.

5.3 Definition of signal and control regions

The topological and kinematic preselection requirements of the resolved and merged event categories and the classification requirements used to distinguish the $\ell^\pm \nu b\bar{b}$ and $q\bar{q}b\bar{b}$ decay chains are summarised in Table 2. The signal and control regions are finally defined by applying additional selection criteria on top of the preselection and event classification requirements.

The signal and control regions of the resolved analysis are obtained based on selection requirements on the $w_{\text{BDT}}^{\text{max}}$ observable. A dedicated signal and control region is defined for each of the four $5j3b$, $5j \geq 4b$, $\geq 6j3b$, and $\geq 6j \geq 4b$ categories. Hence, eight regions are used in the resolved $\ell^\pm \nu b\bar{b}$ channel:

- *Signal regions (SRs)* are defined by $w_{\text{BDT}}^{\text{max}} \geq 0.7$,
- *Control regions (CRs)* are defined in the range of $-0.5 \leq w_{\text{BDT}}^{\text{max}} < 0.5$.

Twelve regions are used in the resolved $q\bar{q}b\bar{b}$ channel:

- *High-purity signal regions* are defined by $w_{\text{BDT}}^{\text{max}} \geq 0.9$,
- *Low-purity signal regions* are defined by $0.0 \leq w_{\text{BDT}}^{\text{max}} < 0.9$ for events with exactly three b -tagged jets and by $0.6 \leq w_{\text{BDT}}^{\text{max}} < 0.9$ for events with at least four b -tagged jets,
- *Control regions* are defined in the range of $-0.5 \leq w_{\text{BDT}}^{\text{max}} < 0.0$ for events with exactly three b -tagged jets and by $-0.5 \leq w_{\text{BDT}}^{\text{max}} < 0.6$ for events with at least four b -tagged jets.

Events enter the signal regions of the merged analysis, if the mass of the $h \rightarrow b\bar{b}$ tagged large- R jet (m_h) is in a window around the Higgs boson pole mass, $95 \text{ GeV} \leq m_h < 140 \text{ GeV}$. The signal regions are further split based on the NN output score. A dedicated signal region is defined for each of the $0b$ and $\geq 1b$ categories. Hence, six regions are used for the merged $\ell^\pm \nu b\bar{b}$ channel:

- *High-NN-score signal regions* are defined by $w_{\text{NN}} \geq 0.83$,
- *Medium-NN-score signal regions* are defined by $0.4 \leq w_{\text{NN}} < 0.83$,
- *Low-NN-score signal regions* are defined by $w_{\text{NN}} < 0.4$.

In the merged $q\bar{q}b\bar{b}$ channel four regions are used:

- *High-NN-score signal regions* are defined by $w_{\text{NN}} \geq 0.2$ ($w_{\text{NN}} \geq 0.1$) for events with (without) additional b -tagged jets,
- *Low-NN-score signal regions* are defined by $w_{\text{NN}} < 0.2$ ($w_{\text{NN}} < 0.1$) for events with (without) additional b -tagged jets.

Furthermore, two sets of sideband control regions are defined in the merged event categories by inverting the selection requirement on m_h . *Low-mass sidebands* ($50 \text{ GeV} \leq m_h < 95 \text{ GeV}$) are defined to constrain the W +jets background, while *high-mass sidebands* ($140 \text{ GeV} \leq m_h < 250 \text{ GeV}$) are defined to target backgrounds containing boosted top quarks. Again, a dedicated region is defined per $0b$ and $\geq 1b$ category. The various signal and control regions are summarised in Table 3.

Table 2: Topological and kinematic selections for each channel and category as described in the text. Events are further classified according to the number of b -tagged jets in the events.

Decay channel	Resolved analysis		Merged analysis	
	$\ell^\pm \nu b\bar{b}$	$q\bar{q}b\bar{b}$	$\ell^\pm \nu b\bar{b}$	$q\bar{q}b\bar{b}$
Preselection	$N^\ell = 1$ $E_T^{\text{miss}} > 30 \text{ GeV}$ $N^{\text{small-}R \text{ jets}} \geq 5$ $N^{b\text{-tags}} \geq 2$		$N^{\text{large-}R \text{ jets}} \geq 1$ $N^{h\text{-tags}} = 1$	
Classification requirement	$m_{\text{top}} > 225 \text{ GeV}$	$m_{\text{top}} < 225 \text{ GeV}$	$N^{W\text{-tags}} = 0$	$N^{W\text{-tags}} = 1$
	$5j3b, 5j \geq 4b, \geq 6j3b, \text{ and } \geq 6j \geq 4b$		$0b \text{ and } \geq 1b$	

Table 3: Summary of signal and control regions considered in the statistical analysis for the resolved and merged channels.

Region	Requirement	$\ell^\pm \nu b\bar{b}$ channel	$q\bar{q}b\bar{b}$ channel
Resolved			
Signal regions	Jet & b -tag multiplicity	$w_{\text{BDT}}^{\text{max}} \geq 0.7$	$5j3b, 5j \geq 4b, \geq 6j3b, \geq 6j \geq 4b$
	BDT score		$w_{\text{BDT}}^{\text{max}} \geq 0.9$
Low-purity signal regions	Jet & b -tag multiplicity	-	$5j3b, 5j \geq 4b, \geq 6j3b, \geq 6j \geq 4b$
	BDT score		$0.0 \leq w_{\text{BDT}}^{\text{max}} < 0.9$ (for events with $5j3b$ or $\geq 6j3b$) $0.6 \leq w_{\text{BDT}}^{\text{max}} < 0.9$ (for events with $5j \geq 4b$ or $\geq 6j \geq 4b$)
Control regions	Jet & b -tag multiplicity	$-0.5 \leq w_{\text{BDT}}^{\text{max}} < 0.5$	$5j3b, 5j \geq 4b, \geq 6j3b, \geq 6j \geq 4b$
	BDT score		$-0.5 \leq w_{\text{BDT}}^{\text{max}} < 0.0$ (for events with $5j3b$ or $\geq 6j3b$) $-0.5 \leq w_{\text{BDT}}^{\text{max}} < 0.6$ (for events with $5j \geq 4b$ or $\geq 6j \geq 4b$)
Merged			
High-NN score signal region	b -tag multiplicity	$w_{\text{NN}} \geq 0.83$	$0b, \geq 1b$
	Mass window		$95 \text{ GeV} \leq m_J < 140 \text{ GeV}$
	NN score		$w_{\text{NN}} \geq 0.2$ (for events with $0b$) $w_{\text{NN}} \geq 0.1$ (for events with $\geq 1b$)
Medium-NN score signal region	b -tag multiplicity	$0.4 \leq w_{\text{NN}} < 0.83$	$0b, \geq 1b$
	Mass window		$95 \text{ GeV} \leq m_J < 140 \text{ GeV}$
	NN score		-
Low-NN score signal region	b -tag multiplicity	$w_{\text{NN}} < 0.4$	$0b, \geq 1b$
	Mass window		$95 \text{ GeV} \leq m_J < 140 \text{ GeV}$
	NN score		$w_{\text{NN}} < 0.2$ (for events with $0b$) $w_{\text{NN}} < 0.1$ (for events with $\geq 1b$)
Low-mass control region	b -tag multiplicity		$0b, \geq 1b$
	Mass window		$m_J < 95 \text{ GeV}$
	NN score		-
High-mass control region	b -tag multiplicity		$0b, \geq 1b$
	Mass window		$m_J \geq 140 \text{ GeV}$
	NN score		-

The products of kinematic acceptance and reconstruction efficiency for $pp \rightarrow tbH^\pm (\rightarrow W^\pm h)$ is presented in Figure 5 and Figure 6 separately for all signal regions of the resolved and merged $\ell^\pm \nu b\bar{b}$ and $q\bar{q}b\bar{b}$ decay channels. In this context, the acceptance is defined as the fraction of simulated signal events for which the expected final state particles satisfy all relevant object definition requirements. The denominator of the acceptance is calculated considering simulated signal events with inclusive decays of the W boson, and $h \rightarrow b\bar{b}$ decays of the 125 GeV Higgs boson. The reconstruction efficiency is defined as the ratio of simulated signal events that satisfy all selection criteria for a given signal region to the total number of simulated signal events that satisfy the acceptance requirements.

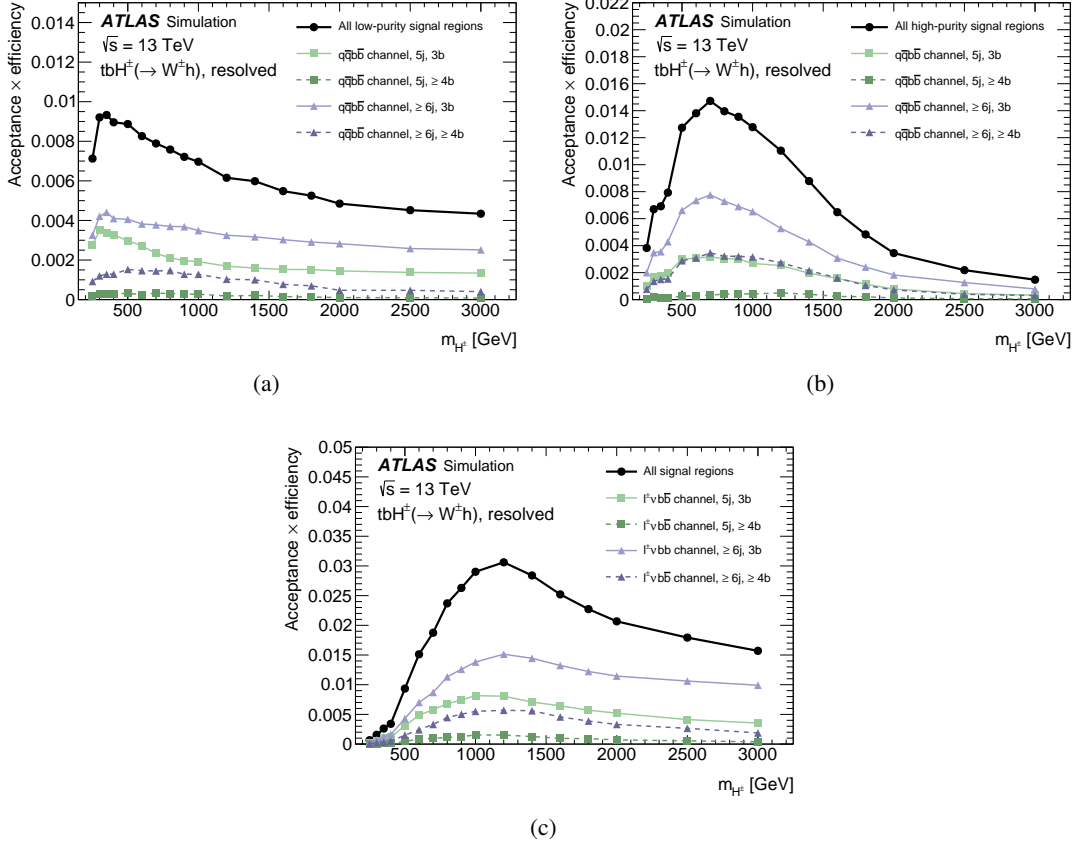


Figure 5: Product of acceptance and efficiency for $pp \rightarrow tbH^\pm(\rightarrow W^\pm h)$ as a function of the charged Higgs boson mass for (a) the resolved $q\bar{q}b\bar{b}$ low-purity signal regions, (b) the resolved $q\bar{q}b\bar{b}$ high-purity signal regions, and (c) the resolved $l^\pm vb\bar{b}$ signal regions.

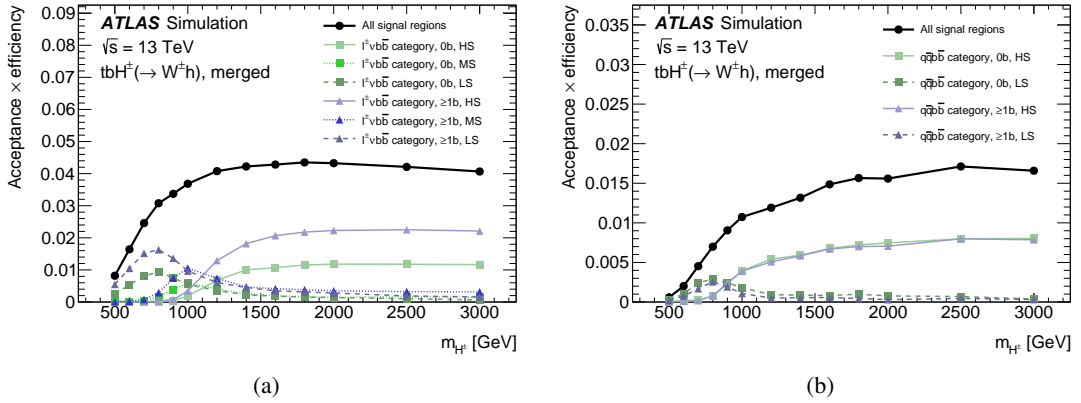


Figure 6: Product of acceptance and efficiency for $pp \rightarrow tbH^\pm(\rightarrow W^\pm h)$ as a function of the charged Higgs boson mass for (a) the merged $l^\pm vb\bar{b}$ high-NN score (HS), medium-NN score (MS) and low-NN score (LS) signal regions, and (b) the merged $q\bar{q}b\bar{b}$ high-NN score and low-NN score signal regions.

6 Background modelling

The background composition in the signal and control regions depends on the event categories and b -jet multiplicities. In the resolved analysis categories, the dominant background source is $t\bar{t}$ + jets production, contributing between 81% and 95% of the total background. Other backgrounds such as W/Z + jets or Wt production are significantly smaller. In the merged categories, the most significant background contributions stem from $t\bar{t}$ + jets and W + jets production. Contributions from diboson, SM Vh , $t\bar{t} + h$, $t\bar{t} + V$, and from the rare top-quark processes (i.e. tZq , tWZ , $tHjb$, tWh , and $t\bar{t}t\bar{t}$) are small in all channels. Background contributions from events containing non-prompt leptons are found to be negligible. These findings are consistent with previous studies in the same and similar final states [30, 118].

Backgrounds are estimated from samples of simulated events, where the normalisation of the dominant backgrounds is obtained from data. In addition, shape corrections are derived for the $t\bar{t}$ + jets production process. These corrections are necessary because the additional jets in the $t\bar{t}$ + jets events are produced by the parton shower, which leads to a mis-modelling of high jet multiplicities and the hardness of additional jet emissions. Hence, in the resolved analysis channels, the simulated $t\bar{t}$ + jets events are reweighted as a function of the H_T^{all} observable.¹⁰ The reweighting function is obtained from fits to the data-to-simulation ratio in events with one charged lepton, $E_T^{\text{miss}} > 30$ GeV, and at least five jets of which exactly two are b -tagged ($\geq 5j2b$) following the approach detailed in Ref. [30] This reweighting procedure is performed separately for different jet multiplicity intervals, distinguishing events with five, six, seven, or at least eight jets. The reweighting factors are expressed as a function of the H_T^{all} observable:

$$r_i(H_T^{\text{all}}) = \frac{N_i^{\text{Data}}(H_T^{\text{all}}) - N_i^{\text{MC,non-}t\bar{t}}(H_T^{\text{all}})}{N_i^{\text{MC},t\bar{t}}(H_T^{\text{all}})},$$

where N_i is the number of events in a H_T^{all} interval and the i -th jet bin. The ensemble of $r_i(H_T^{\text{all}})$ is fitted per jet bin with an exponential plus sigmoid functional form,¹¹ which is then used as a correction function applied to the $5j3b$, $5j \geq 4b$, $\geq 6j3b$ and $\geq 6j \geq 4b$ regions of the $\ell^\pm \nu b\bar{b}$ and $q\bar{q}b\bar{b}$ analysis channels. In contrast, the merged analysis channels are more inclusive in jet multiplicity, making them less dependent on the modelling of the additional jet activity. While a similar correction procedure was tested for the merged analysis, it did not significantly improve the modelling of relevant observables. Thus, no such correction procedure is applied in the merged analysis.

Events containing top-quark pairs are categorised according to the flavour of jets produced in association with the $t\bar{t}$ system. This categorisation procedure is based on generator-level information, where jets are reconstructed from stable particles (i.e. particles with a mean lifetime $\tau > 3 \times 10^{-11}$ s) using the anti- k_t algorithm with the radius parameter set to $R = 0.4$. These jets are required to have $p_T > 15$ GeV and $|\eta| < 2.5$, and their flavour is determined by counting b - or c -hadrons with p_T larger than 5 GeV within a cone of $\Delta R = 0.4$ around the jet axis. Jets including b -hadrons are labelled as b -jets, while jets that do not include any b -hadron, but do include one or more c -hadrons are labelled as c -jets. Events that include at least one b - or c -jet, not considering heavy-flavour jets from top-quark, W -boson, Z -boson or Higgs-boson decays, are labelled as $t\bar{t}$ + HF (with HF denoting ‘heavy flavour’). Events not containing any heavy-flavour

¹⁰ The H_T^{all} observable is defined as the scalar sum of the transverse momenta of all jets and the charged lepton in the event.

¹¹ In addition a hyperbola plus sigmoid functional form and a 2nd order polynomial plus first order exponential functional form were tested. However, the exponential plus sigmoid functional form was found to fit the data best.

jets, aside from those from top-quark or W -boson decays, are labelled as $t\bar{t} + \text{LF}$ (with LF denoting ‘light flavour’).

The subdominant background processes are grouped into four components: single-top-quark production (including s - and t -channels, Wt production, tZq , and tWZ), VV & $V + \text{jets}$ (including $W/Z + \text{jets}$, WW , ZZ , and WZ), $t\bar{t} + X$ (including $t\bar{t} + h$, $t\bar{t} + W$, and $t\bar{t} + Z$), and the remaining backgrounds referred to as ‘Others’ (including $tHjb$, tWh , $t\bar{t}\bar{t}$, and SM Vh).

7 Systematic uncertainties

The distributions of the $m_{W\pm h}$ observable and the event yields in the signal and control regions are affected by both experimental and modelling uncertainties, which enter the final fits as nuisance parameters (NPs). Uncertainties in the modelling of physics objects are correlated between signal and background processes, channels, kinematic regions and distributions of observables. The modelling uncertainties are evaluated separately for the signal and all relevant background processes.

7.1 Experimental systematic uncertainties

All experimental uncertainties, except for the luminosity uncertainty, impact both the normalisation and shape of the simulated distributions. The dominant experimental uncertainties are uncertainties in the flavour-tagging performance, in the jet energy scale and resolution calibration, and in the modelling of the pile-up activity.

Uncertainties in the trigger selection, the charged lepton reconstruction, identification and isolation criteria, as well as the lepton momentum scale and resolution are measured in data applying tag-and-probe techniques to $Z \rightarrow \ell^+\ell^-$ events [92, 94]. These uncertainties have only a small impact on the charged Higgs boson search.

The uncertainties in the small- R jet energy scale and resolution have contributions from *in situ* calibration measurements, from the dependency on the pile-up activity and from the flavour composition of the jets [105]. The uncertainty in the scale and resolution of the large- R jet energy and mass is derived by comparing the ratio of calorimeter-based to track-based measurements in dijet data and simulation, as described in Ref. [106].

Dedicated measurements are performed to calibrate the jet flavour-tagging efficiency for b -jets and the mis-tagging rates for c - and light-flavour jets to the performance in data. The results of these measurements are expressed as p_T dependent correction factors that are derived for b -jets in $t\bar{t}$ events with dilepton final states [119], for c -jets in $t\bar{t}$ events with single-lepton final states [120] and in Z +jets events for light-flavour jets [121]. Uncertainties in these correction factors are decomposed into uncorrelated components and then propagated to the charged Higgs boson search. Additional uncertainties are considered to extrapolate the measured efficiencies to high jet p_T [122]. These terms are calculated from simulated events by considering variations of the quantities affecting the b -tagging performance, such as the impact parameter resolution, percentage of tracks from random combinations of measurements in the ID, description of the detector material, and track multiplicity per jet.

The $h \rightarrow b\bar{b}$ identification efficiencies and the corresponding mis-identification rates for boosted top-quark jets are corrected to data using dedicated measurements. Correction factors and their corresponding

uncertainties in the $h \rightarrow b\bar{b}$ identification efficiencies are obtained from events containing $Z \rightarrow b\bar{b}$ decays [123]. The correction factors are dependent on the large- R jet p_T and vary from approximately 0.96 to 1.34 with uncertainties ranging from around 30% to 35%. The mis-identification efficiency scale factors for boosted top quarks are measured in top-quark pair events. They vary from 1.10 ± 0.12 at low p_T to 1.00 ± 0.16 at high p_T . Mis-identification efficiency uncertainties for QCD jets were estimated in the sideband control regions of the merged analysis by performing a three-component fit to data: one component describing events in which the $h \rightarrow b\bar{b}$ tagged jet originates from the decay of a boosted top quark, one component describing events in which the $h \rightarrow b\bar{b}$ tagged jet originates from a QCD jet, and a third component describing events in which the tagged jet stems from a boosted Z , W , or Higgs boson. The large- R mass distributions of these three components are fitted to data across different jet p_T intervals, excluding the Higgs boson mass region. In these fits, the normalisation factors of the top-quark jet and QCD jet components were allowed to vary freely, while the third component was fixed to the SM prediction. The final uncertainties are determined by summing the deviation of the central value from unity and the uncertainty of a given normalisation factor. These uncertainties range from 7% at low large- R jet p_T to 41% for jets with p_T exceeding 500 GeV.

The uncertainties in the energy scale and resolution of the small- R jets and leptons are propagated to the calculation of E_T^{miss} , which also has additional uncertainties from the modelling of the underlying event and the momentum scale, momentum resolution and reconstruction efficiency of the tracks used to compute the soft-term [111].

Finally, a global luminosity uncertainty of 0.83% is applied to the normalisation of the simulated signal and background samples [42, 45].

7.2 Modelling systematic uncertainties

Modelling uncertainties are taken into account for all simulated signal and relevant background processes and cover three areas: shape uncertainties that account for uncertainties in the $m_{W^\pm h}$ template shapes used for the statistical analysis; absolute normalisation uncertainties; and relative acceptance uncertainties (referred to as extrapolation uncertainties), that account for differences in the acceptance between regions with a common floating normalisation factor, e.g. migration effects between the signal and control regions, the $\ell^\pm \nu b\bar{b}$ and $q\bar{q}b\bar{b}$ channels, and the different jet multiplicity regions. While normalisation and shape uncertainties may be described by a common nuisance parameter, extrapolation uncertainties are always described by separate nuisance parameters. The modelling uncertainties are assessed by comparing nominal and alternative event generators and the underlying event and parton shower models. In general, the perturbative accuracy and the PDF sets used in these alternative configurations match those of the nominal generators (unless explicitly stated). Uncertainties due to the modelling of PDF sets are evaluated following the PDF4LHC recommendations [85], and uncertainties due to missing higher orders are evaluated by varying the renormalisation and factorisation scales, μ_R and μ_F , as described below.

For the signal processes, uncertainties in the acceptance are derived by comparing the predictions of the nominal PDF set with those from the CT14 [124] and MMHT2014 [125] PDF sets and then comparing the larger variation with the difference from the root-mean-square spread of the nominal replica sets. The variation with the largest impact on the results is taken as the final uncertainty. Further uncertainties are obtained by replacing PYTHIA 8.244 by HERWIG 7.2.2 for the showering and hadronisation, and by varying the renormalisation and factorisation scales. The total acceptance uncertainties show substantial variation across different charged Higgs boson masses, decay channels, and event categories.

The modelling uncertainties of the top-quark pair production processes are derived as follows. To assess the uncertainties in the matching of the matrix element to the parton shower, the nominal $t\bar{t}$ + HF and $t\bar{t}$ + LF samples are compared with samples where POWHEG BOX is replaced by MADGRAPH5_AMC@NLO. The parton shower modelling uncertainties are determined by replacing PYTHIA 8.230 by HERWIG 7.0.4 and switching to the H7UE set of tuned parameters [126]. The uncertainties in the modelling of the initial-state radiation (ISR) and the final-state radiation (FSR) are addressed by varying the strong coupling constant α_S independently at the matrix element and the parton shower generation stage. In the matrix element, the parameter α_S is increased (decreased) to 0.140 (0.115) instead of the nominal value 0.127, while in the parton shower α_S is increased (decreased) to 0.142 (0.115) instead of the nominal value. Uncertainties related to missing higher-order terms in the perturbative expansion are estimated by scaling μ_R and μ_F independently up and down by a factor of two. Additional uncertainties in the associated production of top-quark pairs and b -quarks are estimated by comparing the predictions of the nominal POWHEG BOX + PYTHIA sample, in which the extra b -quarks arise from the PS, to the predictions of an alternative POWHEG BOX + PYTHIA sample simulated using the four-flavour scheme. In the latter sample, an additional b -quark pair is produced in association with the top-quark pair ($t\bar{t}b\bar{b}$) in the matrix element, which is calculated at NLO accuracy in QCD. Furthermore, an uncertainty in the relative composition of the additional c - and b -jet contributions in the $t\bar{t}$ + HF sample is taken into account. This uncertainty is evaluated by varying the relative normalisations of the $t\bar{t} + \geq 1b$ and $t\bar{t} + \geq 1c$ contributions according to the predictions of the alternative MC generators relative to the predictions of the nominal MC generator configuration. These variations range from 10% to 30% in the regions of the resolved analysis and from 3% to 30% in the regions of the merged analysis. While varying the $t\bar{t} + \geq 1b$ and $t\bar{t} + \geq 1c$ contributions, the overall normalisation of the $t\bar{t}$ + HF background is kept constant. When calculating the modelling uncertainties for the $t\bar{t}$ + HF and $t\bar{t}$ + LF processes, the same H_T reweighting is applied to the nominal and alternative models.

A 5% uncertainty is considered on the cross-section of the Wt production mode and the s - and t -channel production of single top quarks [127]. Uncertainties associated with the matching of the matrix element and the parton shower and the choice of the parton shower and hadronisation models, are estimated by comparing, for each of these three processes, the nominal POWHEG BOX + PYTHIA 8.230 sample with alternative samples produced using MADGRAPH5_AMC@NLO 2.62 + PYTHIA 8.140 and POWHEG BOX + HERWIG 7.0.4, respectively. Uncertainties associated with the interference between top-quark pair and Wt production at NLO are evaluated by comparing the predictions of the nominal Wt sample with those from an alternative sample generated with POWHEG BOX and PYTHIA 8.230 using the diagram subtraction (DS) scheme [128] instead of the diagram removal scheme. Finally, an 8% uncertainty is considered on the cross-section of the tZq process, and a 50% uncertainty is considered on the tWZ cross-section [30].

An uncertainty of $^{+9\%}_{-12\%}$ in the $t\bar{t} + h$ production cross-section is considered, including effects from varying the factorisation and renormalisation scales, the PDF set, and α_S [71, 129]. The nominal POWHEG BOX + PYTHIA 8.230 sample is compared with a sample produced with MADGRAPH5_AMC@NLO 2.60 + PYTHIA 8.230 to assess the uncertainty associated with the matching of the matrix element and the parton shower, and to a sample generated with POWHEG BOX + HERWIG 7.0.4 for the uncertainty in the modelling of the parton shower.

The uncertainties in the normalisation of the $t\bar{t} + Z$ and $t\bar{t} + W^\pm$ backgrounds are $^{+10.4\%}_{-12.0\%}$ and $^{+13.4\%}_{-12.0\%}$, respectively and include effects from varying the factorisation and renormalisation scales and the PDF set [130]. In addition, uncertainties in the choice of the parton shower and hadronisation models and matching scheme for the $t\bar{t} + Z$ and $t\bar{t} + W^\pm$ processes are estimated by comparing the nominal MADGRAPH5_AMC@NLO 2.33 + PYTHIA 8.210 samples to alternative samples simulated using SHERPA 2.2.1 with the NNPDF3.0NNLO

PDF set. For the alternative $t\bar{t} + W^\pm$ event samples, diagrams with up to one additional parton emission are generated at NLO accuracy in QCD, and diagrams with two, three or four additional parton emissions are generated at LO accuracy in QCD. For the production of $t\bar{t} + Z$ events, diagrams with up to four additional parton emission are generated at LO accuracy in QCD. In both samples, the CKKW matching scale of the additional emissions was set to 30 GeV.

An overall 50% uncertainty is considered in the normalisation of the four-top-quarks background [50, 131], while uncertainties of $^{+7.5\%}_{-15.4\%}$ and $^{+9.1\%}_{-9.2\%}$ are assigned to the $thjb$ and thW backgrounds [50]. These uncertainties cover effects from varying the renormalisation and factorisation scales, the PDF set and α_S .

In the merged event categories, the modelling uncertainties in the W +jets background are determined as follows: uncertainties related to missing higher order terms in the perturbative expansion are estimated by individually varying μ_R and μ_F by a factor of 2 or 0.5. Six combinations are considered: $(\mu_R, \mu_F) = (0.5, 0.5), (0.5, 1.0), (1.0, 0.5), (1.0, 2.0), (2.0, 1.0),$ and $(2.0, 2.0)$ times their nominal value. The final uncertainty is derived as the variation of μ_R and μ_F that has the largest impact on the results. Additionally, variations of the SHERPA merging scale are taken into account, where the nominal value, 20 GeV, is changed to 30 GeV and 15 GeV. Furthermore, uncertainties in the parton shower evolution's upper cutoff scale are assessed by varying the resummation scale by factors of $1/\sqrt{2}$ and $\sqrt{2}$ from its nominal value. Additional modelling uncertainties are derived by comparing the nominal W +jets sample to an alternative sample simulated using MADGRAPH5_AMC@NLO 2.6.5 with the NNPDF3.1NNLO PDF set. The alternative sample includes vector bosons with up to three additional partons at NLO accuracy in QCD. PYTHIA 8.240 with the A14 set of tuned parameters is used for showering and hadronisation, and the different jet multiplicities were merged using the FxFx procedure [132]. In the resolved event categories, where the W +jets background is nearly negligible, a flat 40% uncertainty is considered on the normalisation of the W +jets background.

Both the resolved and merged analyses assign an uncertainty of 35% to the Z +jets background normalisation, and a 50% uncertainty in the normalisation of the diboson backgrounds. These normalisation uncertainties account for effects from varying the renormalisation and factorisation scales, the merging scale and the PDF set and α_S .

Additional uncertainties in the H_T reweighting of the $t\bar{t} + \text{jets}$ background in the resolved analysis regions (cf. Section 6) are evaluated by independently varying the fitted parameters of the exponential plus sigmoid functional form within their uncertainties and reapplying the reweighting procedure. The resulting differences in the normalisation and $m_{W^\pm h}$ shape of the $t\bar{t} + \text{jets}$ background compared with the nominal reweighting are assigned as a systematic uncertainty. These uncertainties are evaluated separately for each jet multiplicity bin. In addition to the nominal reweighting function, two other functional forms (cf. Section 6) were considered for the reweighting procedure. The differences in results between the nominal and alternative functions are negligible compared to the MC statistical uncertainties of the $t\bar{t} + \text{jets}$ sample. Therefore, no additional uncertainty due to the choice of the reweighting function is assigned.

Residual mismodelling (i.e. non-closure in the comparison between data and simulation) of the transverse W -boson momentum, $p_{T,W}$, distribution in the resolved analysis regions and the $p_{T,W}/m_{Wh}$, $\Delta\Phi(W, h)$ and E_T^{miss} distributions in the merged analysis regions are observed in the respective control regions. The non-closure uncertainties are derived by parameterising the data-to-simulation ratios of mis-modelled observables. These parametric functions are then used to reweight the observables and assess the impact on the shape of the $m_{W^\pm h}$ distribution. The magnitude of the $m_{W^\pm h}$ shape differences reach up to 30% in the tails of the distributions. The final uncertainty is quantified as the variation between the reweighted

and nominal $m_{W\neq h}$ distributions, and is incorporated as an additional nuisance parameter affecting all processes.

The relative modelling systematic uncertainties (at the pre-fit stage), impacting the normalisation, cross-region extrapolation, and shape of the signal and background processes are summarised in Table 4.

8 Results

To test for the presence of a massive charged Higgs boson in data, the m_{Wh} templates obtained from the simulated signal and background event samples are fitted to data using a binned maximum-likelihood approach based on the RooFIT/RooSTATS framework [133–135]. Fits are simultaneously performed on the signal and control regions defined in Section 5.3 to constrain the normalisation of the main backgrounds and the nuisance parameters describing the systematic uncertainties detailed in Section 7. Each systematic variation is incorporated in the fit as an individual nuisance parameter using a Gaussian constraint, while nuisance parameters describing statistical uncertainties are incorporated using a Poisson constraint. Systematic variations that are impacted by large statistical fluctuations are smoothed, while systematic variations with negligible impact on the final results are pruned away. Asimov data sets [136] are used to evaluate the expected performance of each fit.

As no significant excess over the SM expectations is found, the results of this search are expressed as upper limits at the 95% confidence level on the production cross-section times branching ratio of charged Higgs bosons for a wide range of resonance masses. The largest deviation from the SM expectations is found for a charged Higgs boson mass of 900 GeV and corresponds to a local significance of about 0.9 standard deviations (and a p -value, i.e. the probability that the background can produce a fluctuation greater than the excess observed in data, of 0.184). The limits are evaluated using the CL_s method [137] and the profile-likelihood-ratio test statistic in the asymptotic approximation [136].

Two separate likelihood fits are performed to search for charged Higgs bosons: one for the resolved analysis and the other for the merged analysis. Each fit includes dedicated SRs and CRs for $q\bar{q}b\bar{b}$ and $\ell^\pm\nu b\bar{b}$ decays (cf. Section 5.3) and the fit models differ between the analyses. The resolved fit has the signal cross-section and the global normalisation factor of the $t\bar{t}$ + HF background as free parameters, while the merged fit has the signal cross-section and the global normalisation factors of the $t\bar{t}$ + HF, $t\bar{t}$ + LF, and VV & V + jets backgrounds as free parameters. Common normalisation factors are applied across all regions used in a fit. However, dedicated nuisance parameters address extrapolation uncertainties between the signal and control regions, decay channels, and the different jet multiplicity regions. The corresponding extrapolation uncertainties are detailed in Table 4. Normalisation factors and uncertainties from background-only fits¹² in the resolved and merged analysis categories are summarised in Table 5. The normalisation factors for the $t\bar{t}$ + HF background exceed unity in both resolved and merged analyses. The normalisation factors are consistent within about one standard deviation across the two analyses. Furthermore, the normalisation factor for the $t\bar{t}$ + LF background component in the merged analysis is below unity, consistent with the corrections obtained from the H_T^{all} reweighting in the resolved analysis.

In addition to constraining the normalisation of the dominant backgrounds, the fit also constrains several modelling uncertainties. Significant constraints are observed in the resolved analysis for nuisance parameters

¹² When performing signal-plus-background fits, the corresponding normalisation factors show minor deviations from those obtained in the background-only fits. However, these differences are insignificant in comparison to the uncertainties in the normalisation factors.

Table 4: Relative modelling systematic uncertainties (at the pre-fit stage) in the normalisation, cross-region extrapolation, and shape of signal and the background processes included in the fits described in the text. An ‘S’ indicates that a shape variation is included for the listed sources. ‘ $A \leftrightarrow B$ ’ indicates relative acceptance uncertainties that account for the relative normalisation differences between two regions, A and B , with a common floating normalisation factor (i.e. these are extrapolation uncertainties). Furthermore, ‘norm.’ is the product of cross-section and acceptance variations, and a value of ‘float’ indicates that the parameter is not constrained in the fit. A range of values means that the size of the uncertainties vary between the regions included in the fit, where the minimum and maximum relative uncertainties in the predicted yields are stated. No dedicated normalisation uncertainty is taken into account for the $t\bar{t}$ + LF background given that the normalisation of this process is fixed by the H_T reweighting. Each of the listed uncertainties is treated as uncorrelated in the fits. The uncertainties are listed separately for (a) the resolved analysis channels and (b) the merged analysis channels.

(a) Relative acceptance and normalisation uncertainties for the resolved analysis channels

	$t\bar{t}$ + HF	$t\bar{t}$ + LF	$t\bar{t}$ + X	Single Top	VV & V + jets	Others	Signal
Norm.	float	fixed	0.8%–12%	1.1%–4.7%	2%–34%	2.9%–47%	float
PDF	S	0.2%–0.5%, S	–	–	–	–	0.5%–6%
ISR	S	0.7%–5%, S	–	–	–	–	–
FSR	S	1.3%–19%, S	–	–	–	–	–
ME-PS matching	S	2.0%–40%, S	0.6%–7%, S	0.6%–53%, S	–	–	–
Parton shower	S	3.3%–22%, S	1.7%–13%, S	2.2%–61%, S	–	–	1.0%–50%, S
4FS vs. 5FS	S	–	–	–	–	–	–
Heavy-flavour composition	S	–	–	–	–	–	–
DS vs. DR scheme (Wt)	–	–	–	3.3%–68%, S	–	–	–
Renormalisation/factorisation scales	S	0.5%–3.0%, S	–	–	–	–	1.0%–13%, S
H_T reweighting	S	0.5%–6%, S	–	–	–	–	–
$p_{T,W}$ non-closure	S	0.5%–0.9%, S	0.7%–1.6%, S	2.7%–4%, S	1.8%–3.3%, S	1.1%–2.0%, S	3.0%–30%, S
$5j \leftrightarrow \geq 6j$	17%–34%	–	–	–	–	–	–
SRs \leftrightarrow CRs	11%–33%	–	–	–	–	–	–
SRs \leftrightarrow low-purity SRs	6.8%–17%	–	–	–	–	–	–
Low-purity SRs \leftrightarrow CRs	5.2%–12%	–	–	–	–	–	–
$\ell^\pm v b \bar{b} \leftrightarrow q \bar{q} b \bar{b}$	5.1%–17%	–	–	–	–	–	–

(b) Relative acceptance and normalisation uncertainties for the merged analysis channels

	$t\bar{t}$ + HF	$t\bar{t}$ + LF	$t\bar{t}$ + X	Single Top	VV & V + jets	Others	Signal
Norm.	float	float	0.5%–11%	5%–50%	float	0.5%–50%	float
PDF	S	S	–	–	–	–	<0.5%
ISR	S	S	–	–	–	–	–
FSR	S	S	–	–	–	–	–
ME-PS matching	S	S	0.5%–28%, S	0.5%–26%, S	S	–	–
Parton shower	S	S	0.5%–18%, S	0.5%–60%, S	S	–	0.8%–60%, S
4FS vs. 5FS	S	–	–	–	–	–	–
Heavy-flavour composition	S	–	–	–	–	–	–
DS vs. DR scheme (Wt)	–	–	–	13%–86%, S	–	–	–
Renormalisation/factorisation scales	S	S	–	–	S	–	0.5%–11%, S
$p_{T,W}/m_{W,h}$ non-closure	S	S	1.0%–4%, S	0.8%–9%, S	S	0.7%–9%, S	0.5%–21%, S
$\Delta\Phi(W, h)$ non-closure	S	S	0.6%–1.2%, S	0.5%–1.2%, S	S	0.5%–0.6%, S	0.5%–3.2%, S
E_T^{miss} non-closure	S	S	0.8%–8%, S	0.6%–8%, S	S	4%–10%, S	0.5%–12%, S
$0b \leftrightarrow \geq 1b$	4%–24%	11%–18%	–	–	8%–70%	–	–
$\ell^\pm v b \bar{b} \leftrightarrow q \bar{q} b \bar{b}$	18%–35%	18%–50%	–	–	16%–60%	–	–
High-mass CRs \leftrightarrow low-mass CRs	3.4%–19%	3.7%–16%	–	–	10%–32%	–	–
CRs \leftrightarrow high-score SR	13.1%–22%	6%–30%	–	–	4%–28%	–	–
CRs \leftrightarrow medium-score SR	11%–17%	6%–22%	–	–	4%–12%	–	–
CRs \leftrightarrow low-score SR	6%–13%	2.7%–23%	–	–	6%–40%	–	–
Low-score SR \leftrightarrow high-score SR	17%–27%	7%–30%	–	–	11%–35%	–	–
Low-score SR \leftrightarrow medium-score SR	13%–19%	7%–23%	–	–	11%–14%	–	–
Medium-score SR \leftrightarrow high-score SR	7%–34%	11%–26%	–	–	14%–20%	–	–

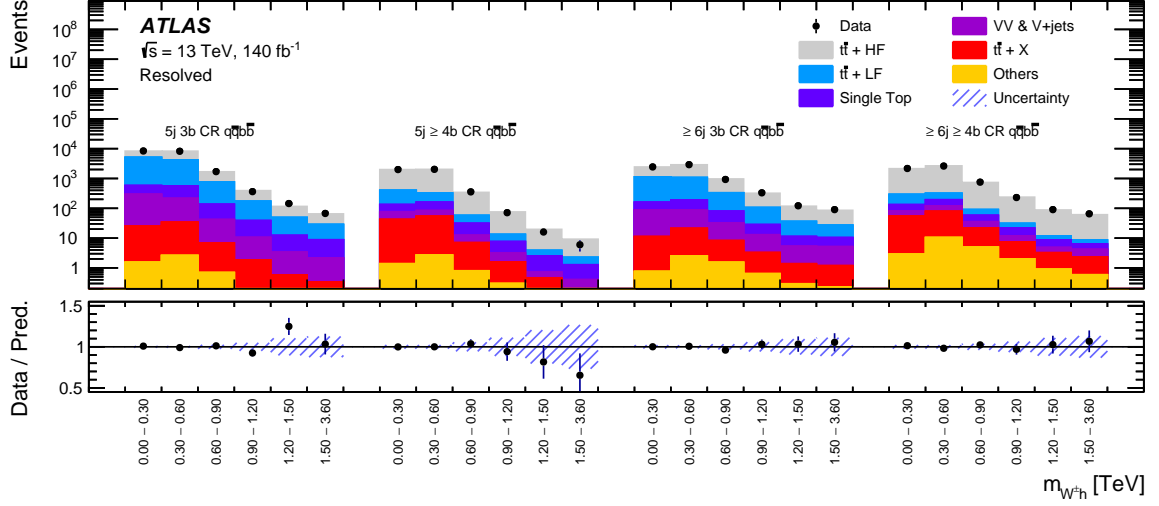
associated with the flavour composition, parton shower modelling and matrix element to parton shower matching of the $t\bar{t}$ + HF background. Furthermore, nuisance parameters associated with the parton shower

Table 5: Post-fit normalisation factors and their uncertainties obtained from a combined background-only fit to the various signal and control regions of the resolved and merged analyses. Numbers are presented for the background components that are allowed to float in the likelihood fit. Uncertainties in the cross-section times branching ratio and the overall acceptance are not considered in the denominators of these normalisation factors.

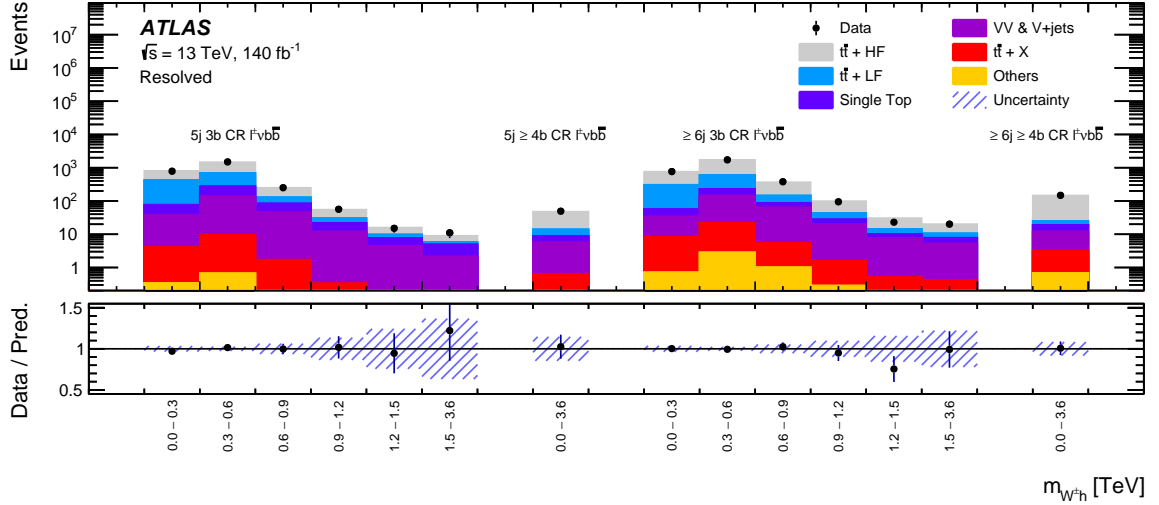
Background	Resolved analysis	Merged analysis
$t\bar{t} + \text{HF}$	1.39 ± 0.18	1.20 ± 0.17
$t\bar{t} + \text{LF}$	–	0.75 ± 0.08
$VV \ \& \ V + \text{jets}$	–	1.17 ± 0.13

modelling of the $t\bar{t} + \text{LF}$ background and the comparison between the DS and DR schemes of the Wt background are constrained substantially. The nuisance parameter corresponding to the flavour composition of the $t\bar{t} + \text{HF}$ background is constrained to 20% of its initial value, while the other nuisance parameters listed above are constrained to about 40%-60% of their initial values. In addition to the constraints, a few significantly pulled nuisance parameters are observed in both analyses. In the resolved analysis, the nuisance parameter associated with the $p_{T,W}$ non-closure uncertainty is pulled by about one standard deviation. In the merged analyses, the nuisance parameters associated with the E_T^{miss} non-closure uncertainty, the uncertainties related to missing higher order terms in the perturbative expansion of the $W + \text{jets}$ background, and the matrix element to parton shower matching of the $t\bar{t} + \text{LF}$ background are each pulled by around 0.7 to 0.8 standard deviations.

The $m_{W\pm h}$ distributions after a background-only fit to data are shown in Figures 7 to 8 for the control regions of the resolved and merged analyses. The corresponding signal region distributions are shown in Figures 9 to 11 for the signal regions of the resolved analysis and in Figures 12 to 14 for the signal regions of the merged analysis. Additionally, the expected and observed event yields after fits of the backgrounds to data performed under the background-only hypothesis are shown in Table 6.

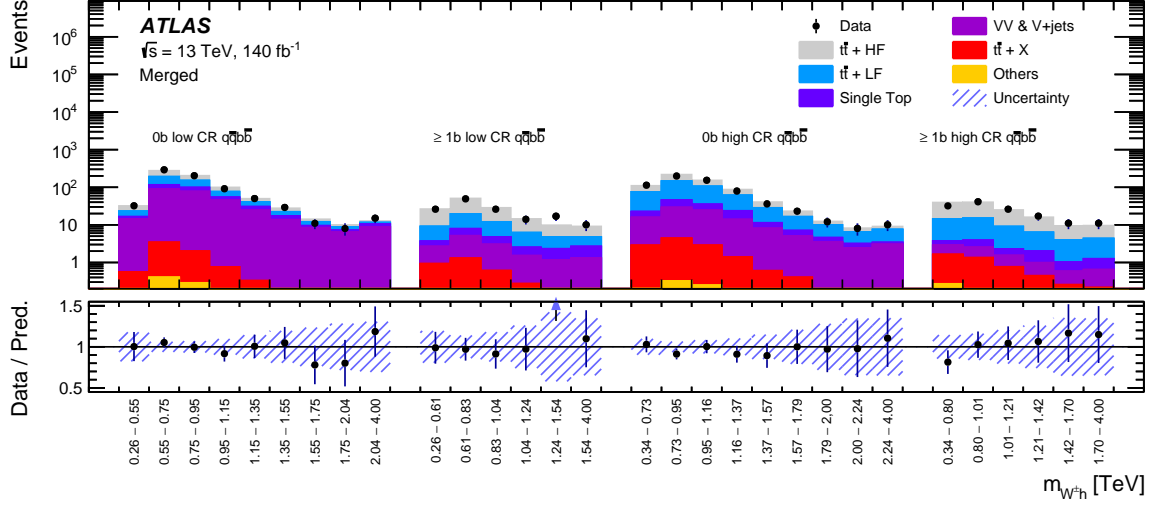


(a)

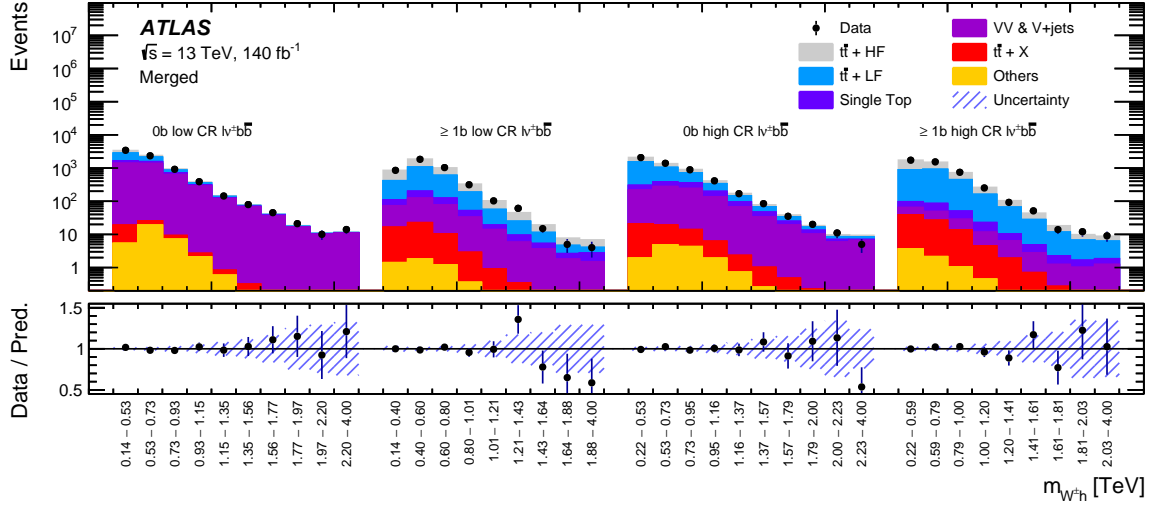


(b)

Figure 7: Distributions of the $m_{W^{\pm}h}$ observable in the control regions of the resolved (a) $q\bar{q}b\bar{b}$ and (b) $\ell^{\pm}v\bar{b}\bar{b}$ event categories. The term ‘Others’ summarises events from $tHj\bar{b}$, tWh , $t\bar{t}t\bar{t}$, and SM Vh production. The distributions are presented after a background-only maximum-likelihood fit to data. The lower panels show the ratio of the observed to the estimated SM background. The shaded bands show the total post-fit uncertainty in the background.



(a)



(b)

Figure 8: Distributions of the $m_{W^\pm h}$ observable in the control regions of the merged (a) $q\bar{q}b\bar{b}$ and (b) $\ell^\pm v b\bar{b}$ event categories. The term ‘Others’ summarises events from $tHj b$, tWh , $t\bar{t}t$, and SM Vh production. The distributions are presented after a background-only maximum-likelihood fit to data. The lower panels show the ratio of the observed to the estimated SM background. The shaded bands show the total post-fit uncertainty in the background.

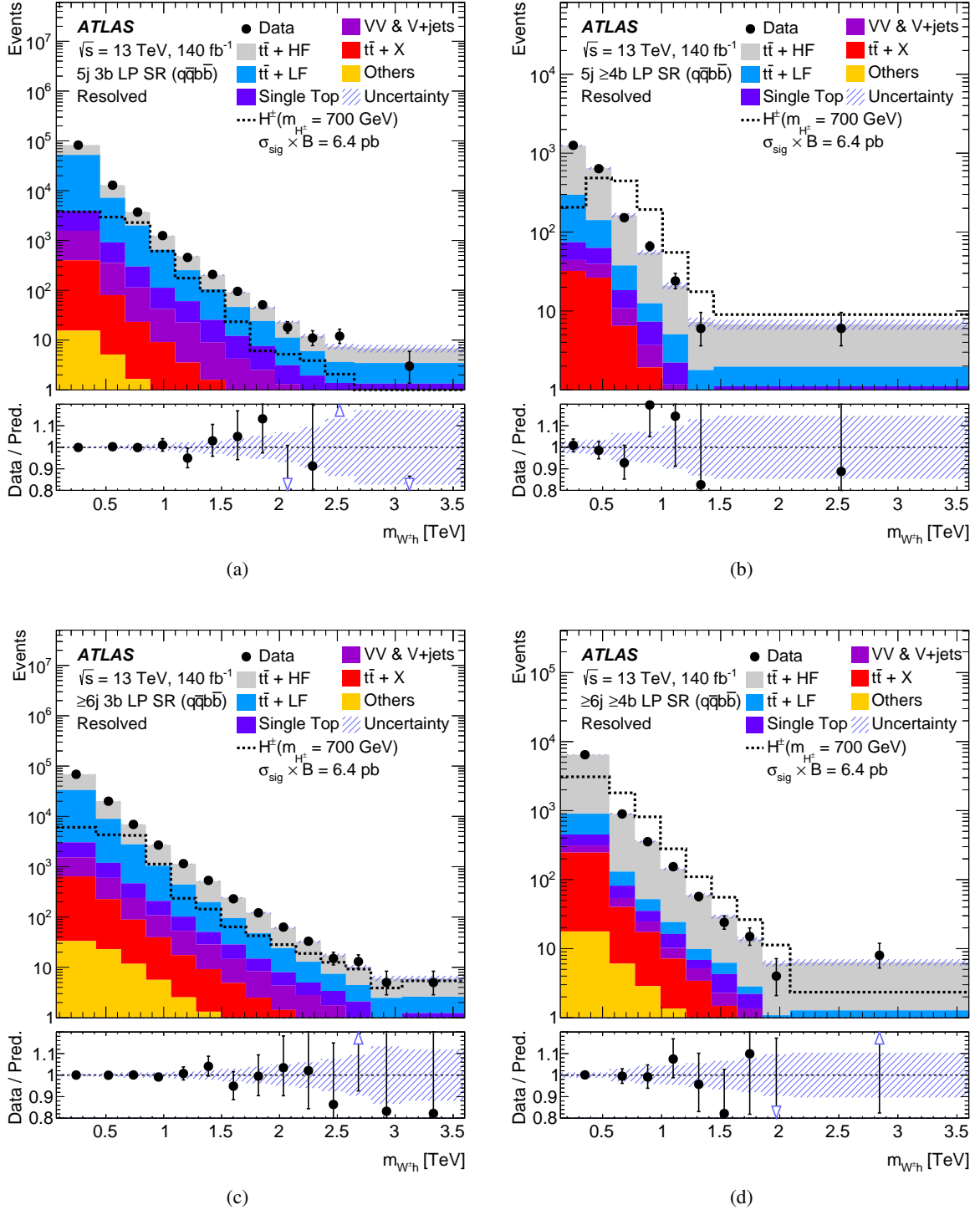


Figure 9: The $m_{W^{\pm}h}$ distributions in the low-purity signal regions (LP SR) of the resolved $q\bar{q}b\bar{b}$ event categories. The term ‘Others’ summarises events from $tHj b$, tWh , $t\bar{t}t\bar{t}$, and SM Vh production. The background prediction is shown after a background-only maximum-likelihood fit to data. The lower panels show the ratio of the observed to the estimated SM background. The shaded bands show the total post-fit uncertainty in the background. The expected signal contribution assuming $m_{H^{\pm}} = 700\text{ GeV}$, normalised to a cross-section times branching ratio ($\sigma_{\text{sig}} \times B$) of 6.4 pb , is shown as a dashed histogram.

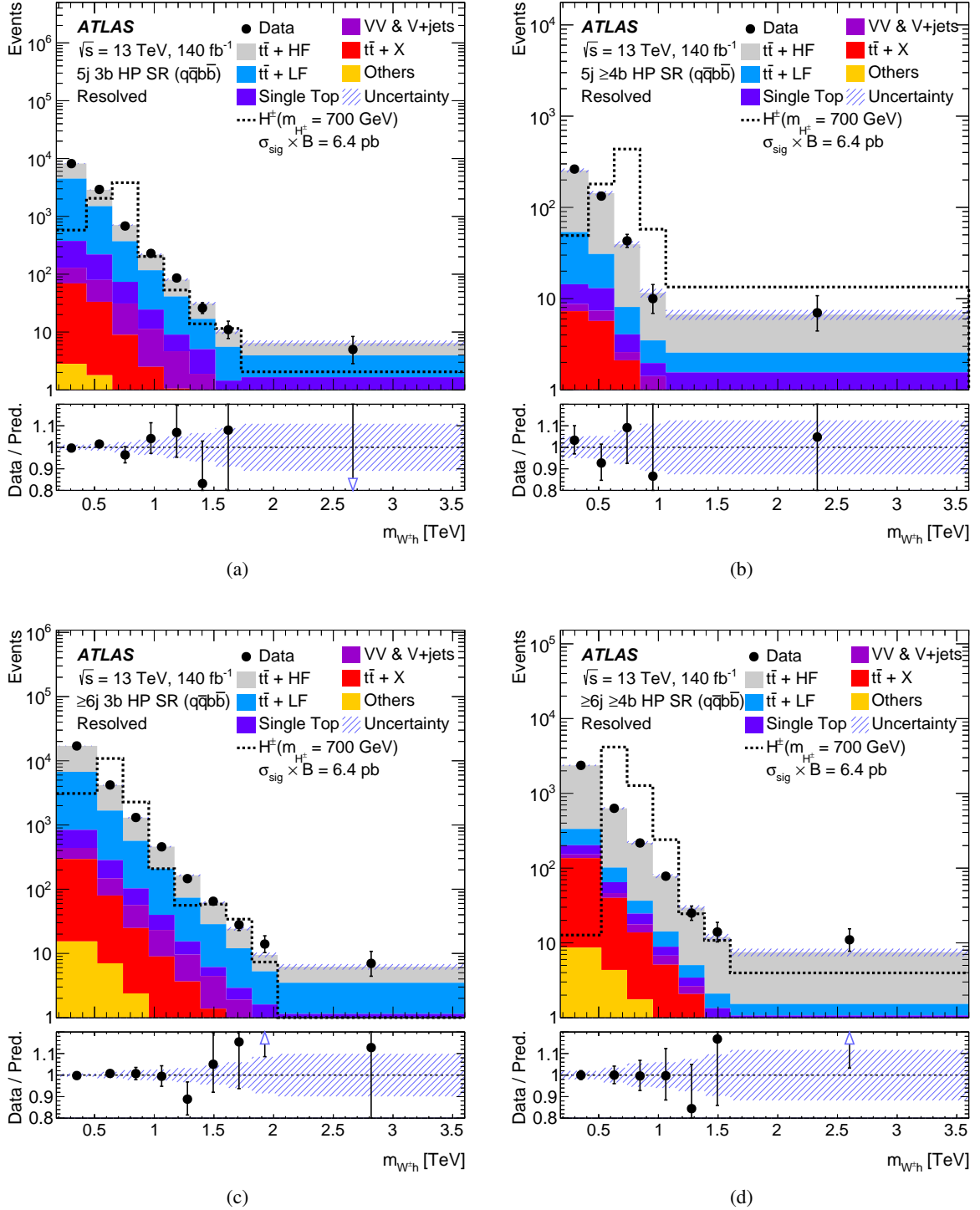


Figure 10: The $m_{W^{\pm}h}$ distributions in the high-purity signal regions (HP SR) of the resolved $q\bar{q}b\bar{b}$ event categories. The term ‘Others’ summarises events from $tHjb$, tWh , $t\bar{t}t\bar{t}$, and SM Vh production. The background prediction is shown after a background-only maximum-likelihood fit to data. The lower panels show the ratio of the observed to the estimated SM background. The shaded bands show the total post-fit uncertainty in the background. The expected signal contribution assuming $m_{H^{\pm}} = 700 \text{ GeV}$, normalised to a cross-section times branching ratio ($\sigma_{\text{sig}} \times B$) of 6.4 pb, is shown as a dashed histogram.

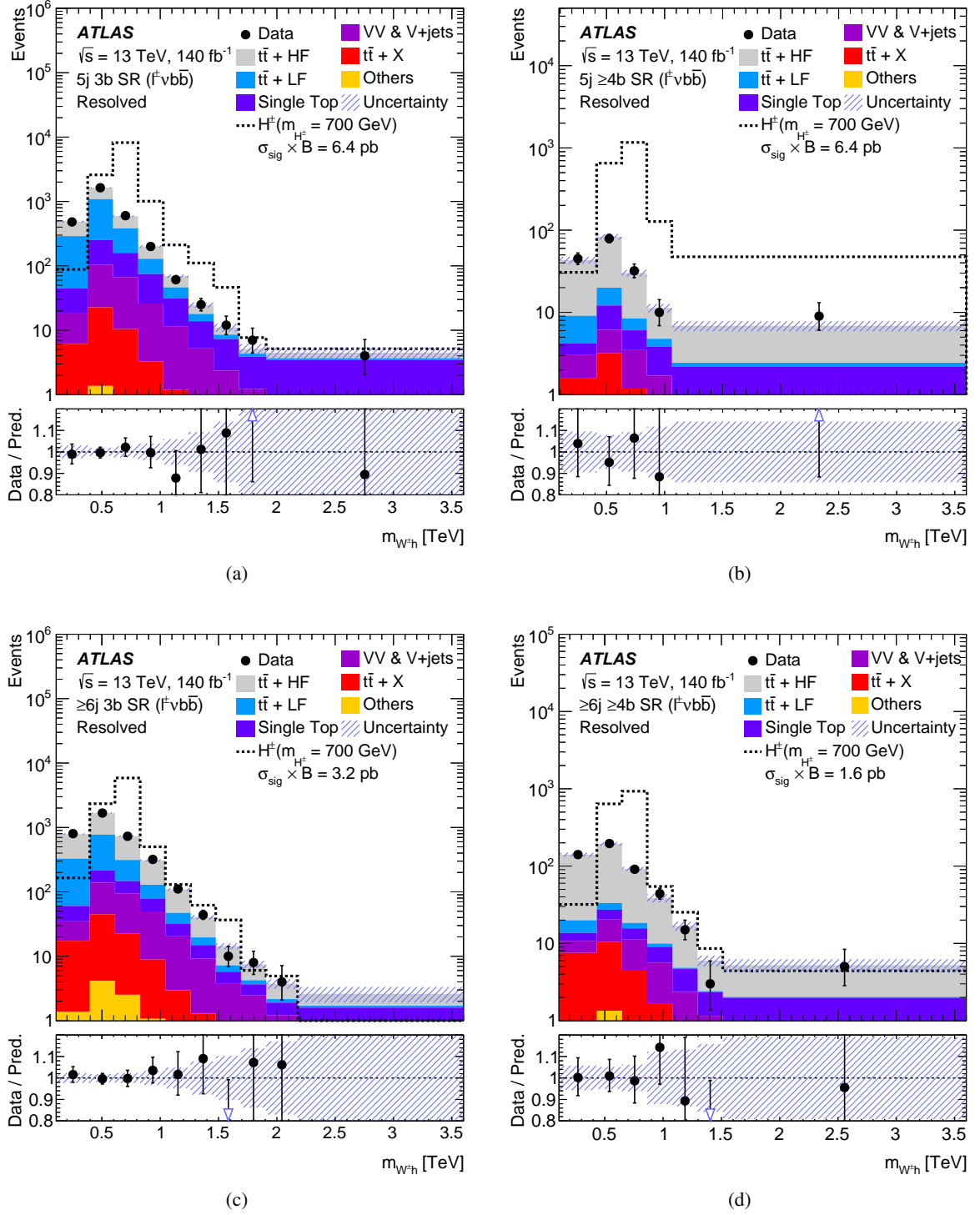


Figure 11: The $m_{W^{\pm}h}$ distributions in the signal regions of the resolved $\ell^{\pm} \nu b \bar{b}$ event categories. The term ‘Others’ summarises events from $tHjb$, tWh , $t\bar{t}\bar{t}$, and SM Vh production. The background prediction is shown after a background-only maximum-likelihood fit to data. The lower panels show the ratio of the observed to the estimated SM background. The shaded bands show the total post-fit uncertainty in the background. The expected signal contribution assuming $m_{H^{\pm}} = 700$ GeV, normalised to different values of the cross-section times branching ratio ($\sigma_{\text{sig}} \times B$), is shown as a dashed histogram.

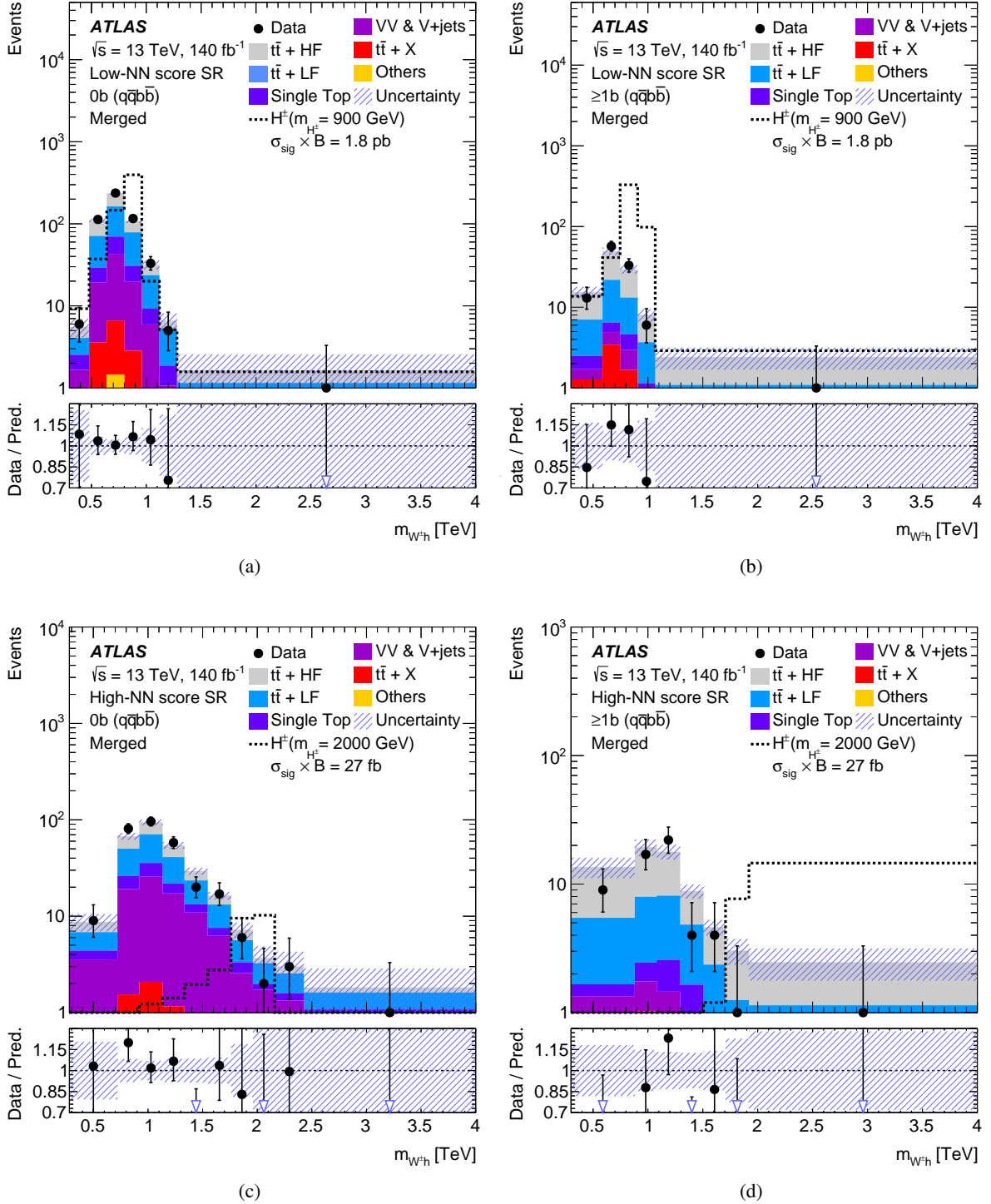


Figure 12: The $m_{W^{\pm}h}$ distributions in the low-NN-score SRs (top) and high-NN-score SRs (bottom) of the merged $q\bar{q}b\bar{b}$ event categories. The term ‘Others’ summarises events from $tHjb$, tWh , $t\bar{t}t\bar{t}$, and SM Vh production. The background prediction is shown after a background-only maximum-likelihood fit to data. The lower panels show the ratio of the observed to the estimated SM background. The shaded bands show the total post-fit uncertainty in the background. The expected signal contributions assuming $m_{H^{\pm}} = 900 \text{ GeV}$ and $m_{H^{\pm}} = 2000 \text{ GeV}$, normalised to cross-section times branching ratio ($\sigma_{\text{sig}} \times B$) values of 1.8 pb and 27 fb respectively, are shown as dashed histograms.

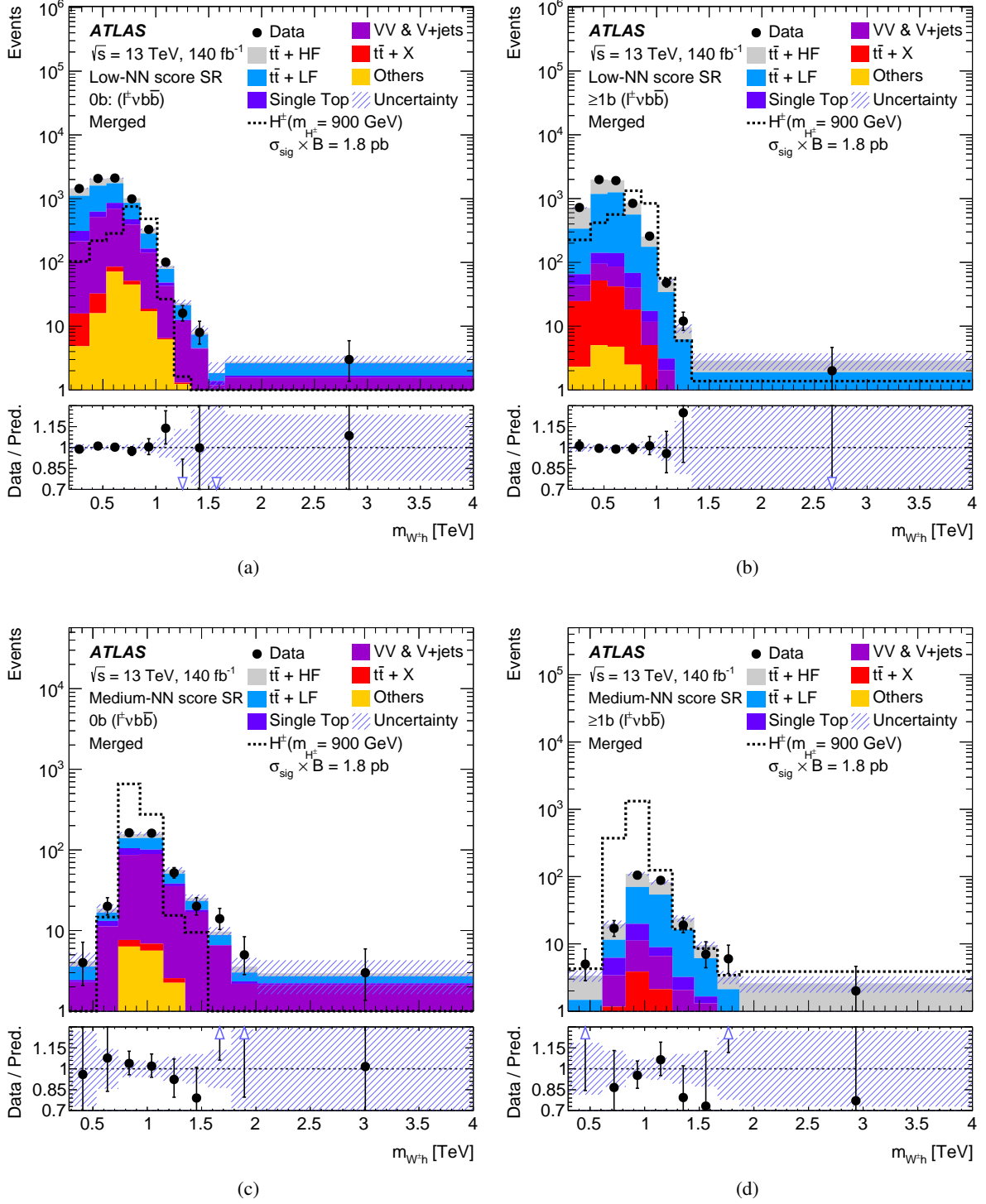


Figure 13: The $m_{W \neq h}$ distributions in the low-NN-score SRs (top) and medium-NN-score SRs (bottom) of the merged $\ell^\pm \nu b \bar{b}$ event categories. The term ‘Others’ summarises events from $tHjb$, tWh , $t\bar{t}i\bar{i}$, and SM Vh production. The background prediction is shown after a background-only maximum-likelihood fit to data. The lower panels show the ratio of the observed to the estimated SM background. The shaded bands show the total post-fit uncertainty in the background. The expected signal contribution assuming $m_{H^\pm} = 900 \text{ GeV}$, normalised to a cross-section times branching ratio ($\sigma_{\text{sig}} \times B$) values of 1.8 pb , is shown as a dashed histogram.

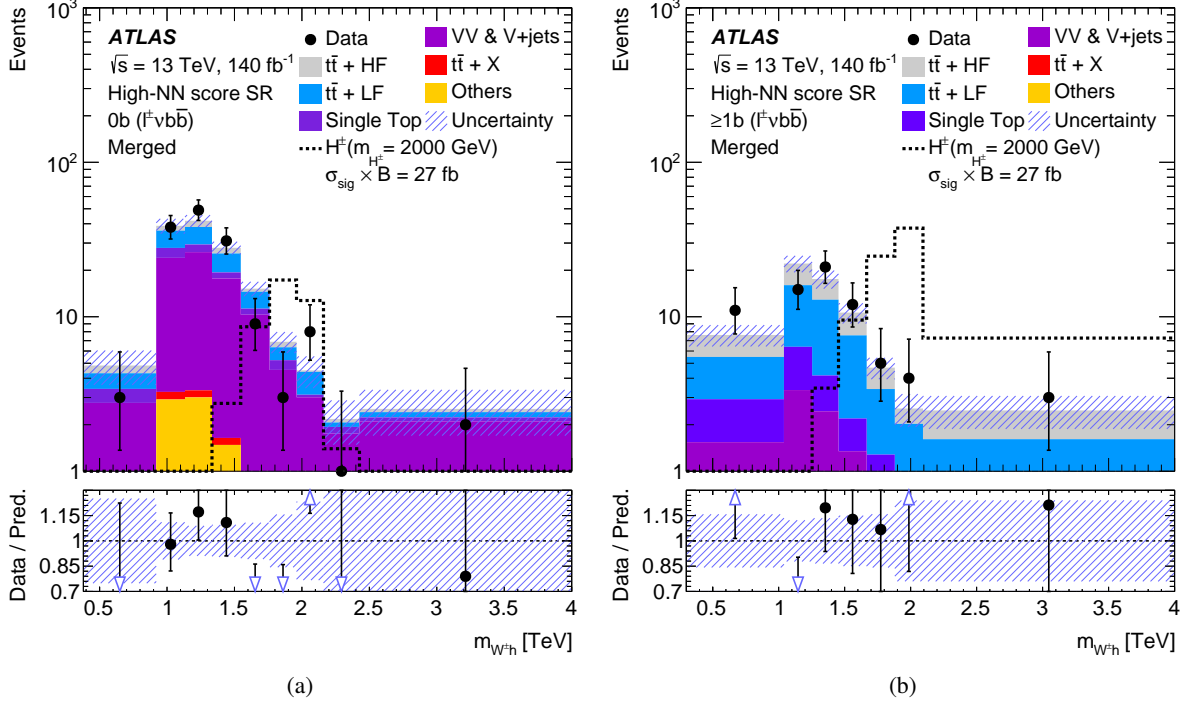


Figure 14: The $m_{W^{\pm}h}$ distributions in the high-NN-score SRs of the merged $\ell^{\pm}\nu b\bar{b}$ event categories. The term ‘Others’ summarises events from $tHjb$, tWh , $t\bar{t}\bar{t}$, and SM Vh production. The background prediction is shown after a background-only maximum-likelihood fit to data. The lower panels show the ratio of the observed to the estimated SM background. The shaded bands show the total post-fit uncertainty in the background. The expected signal contribution assuming $m_{H^{\pm}} = 2000$ GeV, normalised to a cross-section times branching ratio ($\sigma_{\text{sig}} \times B$) of 27 fb, is shown as a dashed histogram.

This search probes for charged Higgs bosons in the mass range from 250 GeV to 3 TeV. In total, 17 signal mass hypotheses are tested. The resolved and merged analyses show complementary sensitivities to different charged Higgs boson mass regions. The resolved analysis is more sensitive for masses up to (and including) 900 GeV, while the merged analysis dominates at higher masses. Instead of performing a statistical combination of the two analyses, the analysis with the more stringent expected upper limit on the production cross-section times branching ratio is used at each mass point.

The 95% CL upper limits on the production cross-section times branching ratio for a charged Higgs boson decaying via $H^{\pm} \rightarrow W^{\pm}h$ are presented in Figure 15 as a function of the charged Higgs boson mass. The observed limits range from 2.8 pb for a mass value of 250 GeV to 1.2 fb for a mass of 3 TeV. The limits on the signal hypotheses with $m_{H^{\pm}} \geq 0.7$ TeV were also calculated using pseudo-experiments to validate the asymptotic approximation approach in a phase-space region strongly limited by a low number of data events. It was found that the asymptotic approximation is valid within 10%.

The expected exclusion limits are dominated by the $\ell^{\pm}\nu b\bar{b}$ channel except for the 250 GeV mass hypothesis, where the $q\bar{q}b\bar{b}$ channel is stronger. In the resolved analysis, the $\ell^{\pm}\nu b\bar{b}$ channel provides a cross-section times branching ratio limit that is 1.1 times lower at 350 GeV and 2.5 times lower at 800 GeV. In the merged analysis, the $\ell^{\pm}\nu b\bar{b}$ channel provides a limit that is 1.4 times lower at 900 GeV and 2.5 times lower at 3000 GeV.

Table 6: Event yields in the various signal and control regions of the (a) resolved and (b) merged analyses after a background-only fit to data. The quoted uncertainties are the total post-fit uncertainties. The uncertainties in the individual background predictions are larger than the total background uncertainty due to correlations resulting from the fit to data.

(a) Post-fit event yields of the resolved event categories

	$t\bar{t}$ + LF	$t\bar{t}$ + HF	Single top	VV & V + jets	$t\bar{t}$ + X	Others	Total bkg.	Data
$5j3b$ CR ($q\bar{q}b\bar{b}$)	9000 ± 500	8400 ± 600	770 ± 190	500 ± 150	64 ± 11	5.0 ± 0.6	18720 ± 150	18737
$5j \geq 4b$ CR ($q\bar{q}b\bar{b}$)	470 ± 80	3640 ± 130	160 ± 50	69 ± 20	100 ± 15	5.3 ± 0.6	4450 ± 70	4449
$\geq 6j3b$ CR ($q\bar{q}b\bar{b}$)	2200 ± 400	4100 ± 400	250 ± 80	180 ± 60	41 ± 8	6.0 ± 2.4	6790 ± 90	6788
$\geq 6j \geq 4b$ CR ($q\bar{q}b\bar{b}$)	330 ± 110	5140 ± 150	160 ± 60	87 ± 25	147 ± 18	22 ± 9	5890 ± 80	5889
$5j3b$ low-purity SR ($q\bar{q}b\bar{b}$)	57000 ± 4000	38000 ± 4000	3300 ± 900	1600 ± 500	500 ± 80	23.4 ± 1.4	100970 ± 330	100957
$5j \geq 4b$ low-purity SR ($q\bar{q}b\bar{b}$)	330 ± 60	1650 ± 90	67 ± 24	32 ± 9	66 ± 10	2.44 ± 0.22	2140 ± 50	2145
$\geq 6j3b$ low-purity SR ($q\bar{q}b\bar{b}$)	42000 ± 6000	53000 ± 6000	2500 ± 700	1600 ± 500	960 ± 160	79 ± 31	100500 ± 500	100485
$\geq 6j \geq 4b$ low-purity SR ($q\bar{q}b\bar{b}$)	530 ± 140	6830 ± 200	190 ± 80	94 ± 27	290 ± 40	29 ± 13	7960 ± 90	7963
$5j3b$ high-purity SR ($q\bar{q}b\bar{b}$)	5800 ± 700	5600 ± 700	450 ± 160	140 ± 40	110 ± 19	5.53 ± 0.29	12130 ± 140	12130
$5j \geq 4b$ high-purity SR ($q\bar{q}b\bar{b}$)	64 ± 16	357 ± 28	14 ± 11	4.5 ± 1.7	16.0 ± 2.9	0.58 ± 0.16	456 ± 21	456
$\geq 6j3b$ high-purity SR ($q\bar{q}b\bar{b}$)	8000 ± 1400	14000 ± 1400	610 ± 220	270 ± 80	390 ± 60	26 ± 10	23260 ± 160	23258
$\geq 6j \geq 4b$ high-purity SR ($q\bar{q}b\bar{b}$)	190 ± 60	2850 ± 100	80 ± 40	30 ± 10	182 ± 27	16 ± 7	3340 ± 60	3343
$5j3b$ CR ($\ell^\pm v b \bar{b}$)	820 ± 80	1310 ± 130	230 ± 90	220 ± 70	14 ± 4	1.22 ± 0.16	2600 ± 50	2599
$5j \geq 4b$ CR ($\ell^\pm v b \bar{b}$)	5.2 ± 2.2	34 ± 6	3.0 ± 1.9	5.0 ± 1.7	0.60 ± 0.15	0.05 ± 0.05	48 ± 6	49
$\geq 6j3b$ CR ($\ell^\pm v b \bar{b}$)	710 ± 120	1870 ± 180	140 ± 70	240 ± 70	33 ± 7	5.0 ± 2.2	3000 ± 50	2991
$\geq 6j \geq 4b$ CR ($\ell^\pm v b \bar{b}$)	6.2 ± 2.7	121 ± 14	7 ± 5	8.9 ± 2.7	2.5 ± 0.4	0.68 ± 0.32	146 ± 12	147
$5j3b$ SR ($\ell^\pm v b \bar{b}$)	1380 ± 140	1060 ± 180	350 ± 80	190 ± 60	42 ± 8	2.72 ± 0.24	3030 ± 50	3026
$5j \geq 4b$ SR ($\ell^\pm v b \bar{b}$)	16 ± 4	130 ± 15	13 ± 6	8.8 ± 2.7	6.2 ± 0.9	0.43 ± 0.08	175 ± 13	175
$\geq 6j3b$ SR ($\ell^\pm v b \bar{b}$)	1060 ± 170	2060 ± 220	210 ± 100	260 ± 80	89 ± 16	10 ± 4	3690 ± 60	3703
$\geq 6j \geq 4b$ SR ($\ell^\pm v b \bar{b}$)	16 ± 5	403 ± 32	23 ± 18	27 ± 8	21.7 ± 2.9	3.5 ± 1.7	494 ± 22	495

(b) Post-fit event yields of the merged event categories

	$t\bar{t}$ + LF	$t\bar{t}$ + HF	Single top	VV & V + jets	$t\bar{t}$ + X	Others	Total bkg.	Data
High- $m_h \geq 1b$ CR ($q\bar{q}b\bar{b}$)	39 ± 9	86 ± 14	5.0 ± 3.5	4.6 ± 0.8	4.0 ± 1.5	0.6 ± 0.3	139 ± 10	138
Low- $m_h \geq 1b$ CR ($q\bar{q}b\bar{b}$)	33 ± 7	82 ± 11	9 ± 5	11.4 ± 1.9	3.2 ± 0.9	0.24 ± 0.11	139 ± 9	142
High- m_h 0b CR ($q\bar{q}b\bar{b}$)	300 ± 50	202 ± 35	50 ± 30	92 ± 16	12.0 ± 2.5	0.9 ± 0.3	659 ± 22	632
Low- m_h 0b CR ($q\bar{q}b\bar{b}$)	180 ± 30	187 ± 28	70 ± 40	281 ± 42	6.4 ± 1.2	1.0 ± 0.4	724 ± 24	728
Low-NN-score 0b SR ($q\bar{q}b\bar{b}$)	203 ± 29	152 ± 24	53 ± 27	77 ± 16	11.1 ± 2.2	3.0 ± 1.2	499 ± 17	511
Low-NN-score $\geq 1b$ SR ($q\bar{q}b\bar{b}$)	32 ± 10	58 ± 11	4.6 ± 1.3	3.6 ± 1.8	6.2 ± 1.3	0.64 ± 0.20	105 ± 8	110
High-NN-score 0b SR ($q\bar{q}b\bar{b}$)	102 ± 16	68 ± 17	28 ± 17	83 ± 22	4.4 ± 0.9	1.8 ± 0.8	286 ± 14	293
High-NN-score $\geq 1b$ SR ($q\bar{q}b\bar{b}$)	21 ± 4	39 ± 7	3.5 ± 2.7	3.0 ± 0.8	2.9 ± 0.8	0.27 ± 0.08	70 ± 6	58
High- $m_h \geq 1b$ CR ($\ell^\pm v b \bar{b}$)	2230 ± 240	1870 ± 250	110 ± 40	78 ± 13	79 ± 16	7.6 ± 2.8	4380 ± 60	4414
Low- $m_h \geq 1b$ CR ($\ell^\pm v b \bar{b}$)	1840 ± 200	1860 ± 220	190 ± 60	278 ± 53	48 ± 9	5.0 ± 1.2	4220 ± 60	4202
High- m_h 0b CR ($\ell^\pm v b \bar{b}$)	2480 ± 240	1160 ± 170	420 ± 160	940 ± 240	50 ± 9	14 ± 7	5060 ± 70	5063
Low- m_h 0b CR ($\ell^\pm v b \bar{b}$)	1950 ± 250	930 ± 130	560 ± 160	3840 ± 280	23 ± 5	34 ± 17	7340 ± 80	7357
Low-NN-score 0b SR ($\ell^\pm v b \bar{b}$)	3210 ± 310	1360 ± 200	480 ± 130	1820 ± 250	50 ± 9	160 ± 80	7070 ± 80	7066
Low-NN-score $\geq 1b$ SR ($\ell^\pm v b \bar{b}$)	3120 ± 310	2260 ± 310	160 ± 50	137 ± 19	127 ± 25	15.3 ± 3.0	5810 ± 70	5785
Medium-NN-score 0b SR ($\ell^\pm v b \bar{b}$)	101 ± 28	46 ± 12	36 ± 22	230 ± 30	3.3 ± 0.7	16 ± 8	435 ± 20	442
Medium-NN-score $\geq 1b$ SR ($\ell^\pm v b \bar{b}$)	121 ± 16	92 ± 18	16 ± 8	18 ± 6	6.9 ± 1.4	1.2 ± 0.4	255 ± 14	249
High-NN-score 0b SR ($\ell^\pm v b \bar{b}$)	30 ± 12	11 ± 5	11 ± 11	82 ± 18	1.1 ± 0.2	9 ± 5	145 ± 11	144
High-NN-score $\geq 1b$ SR ($\ell^\pm v b \bar{b}$)	30 ± 13	19 ± 6	8 ± 7	8 ± 6	2.1 ± 0.3	0.62 ± 0.25	68 ± 8	71

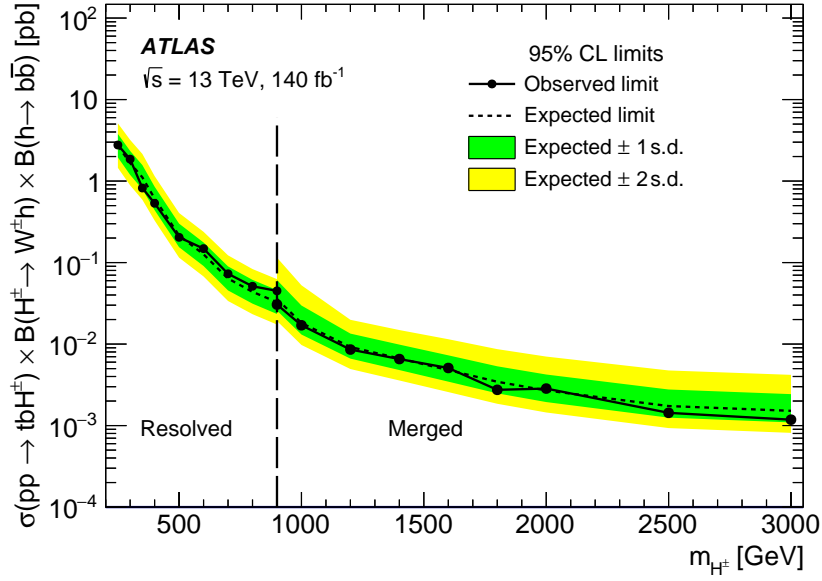


Figure 15: Upper limits at 95% CL on the product of the cross-section for $pp \rightarrow tbH^\pm$ and the branching ratio $\mathcal{B}(W^\pm h) \times \mathcal{B}(h \rightarrow b\bar{b})$ from the combined fit to all signal and control regions of the resolved and merged analyses. The bands surrounding the expected limit correspond to the ± 1 and ± 2 standard deviation (s.d.) intervals around the expected limit. The results of the resolved analysis are used up to a mass of 900 GeV and those of the merged analysis are used at higher masses.

The dominant uncertainties for low charged Higgs boson masses (e.g. $m_{H^\pm} = 0.4$ TeV) are related to the modelling of the $t\bar{t} + \text{HF}$ and $t\bar{t} + \text{LF}$ backgrounds, while at high charged Higgs boson masses (e.g. $m_{H^\pm} = 2.0$ TeV) the dominant uncertainties are related to the data statistical uncertainty. The relative impact of the dominant uncertainties on the best-fit signal-strength parameter μ , i.e. the ratio of the extracted to injected signal cross-section times branching ratio, are detailed in Table 7.

Table 7: Breakdown of the relative contributions to the uncertainty in the best-fit signal-strength parameter μ of the hypothesised production of a charged Higgs boson for two signal mass hypotheses: $m_{H^\pm} = 0.4$ TeV and $m_{H^\pm} = 2.0$ TeV. The contributions are obtained by fixing the relevant nuisance parameters to their post-fit values in the likelihood fit to data. The relative impact is determined as the square-root of the difference of the squares of the nominal uncertainty and the varied uncertainty, divided by the nominal uncertainty. The sum in quadrature of the individual components differs from the total uncertainty due to correlations between uncertainties in the different groups. The uncertainty from data statistical uncertainties is determined from fits with all nuisance parameters fixed to their post-fit values. The breakdown of uncertainties for the $m_{H^\pm} = 0.4$ TeV mass point corresponds to the resolved analysis, while for the $m_{H^\pm} = 2.0$ TeV mass point, the breakdown of uncertainties corresponds to the merged analysis. The signal cross-section times branching ratio is assumed to be 0.6 pb at 400 GeV and 2.7 fb at 2 TeV, corresponding to the expected upper limits for these two mass hypotheses.

$m_{H^\pm} = 0.4$ TeV		$m_{H^\pm} = 2$ TeV	
Category	Relative contribution	Category	Relative contribution
Modelling uncertainties			
$t\bar{t}$ + HF modelling	74%	Extrapolation/migration	25%
$t\bar{t}$ + LF modelling	34%	$t\bar{t}$ + LF modelling	17%
Extrapolation/migration	20%	Non- $t\bar{t}$ modelling	16%
Non- $t\bar{t}$ modelling	9%	MC statistical uncertainty	12%
Signal modelling	5%	$t\bar{t}$ + HF normalisation	10%
$t\bar{t}$ + HF normalisation	5%	Non-closure	7%
Non-closure	5%	$t\bar{t}$ + LF normalisation	6%
MC statistical uncertainty	4%	$t\bar{t}$ + HF modelling	6%
		VV modelling	4%
		Signal modelling	3%
		VV normalisation	1%
Experimental uncertainties			
Small- R jets	15%	$h \rightarrow b\bar{b}$ tagging	12%
Flavour tagging	14%	Larger- R -jets	4%
Pile-up	7%	Small- R jets	4%
Electrons	4%	Flavour tagging	3%
Luminosity	3%	Pile-up	1%
Muons	1%	Electrons	1%
Missing transverse momentum	<0.1%	Missing transverse momentum	0.1%
		Muons	<0.1%
		Luminosity	<0.1%
Total systematic uncertainty	93%	Total systematic uncertainty	49%
Data statistical uncertainty	37%	Data statistical uncertainty	87%

9 Conclusion

A search for a heavy charged Higgs boson produced in association with a top quark and a bottom quark and decaying into a W boson and a 125 GeV Higgs boson is performed in the mass range from 250 GeV to 3000 GeV. This search uses pp collision data at $\sqrt{s} = 13$ TeV collected with the ATLAS detector at the LHC from 2015 to 2018, corresponding to an integrated luminosity of 140 fb^{-1} .

Two different analysis strategies are applied to ensure high sensitivity to both low- and high-mass charged Higgs bosons. The mass range up to 900 GeV is probed in final states with exactly one charged electron or muon, missing transverse momentum and at least five small- R jets. Events are classified based on kinematic requirements and the multiplicity of b -tagged jets per event. Finally, two sets of boosted decision trees are used to reconstruct the four-momentum of the charged Higgs boson candidate. The mass range above 900 GeV is probed in final states with exactly one charged electron or muon, missing transverse momentum and at least one large- R jet. A recently developed boosted $h \rightarrow b\bar{b}$ tagging technique is used to identify the decay of boosted Higgs bosons and sets of neural networks are employed to further separate between the signal and the background processes.

Both analyses search for a localised excess in the distribution of the reconstructed invariant mass of the charged Higgs boson. Neither analyses observe a significant excess of events above the SM prediction and upper limits at 95% CL are set on the production cross-section times branching ratio. The upper limits range from 2.8 pb for $m_{H^\pm} = 250$ GeV to 1.2 fb for $m_{H^\pm} = 3000$ GeV.

This search is performed for the first time at the LHC, complementing previous searches for $H^\pm \rightarrow tb$ and $H^\pm \rightarrow \tau^\pm \nu$ decays by the ATLAS and CMS collaborations. While the $H^\pm \rightarrow W^\pm h$ decay mode is predicted to be subdominant in common two-Higgs-doublet models, its branching ratio is predicted to be significant in other extended scalar sector models such as the Georgi-Machacek model, or the three-Higgs-doublet model.

Acknowledgements

We thank CERN for the very successful operation of the LHC and its injectors, as well as the support staff at CERN and at our institutions worldwide without whom ATLAS could not be operated efficiently.

The crucial computing support from all WLCG partners is acknowledged gratefully, in particular from CERN, the ATLAS Tier-1 facilities at TRIUMF/SFU (Canada), NDGF (Denmark, Norway, Sweden), CC-IN2P3 (France), KIT/GridKA (Germany), INFN-CNAF (Italy), NL-T1 (Netherlands), PIC (Spain), RAL (UK) and BNL (USA), the Tier-2 facilities worldwide and large non-WLCG resource providers. Major contributors of computing resources are listed in Ref. [138].

We gratefully acknowledge the support of ANPCyT, Argentina; YerPhI, Armenia; ARC, Australia; BMWFW and FWF, Austria; ANAS, Azerbaijan; CNPq and FAPESP, Brazil; NSERC, NRC and CFI, Canada; CERN; ANID, Chile; CAS, MOST and NSFC, China; Minciencias, Colombia; MEYS CR, Czech Republic; DNRF and DNSRC, Denmark; IN2P3-CNRS and CEA-DRF/IRFU, France; SRNSFG, Georgia; BMBF, HGF and MPG, Germany; GSRI, Greece; RGC and Hong Kong SAR, China; ICHEP and Academy of Sciences and Humanities, Israel; INFN, Italy; MEXT and JSPS, Japan; CNRST, Morocco; NWO, Netherlands; RCN, Norway; MNiSW, Poland; FCT, Portugal; MNE/IFA, Romania; MSTDI, Serbia; MSSR, Slovakia; ARIS and MVZI, Slovenia; DSI/NRF, South Africa; MICIU/AEI, Spain; SRC and Wallenberg Foundation,

Sweden; SERI, SNSF and Cantons of Bern and Geneva, Switzerland; NSTC, Taipei; TENMAK, Türkiye; STFC/UKRI, United Kingdom; DOE and NSF, United States of America.

Individual groups and members have received support from BCKDF, CANARIE, CRC and DRAC, Canada; CERN-CZ, FORTE and PRIMUS, Czech Republic; COST, ERC, ERDF, Horizon 2020, ICSC-NextGenerationEU and Marie Skłodowska-Curie Actions, European Union; Investissements d'Avenir Labex, Investissements d'Avenir Idex and ANR, France; DFG and AvH Foundation, Germany; Herakleitos, Thales and Aristeia programmes co-financed by EU-ESF and the Greek NSRF, Greece; BSF-NSF and MINERVA, Israel; NCN and NAWA, Poland; La Caixa Banking Foundation, CERCA Programme Generalitat de Catalunya and PROMETEO and GenT Programmes Generalitat Valenciana, Spain; Göran Gustafssons Stiftelse, Sweden; The Royal Society and Leverhulme Trust, United Kingdom.

In addition, individual members wish to acknowledge support from Armenia: Yerevan Physics Institute (FAPERJ); CERN: European Organization for Nuclear Research (CERN DOCT); Chile: Agencia Nacional de Investigación y Desarrollo (FONDECYT 1230812, FONDECYT 1230987, FONDECYT 1240864); China: Chinese Ministry of Science and Technology (MOST-2023YFA1605700), National Natural Science Foundation of China (NSFC - 12175119, NSFC 12275265, NSFC-12075060); Czech Republic: Czech Science Foundation (GACR - 24-11373S), Ministry of Education Youth and Sports (FORTE CZ.02.01.01/00/22_008/0004632), PRIMUS Research Programme (PRIMUS/21/SCI/017); EU: H2020 European Research Council (ERC - 101002463); European Union: European Research Council (ERC - 948254, ERC 101089007), European Union, Future Artificial Intelligence Research (FAIR-NextGenerationEU PE00000013), Italian Center for High Performance Computing, Big Data and Quantum Computing (ICSC, NextGenerationEU); France: Agence Nationale de la Recherche (ANR-20-CE31-0013, ANR-21-CE31-0013, ANR-21-CE31-0022, ANR-22-EDIR-0002); Germany: Baden-Württemberg Stiftung (BW Stiftung-Postdoc Eliteprogramme), Deutsche Forschungsgemeinschaft (DFG - 469666862, DFG - CR 312/5-2); Italy: Istituto Nazionale di Fisica Nucleare (ICSC, NextGenerationEU), Ministero dell'Università e della Ricerca (PRIN - 20223N7F8K - PNRR M4.C2.1.1); Japan: Japan Society for the Promotion of Science (JSPS KAKENHI JP22H01227, JSPS KAKENHI JP22H04944, JSPS KAKENHI JP22KK0227, JSPS KAKENHI JP23KK0245); Norway: Research Council of Norway (RCN-314472); Poland: Ministry of Science and Higher Education (IDUB AGH, POB8, D4 no 9722), Polish National Agency for Academic Exchange (PPN/PPO/2020/1/00002/U/00001), Polish National Science Centre (NCN 2021/42/E/ST2/00350, NCN OPUS 2023/51/B/ST2/02507, NCN OPUS nr 2022/47/B/ST2/03059, NCN UMO-2019/34/E/ST2/00393, NCN & H2020 MSCA 945339, UMO-2020/37/B/ST2/01043, UMO-2021/40/C/ST2/00187, UMO-2022/47/O/ST2/00148, UMO-2023/49/B/ST2/04085, UMO-2023/51/B/ST2/00920); Spain: Generalitat Valenciana (Artemisa, FEDER, IDIFEDER/2018/048), Ministry of Science and Innovation (MCIN & NextGenEU PCI2022-135018-2, MICIN & FEDER PID2021-125273NB, RYC2019-028510-I, RYC2020-030254-I, RYC2021-031273-I, RYC2022-038164-I); Sweden: Carl Trygger Foundation (Carl Trygger Foundation CTS 22:2312), Swedish Research Council (Swedish Research Council 2023-04654, VR 2018-00482, VR 2022-03845, VR 2022-04683, VR 2023-03403, VR grant 2021-03651), Knut and Alice Wallenberg Foundation (KAW 2018.0458, KAW 2019.0447, KAW 2022.0358); Switzerland: Swiss National Science Foundation (SNSF - PCEFP2_194658); United Kingdom: Leverhulme Trust (Leverhulme Trust RPG-2020-004), Royal Society (NIF-R1-231091); United States of America: U.S. Department of Energy (ECA DE-AC02-76SF00515), Neubauer Family Foundation.

References

- [1] ATLAS Collaboration, *Observation of a new particle in the search for the Standard Model Higgs boson with the ATLAS detector at the LHC*, *Phys. Lett. B* **716** (2012) 1, arXiv: [1207.7214 \[hep-ex\]](#).
- [2] CMS Collaboration, *Observation of a new boson at a mass of 125 GeV with the CMS experiment at the LHC*, *Phys. Lett. B* **716** (2012) 30, arXiv: [1207.7235 \[hep-ex\]](#).
- [3] G. C. Branco et al., *Theory and phenomenology of two-Higgs-doublet models*, *Phys. Rept.* **516** (2012) 1, arXiv: [1106.0034 \[hep-ph\]](#).
- [4] J. F. Gunion and H. E. Haber, *CP-conserving two-Higgs-doublet model: The approach to the decoupling limit*, *Phys. Rev. D* **67** (2003) 075019, arXiv: [hep-ph/0207010](#).
- [5] T. P. Cheng and L.-F. Li, *Neutrino masses, mixings, and oscillations in $SU(2) \times U(1)$ models of electroweak interactions*, *Phys. Rev. D* **22** (1980) 2860.
- [6] J. Schechter and J. W. F. Valle, *Neutrino masses in $SU(2) \otimes U(1)$ theories*, *Phys. Rev. D* **22** (1980) 2227.
- [7] G. Lazarides, Q. Shafi, and C. Wetterich, *Proton lifetime and fermion masses in an $SO(10)$ model*, *Nucl. Phys. B* **181** (1981) 287.
- [8] M. S. Chanowitz and M. Golden, *Higgs boson triplets with $M_W = M_Z \cos \theta_W$* , *Phys. Lett. B* **165** (1985) 105.
- [9] J. F. Gunion, R. Vega and J. Wudka, *Higgs triplets in the standard model*, *Phys. Rev. D* **42** (1990) 1673.
- [10] J. Bernon et al., *Scrutinizing the alignment limit in two-Higgs-doublet models: $m_h=125$ GeV*, *Phys. Rev. D* **92** (2015) 075004, arXiv: [1507.00933 \[hep-ph\]](#).
- [11] C.-Y. Chen, M. Freid and M. Sher, *Next-to-minimal two Higgs doublet model*, *Phys. Rev. D* **89** (2014) 075009, arXiv: [1312.3949 \[hep-ph\]](#).
- [12] M. Mühlleitner, M. O. P. Sampaio, R. Santos and J. Wittbrodt, *The N2HDM under Theoretical and Experimental Scrutiny*, *JHEP* **03** (2017) 094, arXiv: [1612.01309 \[hep-ph\]](#).
- [13] V. Keus, S. F. King and S. Moretti, *Three-Higgs-doublet models: symmetries, potentials and Higgs boson masses*, *JHEP* **01** (2014) 052, arXiv: [1310.8253 \[hep-ph\]](#).
- [14] H. Georgi and M. Machacek, *Doubly charged Higgs bosons*, *Nucl. Phys. B* **262** (1985) 463.
- [15] T. Biekötter, M. Chakraborti and S. Heinemeyer, ‘The ’96 GeV excess’ in the N2HDM’, *31st Rencontres de Blois on Particle Physics and Cosmology*, 2019, arXiv: [1910.06858 \[hep-ph\]](#).
- [16] R. Boto, J. C. Romão and J. P. Silva, *Current bounds on the type-Z Z3 three-Higgs-doublet model*, *Phys. Rev. D* **104** (2021) 095006, arXiv: [2106.11977 \[hep-ph\]](#).
- [17] N. Ghosh, S. Ghosh and I. Saha, *Charged Higgs boson searches in the Georgi-Machacek model at the LHC*, *Phys. Rev. D* **101** (2020) 015029, arXiv: [1908.00396 \[hep-ph\]](#).

- [18] V. Keus, S. F. King, S. Moretti and K. Yagyu, *CP Violating Two-Higgs-Doublet Model: Constraints and LHC Predictions*, **JHEP** **04** (2016) 048, arXiv: [1510.04028 \[hep-ph\]](#).
- [19] ATLAS Collaboration, *Search for charged Higgs bosons decaying via $H^\pm \rightarrow \tau\nu$ in $t\bar{t}$ events using pp collision data at $\sqrt{s} = 7$ TeV with the ATLAS detector*, **JHEP** **06** (2012) 039, arXiv: [1204.2760 \[hep-ex\]](#).
- [20] ATLAS Collaboration, *Search for charged Higgs bosons through the violation of lepton universality in $t\bar{t}$ events using pp collision data at $\sqrt{s} = 7$ TeV with the ATLAS experiment*, **JHEP** **03** (2013) 076, arXiv: [1212.3572 \[hep-ex\]](#).
- [21] ATLAS Collaboration, *Search for charged Higgs bosons decaying via $H^\pm \rightarrow \tau^\pm\nu$ in fully hadronic final states using pp collision data at $\sqrt{s} = 8$ TeV with the ATLAS detector*, **JHEP** **03** (2015) 088, arXiv: [1412.6663 \[hep-ex\]](#).
- [22] CMS Collaboration, *Search for a light charged Higgs boson in top quark decays in pp collisions at $\sqrt{s} = 7$ TeV*, **JHEP** **07** (2012) 143, arXiv: [1205.5736 \[hep-ex\]](#).
- [23] CMS Collaboration, *Search for a charged Higgs boson in pp collisions at $\sqrt{s} = 8$ TeV*, **JHEP** **11** (2015) 018, arXiv: [1508.07774 \[hep-ex\]](#).
- [24] ATLAS Collaboration, *Search for charged Higgs bosons decaying via $H^\pm \rightarrow \tau^\pm\nu_\tau$ in the τ +jets and τ +lepton final states with 36 fb^{-1} of pp collision data recorded at $\sqrt{s} = 13$ TeV with the ATLAS experiment*, **JHEP** **09** (2018) 139, arXiv: [1807.07915 \[hep-ex\]](#).
- [25] ATLAS Collaboration, *Search for a light charged Higgs boson in the decay channel $H^+ \rightarrow c\bar{s}$ in $t\bar{t}$ events using pp collisions at $\sqrt{s} = 7$ TeV with the ATLAS detector*, **Eur. Phys. J. C** **73** (2013) 2465, arXiv: [1302.3694 \[hep-ex\]](#).
- [26] CMS Collaboration, *Search for a light charged Higgs boson decaying to $c\bar{s}$ in pp collisions at $\sqrt{s} = 8$ TeV*, **JHEP** **12** (2015) 178, arXiv: [1510.04252 \[hep-ex\]](#).
- [27] CMS Collaboration, *Search for a charged Higgs boson decaying to charm and bottom quarks in proton–proton collisions at $\sqrt{s} = 8$ TeV*, **JHEP** **11** (2018) 115, arXiv: [1808.06575 \[hep-ex\]](#).
- [28] ATLAS Collaboration, *Search for a light charged Higgs boson in $t \rightarrow H^\pm b$ decays, with $H^\pm \rightarrow cb$, in the lepton+jets final state in proton-proton collisions at $\sqrt{s} = 13$ TeV with the ATLAS detector*, **JHEP** **09** (2023) 004, arXiv: [2302.11739 \[hep-ex\]](#).
- [29] ATLAS Collaboration, *Search for charged Higgs bosons produced in association with a top quark and decaying via $H^\pm \rightarrow \tau\nu$ using pp collision data recorded at $\sqrt{s} = 13$ TeV by the ATLAS detector*, **Phys. Lett. B** **759** (2016) 555, arXiv: [1603.09203 \[hep-ex\]](#).
- [30] ATLAS Collaboration, *Search for charged Higgs bosons decaying into a top quark and a bottom quark at $\sqrt{s} = 13$ TeV with the ATLAS detector*, **JHEP** **06** (2021) 145, arXiv: [2102.10076 \[hep-ex\]](#).
- [31] CMS Collaboration, *Search for a charged Higgs boson decaying into top and bottom quarks in events with electrons or muons in proton–proton collisions at $\sqrt{s} = 13$ TeV*, **JHEP** **01** (2020) 096, arXiv: [1908.09206 \[hep-ex\]](#).

- [32] CMS Collaboration, *Search for charged Higgs bosons decaying into a top and a bottom quark in the all-jet final state of pp collisions at $\sqrt{s} = 13$ TeV*, *JHEP* **07** (2020) 126, arXiv: [2001.07763 \[hep-ex\]](#).
- [33] ATLAS Collaboration, *Search for a Charged Higgs Boson Produced in the Vector-Boson Fusion Mode with Decay $H^\pm \rightarrow W^\pm Z$ using pp Collisions at $\sqrt{s} = 8$ TeV with the ATLAS Experiment*, *Phys. Rev. Lett.* **114** (2015) 231801, arXiv: [1503.04233 \[hep-ex\]](#).
- [34] CMS Collaboration, *Search for charged Higgs bosons produced via vector boson fusion and decaying into a pair of W and Z bosons using pp collisions at $\sqrt{s} = 13$ TeV*, *Phys. Rev. Lett.* **119** (2017) 141802, arXiv: [1705.02942 \[hep-ex\]](#).
- [35] CMS Collaboration, *Search for charged Higgs bosons produced in vector boson fusion processes and decaying into vector boson pairs in proton–proton collisions at $\sqrt{s} = 13$ TeV*, *Eur. Phys. J. C* **81** (2021) 723, arXiv: [2104.04762 \[hep-ex\]](#).
- [36] CMS Collaboration, *A search for a doubly-charged Higgs boson in pp collisions at $\sqrt{s} = 7$ TeV*, *Eur. Phys. J. C* **72** (2012) 2189, arXiv: [1207.2666 \[hep-ex\]](#).
- [37] ATLAS Collaboration, *Search for doubly charged Higgs boson production in multi-lepton final states using 139 fb^{-1} of proton–proton collisions at $\sqrt{s} = 13$ TeV with the ATLAS detector*, *Eur. Phys. J. C* **83** (2023) 605, arXiv: [2211.07505 \[hep-ex\]](#).
- [38] ATLAS Collaboration, *Search for doubly and singly charged Higgs bosons decaying into vector bosons in multi-lepton final states with the ATLAS detector using proton–proton collisions at $\sqrt{s} = 13$ TeV*, *JHEP* **06** (2021) 146, arXiv: [2101.11961 \[hep-ex\]](#).
- [39] ATLAS Collaboration, *The ATLAS Experiment at the CERN Large Hadron Collider*, *JINST* **3** (2008) S08003.
- [40] ATLAS Collaboration, *ATLAS Insertable B-Layer: Technical Design Report*, ATLAS-TDR-19; CERN-LHCC-2010-013, 2010, URL: <https://cds.cern.ch/record/1291633>, Addendum: ATLAS-TDR-19-ADD-1; CERN-LHCC-2012-009, 2012, URL: <https://cds.cern.ch/record/1451888>.
- [41] B. Abbott et al., *Production and integration of the ATLAS Insertable B-Layer*, *JINST* **13** (2018) T05008, arXiv: [1803.00844 \[physics.ins-det\]](#).
- [42] G. Avoni et al., *The new LUCID-2 detector for luminosity measurement and monitoring in ATLAS*, *JINST* **13** (2018) P07017.
- [43] ATLAS Collaboration, *Performance of the ATLAS trigger system in 2015*, *Eur. Phys. J. C* **77** (2017) 317, arXiv: [1611.09661 \[hep-ex\]](#).
- [44] ATLAS Collaboration, *Software and computing for Run 3 of the ATLAS experiment at the LHC*, (2024), arXiv: [2404.06335 \[hep-ex\]](#).
- [45] ATLAS Collaboration, *Luminosity determination in pp collisions at $\sqrt{s} = 13$ TeV using the ATLAS detector at the LHC*, *Eur. Phys. J. C* **83** (2023) 982, arXiv: [2212.09379 \[hep-ex\]](#).
- [46] ATLAS Collaboration, *ATLAS data quality operations and performance for 2015–2018 data-taking*, *JINST* **15** (2020) P04003, arXiv: [1911.04632 \[physics.ins-det\]](#).

- [47] ATLAS Collaboration, *The ATLAS Simulation Infrastructure*, *Eur. Phys. J. C* **70** (2010) 823, arXiv: [1005.4568 \[physics.ins-det\]](#).
- [48] S. Agostinelli et al., *GEANT4 – a simulation toolkit*, *Nucl. Instrum. Meth. A* **506** (2003) 250.
- [49] ATLAS Collaboration, *The simulation principle and performance of the ATLAS fast calorimeter simulation FastCaloSim*, ATL-PHYS-PUB-2010-013, 2010, URL: <https://cds.cern.ch/record/1300517>.
- [50] J. Alwall et al., *The automated computation of tree-level and next-to-leading order differential cross sections, and their matching to parton shower simulations*, *JHEP* **07** (2014) 079, arXiv: [1405.0301 \[hep-ph\]](#).
- [51] NNPDF Collaboration, R. D. Ball et al., *Parton distributions for the LHC run II*, *JHEP* **04** (2015) 040, arXiv: [1410.8849 \[hep-ph\]](#).
- [52] T. Sjöstrand et al., *An introduction to PYTHIA 8.2*, *Comput. Phys. Commun.* **191** (2015) 159, arXiv: [1410.3012 \[hep-ph\]](#).
- [53] ATLAS Collaboration, *ATLAS Pythia 8 tunes to 7 TeV data*, ATL-PHYS-PUB-2014-021, 2014, URL: <https://cds.cern.ch/record/1966419>.
- [54] A. Alloul, N. D. Christensen, C. Degrande, C. Duhr and B. Fuks, *FeynRules 2.0 - A complete toolbox for tree-level phenomenology*, *Comput. Phys. Commun.* **185** (2014) 2250, arXiv: [1310.1921 \[hep-ph\]](#).
- [55] C. Degrande, *Automatic evaluation of UV and R2 terms for beyond the Standard Model Lagrangians: a proof-of-principle*, *Comput. Phys. Commun.* **197** (2015) 239, arXiv: [1406.3030 \[hep-ph\]](#).
- [56] S. Frixione, G. Ridolfi and P. Nason, *A positive-weight next-to-leading-order Monte Carlo for heavy flavour hadroproduction*, *JHEP* **09** (2007) 126, arXiv: [0707.3088 \[hep-ph\]](#).
- [57] P. Nason, *A new method for combining NLO QCD with shower Monte Carlo algorithms*, *JHEP* **11** (2004) 040, arXiv: [hep-ph/0409146](#).
- [58] S. Frixione, P. Nason and C. Oleari, *Matching NLO QCD computations with parton shower simulations: the POWHEG method*, *JHEP* **11** (2007) 070, arXiv: [0709.2092 \[hep-ph\]](#).
- [59] S. Alioli, P. Nason, C. Oleari and E. Re, *A general framework for implementing NLO calculations in shower Monte Carlo programs: the POWHEG BOX*, *JHEP* **06** (2010) 043, arXiv: [1002.2581 \[hep-ph\]](#).
- [60] ATLAS Collaboration, *Studies on top-quark Monte Carlo modelling for Top2016*, ATL-PHYS-PUB-2016-020, 2016, URL: <https://cds.cern.ch/record/2216168>.
- [61] S. Frixione, E. Laenen, P. Motylinski and B. R. Webber, *Angular correlations of lepton pairs from vector boson and top quark decays in Monte Carlo simulations*, *JHEP* **04** (2007) 081, arXiv: [hep-ph/0702198](#).
- [62] P. Artoisenet, R. Frederix, O. Mattelaer and R. Rietkerk, *Automatic spin-entangled decays of heavy resonances in Monte Carlo simulations*, *JHEP* **03** (2013) 015, arXiv: [1212.3460 \[hep-ph\]](#).
- [63] NNPDF Collaboration, R. D. Ball et al., *Parton distributions with LHC data*, *Nucl. Phys. B* **867** (2013) 244, arXiv: [1207.1303 \[hep-ph\]](#).

- [64] M. Beneke, P. Falgari, S. Klein and C. Schwinn, *Hadronic top-quark pair production with NNLL threshold resummation*, *Nucl. Phys. B* **855** (2012) 695, arXiv: [1109.1536 \[hep-ph\]](#).
- [65] M. Cacciari, M. Czakon, M. Mangano, A. Mitov and P. Nason, *Top-pair production at hadron colliders with next-to-next-to-leading logarithmic soft-gluon resummation*, *Phys. Lett. B* **710** (2012) 612, arXiv: [1111.5869 \[hep-ph\]](#).
- [66] P. Bärnreuther, M. Czakon and A. Mitov, *Percent-Level-Precision Physics at the Tevatron: Next-to-Next-to-Leading Order QCD Corrections to $q\bar{q} \rightarrow t\bar{t} + X$* , *Phys. Rev. Lett.* **109** (2012) 132001, arXiv: [1204.5201 \[hep-ph\]](#).
- [67] M. Czakon and A. Mitov, *NNLO corrections to top-pair production at hadron colliders: the all-fermionic scattering channels*, *JHEP* **12** (2012) 054, arXiv: [1207.0236 \[hep-ph\]](#).
- [68] M. Czakon and A. Mitov, *NNLO corrections to top pair production at hadron colliders: the quark-gluon reaction*, *JHEP* **01** (2013) 080, arXiv: [1210.6832 \[hep-ph\]](#).
- [69] M. Czakon, P. Fiedler and A. Mitov, *Total Top-Quark Pair-Production Cross Section at Hadron Colliders Through $O(\alpha_S^4)$* , *Phys. Rev. Lett.* **110** (2013) 252004, arXiv: [1303.6254 \[hep-ph\]](#).
- [70] M. Czakon and A. Mitov, *Top++: A program for the calculation of the top-pair cross-section at hadron colliders*, *Comput. Phys. Commun.* **185** (2014) 2930, arXiv: [1112.5675 \[hep-ph\]](#).
- [71] D. de Florian et al., *Handbook of LHC Higgs Cross Sections: 4. Deciphering the Nature of the Higgs Sector*, (2017), arXiv: [1610.07922 \[hep-ph\]](#).
- [72] S. Frixione, E. Laenen, P. Motylinski, C. White and B. R. Webber, *Single-top hadroproduction in association with a W boson*, *JHEP* **07** (2008) 029, arXiv: [0805.3067 \[hep-ph\]](#).
- [73] E. Bothmann et al., *Event generation with Sherpa 2.2*, *SciPost Phys.* **7** (2019) 034, arXiv: [1905.09127 \[hep-ph\]](#).
- [74] T. Gleisberg and S. Höche, *Comix, a new matrix element generator*, *JHEP* **12** (2008) 039, arXiv: [0808.3674 \[hep-ph\]](#).
- [75] F. Buccioni et al., *OpenLoops 2*, *Eur. Phys. J. C* **79** (2019) 866, arXiv: [1907.13071 \[hep-ph\]](#).
- [76] F. Cascioli, P. Maierhöfer and S. Pozzorini, *Scattering Amplitudes with Open Loops*, *Phys. Rev. Lett.* **108** (2012) 111601, arXiv: [1111.5206 \[hep-ph\]](#).
- [77] A. Denner, S. Dittmaier and L. Hofer, *COLLIER: A fortran-based complex one-loop library in extended regularizations*, *Comput. Phys. Commun.* **212** (2017) 220, arXiv: [1604.06792 \[hep-ph\]](#).
- [78] S. Höche, F. Krauss, M. Schönherr and F. Siegert, *A critical appraisal of NLO+PS matching methods*, *JHEP* **09** (2012) 049, arXiv: [1111.1220 \[hep-ph\]](#).
- [79] S. Höche, F. Krauss, M. Schönherr and F. Siegert, *QCD matrix elements + parton showers. The NLO case*, *JHEP* **04** (2013) 027, arXiv: [1207.5030 \[hep-ph\]](#).

- [80] S. Catani, F. Krauss, B. R. Webber and R. Kuhn, *QCD Matrix Elements + Parton Showers*, **JHEP** **11** (2001) 063, arXiv: [hep-ph/0109231](#).
- [81] S. Höche, F. Krauss, S. Schumann and F. Siegert, *QCD matrix elements and truncated showers*, **JHEP** **05** (2009) 053, arXiv: [0903.1219](#) [[hep-ph](#)].
- [82] S. Schumann and F. Krauss, *A parton shower algorithm based on Catani–Seymour dipole factorisation*, **JHEP** **03** (2008) 038, arXiv: [0709.1027](#) [[hep-ph](#)].
- [83] C. Anastasiou, L. Dixon, K. Melnikov and F. Petriello, *High-precision QCD at hadron colliders: Electroweak gauge boson rapidity distributions at next-to-next-to leading order*, **Phys. Rev. D** **69** (2004) 094008, arXiv: [hep-ph/0312266](#).
- [84] A. Denner, S. Dittmaier, M. Roth, and M. M. Weber, *Electroweak radiative corrections to $e^+ e^- \rightarrow \nu$ anti- ν H* , **Nucl. Phys. B** **660** (2003) 289, arXiv: [hep-ph/0302198](#).
- [85] J. Butterworth et al., *PDF4LHC recommendations for LHC Run II*, **J. Phys. G** **43** (2016) 023001, arXiv: [1510.03865](#) [[hep-ph](#)].
- [86] ATLAS Collaboration, *Measurement of the Z/γ^* boson transverse momentum distribution in pp collisions at $\sqrt{s} = 7$ TeV with the ATLAS detector*, **JHEP** **09** (2014) 145, arXiv: [1406.3660](#) [[hep-ex](#)].
- [87] R. V. Harlander, A. Kulesza, V. Theeuwes and T. Zirke, *Soft gluon resummation for gluon-induced Higgs Strahlung*, **JHEP** **11** (2014) 082, arXiv: [1410.0217](#) [[hep-ph](#)].
- [88] ATLAS Collaboration, *The Pythia 8 A3 tune description of ATLAS minimum bias and inelastic measurements incorporating the Donnachie–Landshoff diffractive model*, ATL-PHYS-PUB-2016-017, 2016, URL: <https://cds.cern.ch/record/2206965>.
- [89] D. J. Lange, *The EvtGen particle decay simulation package*, **Nucl. Instrum. Meth. A** **462** (2001) 152.
- [90] ATLAS Collaboration, *Performance of the ATLAS track reconstruction algorithms in dense environments in LHC Run 2*, **Eur. Phys. J. C** **77** (2017) 673, arXiv: [1704.07983](#) [[hep-ex](#)].
- [91] ATLAS Collaboration, *Vertex Reconstruction Performance of the ATLAS Detector at $\sqrt{s} = 13$ TeV*, ATL-PHYS-PUB-2015-026, 2015, URL: <https://cds.cern.ch/record/2037717>.
- [92] ATLAS Collaboration, *Electron and photon performance measurements with the ATLAS detector using the 2015–2017 LHC proton–proton collision data*, **JINST** **14** (2019) P12006, arXiv: [1908.00005](#) [[hep-ex](#)].
- [93] ATLAS Collaboration, *Tools for estimating fake/non-prompt lepton backgrounds with the ATLAS detector at the LHC*, **JINST** **18** (2023) T11004, arXiv: [2211.16178](#) [[hep-ex](#)].
- [94] ATLAS Collaboration, *Muon reconstruction and identification efficiency in ATLAS using the full Run 2 pp collision data set at $\sqrt{s} = 13$ TeV*, **Eur. Phys. J. C** **81** (2021) 578, arXiv: [2012.00578](#) [[hep-ex](#)].
- [95] M. Cacciari, G. P. Salam, and G. Soyez, *The anti- k_t jet clustering algorithm*, **JHEP** **04** (2008) 063, arXiv: [0802.1189](#) [[hep-ph](#)].

- [96] M. Cacciari, G. P. Salam, and G. Soyez, *FastJet user manual*, [Eur. Phys. J. C **72** \(2012\) 1896](#), arXiv: [1111.6097 \[hep-ph\]](#).
- [97] ATLAS Collaboration, *Jet reconstruction and performance using particle flow with the ATLAS Detector*, [Eur. Phys. J. C **77** \(2017\) 466](#), arXiv: [1703.10485 \[hep-ex\]](#).
- [98] ATLAS Collaboration, *Performance of pile-up mitigation techniques for jets in pp collisions at $\sqrt{s} = 8$ TeV using the ATLAS detector*, [Eur. Phys. J. C **76** \(2016\) 581](#), arXiv: [1510.03823 \[hep-ex\]](#).
- [99] ATLAS Collaboration, *Topological cell clustering in the ATLAS calorimeters and its performance in LHC Run 1*, [Eur. Phys. J. C **77** \(2017\) 490](#), arXiv: [1603.02934 \[hep-ex\]](#).
- [100] ATLAS Collaboration, *Jet energy measurement with the ATLAS detector in proton–proton collisions at $\sqrt{s} = 7$ TeV*, [Eur. Phys. J. C **73** \(2013\) 2304](#), arXiv: [1112.6426 \[hep-ex\]](#).
- [101] D. Krohn, J. Thaler and L.-T. Wang, *Jet Trimming*, [JHEP **02** \(2010\) 084](#), arXiv: [0912.1342 \[hep-ph\]](#).
- [102] S. Catani, Yu. L. Dokshitzer, M. H. Seymour, and B. R. Webber, *Longitudinally-invariant k_{\perp} clustering algorithms for hadron-hadron collisions*, [Nucl. Phys. B **406** \(1993\) 187](#).
- [103] S. D. Ellis, and D. E. Soper, *Successive combination jet algorithm for hadron collisions*, [Phys. Rev. D **48** \(1993\) 3160](#), arXiv: [hep-ph/9305266](#).
- [104] ATLAS Collaboration, *Identification of Boosted, Hadronically-Decaying W and Z Bosons in $\sqrt{s} = 13$ TeV Monte Carlo Simulations for ATLAS*, ATL-PHYS-PUB-2015-033, 2015, URL: <https://cds.cern.ch/record/2041461>.
- [105] ATLAS Collaboration, *Jet energy scale and resolution measured in proton–proton collisions at $\sqrt{s} = 13$ TeV with the ATLAS detector*, [Eur. Phys. J. C **81** \(2021\) 689](#), arXiv: [2007.02645 \[hep-ex\]](#).
- [106] ATLAS Collaboration, *In situ calibration of large-radius jet energy and mass in 13 TeV proton–proton collisions with the ATLAS detector*, [Eur. Phys. J. C **79** \(2019\) 135](#), arXiv: [1807.09477 \[hep-ex\]](#).
- [107] ATLAS Collaboration, *Variable Radius, Exclusive- k_T , and Center-of-Mass Subjet Reconstruction for Higgs($\rightarrow b\bar{b}$) Tagging in ATLAS*, ATL-PHYS-PUB-2017-010, 2017, URL: <https://cds.cern.ch/record/2268678>.
- [108] ATLAS Collaboration, *ATLAS flavour-tagging algorithms for the LHC Run 2 pp collision dataset*, [Eur. Phys. J. C **83** \(2023\) 681](#), arXiv: [2211.16345 \[physics.data-an\]](#).
- [109] ATLAS Collaboration, *Identification of boosted Higgs bosons decaying into b-quark pairs with the ATLAS detector at 13 TeV*, [Eur. Phys. J. C **79** \(2019\) 836](#), arXiv: [1906.11005 \[hep-ex\]](#).
- [110] ATLAS Collaboration, *Identification of Boosted Higgs Bosons Decaying Into $b\bar{b}$ With Neural Networks and Variable Radius Subjets in ATLAS*, ATL-PHYS-PUB-2020-019, 2020, URL: <https://cds.cern.ch/record/2724739>.
- [111] ATLAS Collaboration, *The performance of missing transverse momentum reconstruction and its significance with the ATLAS detector using 140fb^{-1} of $\sqrt{s} = 13$ TeV pp collisions*, (2024), arXiv: [2402.05858 \[hep-ex\]](#).

- [112] ATLAS Collaboration, *Performance of electron and photon triggers in ATLAS during LHC Run 2*, *Eur. Phys. J. C* **80** (2020) 47, arXiv: [1909.00761 \[hep-ex\]](#).
- [113] ATLAS Collaboration, *Performance of the ATLAS muon triggers in Run 2*, *JINST* **15** (2020) P09015, arXiv: [2004.13447 \[physics.ins-det\]](#).
- [114] ATLAS Collaboration, *A search for $t\bar{t}$ resonances using lepton-plus-jets events in proton–proton collisions at $\sqrt{s} = 8$ TeV with the ATLAS detector*, *JHEP* **08** (2015) 148, arXiv: [1505.07018 \[hep-ex\]](#).
- [115] A. Hoecker et al., *TMVA - Toolkit for Multivariate Data Analysis*, 2009, arXiv: [physics/0703039 \[physics.data-an\]](#).
- [116] F. Chollet et al., *Keras*, 2015, URL: <https://keras.io>.
- [117] D. P. Kingma, and J. Ba, *Adam: A Method for Stochastic Optimization*, 2014, arXiv: [1412.6980 \[cs.LG\]](#).
- [118] ATLAS Collaboration, *Search for heavy resonances decaying into a Z or W boson and a Higgs boson in final states with leptons and b-jets in 139fb^{-1} of pp collisions at $\sqrt{s} = 13$ TeV with the ATLAS detector*, *JHEP* **06** (2023) 016, arXiv: [2207.00230 \[hep-ex\]](#).
- [119] ATLAS Collaboration, *ATLAS b-jet identification performance and efficiency measurement with $t\bar{t}$ events in pp collisions at $\sqrt{s} = 13$ TeV*, *Eur. Phys. J. C* **79** (2019) 970, arXiv: [1907.05120 \[hep-ex\]](#).
- [120] ATLAS Collaboration, *Measurement of the c-jet mistagging efficiency in $t\bar{t}$ events using pp collision data at $\sqrt{s} = 13$ TeV collected with the ATLAS detector*, *Eur. Phys. J. C* **82** (2022) 95, arXiv: [2109.10627 \[hep-ex\]](#).
- [121] ATLAS Collaboration, *Calibration of the light-flavour jet mistagging efficiency of the b-tagging algorithms with Z+jets events using 139fb^{-1} of ATLAS proton–proton collision data at $\sqrt{s} = 13$ TeV*, *Eur. Phys. J. C* **83** (2023) 728, arXiv: [2301.06319 \[hep-ex\]](#).
- [122] ATLAS Collaboration, *Simulation-based extrapolation of b-tagging calibrations towards high transverse momenta in the ATLAS experiment*, ATL-PHYS-PUB-2021-003, 2021, URL: <https://cds.cern.ch/record/2753444>.
- [123] ATLAS Collaboration, *Efficiency corrections for a tagger for boosted $H \rightarrow b\bar{b}$ decays in pp collisions at $\sqrt{s} = 13$ TeV with the ATLAS detector*, ATL-PHYS-PUB-2021-035, 2021, URL: <https://cds.cern.ch/record/2777811>.
- [124] S. Dulat, L. A. Harland-Lang, A. D. Martin, P. Motylinski, and R. S. Thorne, *New parton distribution functions from a global analysis of quantum chromodynamics*, *Phys. Rev. D* **93** (2016) 033006, arXiv: [1506.07443 \[hep-ph\]](#).
- [125] L. A. Harland-Lang et al., *Parton distributions in the LHC era: MMHT 2014 PDFs*, *Eur. Phys. J. C* **75** (2015) 204, arXiv: [1412.3989 \[hep-ph\]](#).
- [126] J. Bellm et al., *Herwig 7.0/Herwig++ 3.0 release note*, *Eur. Phys. J. C* **76** (2016) 196, arXiv: [1512.01178 \[hep-ph\]](#).
- [127] P. Kant et al., *HatHor for single top-quark production: Updated predictions and uncertainty estimates for single top-quark production in hadronic collisions*, *Comput. Phys. Commun.* **191** (2015) 74, arXiv: [1406.4403 \[hep-ph\]](#).

- [128] S. Frixione, E. Laenen, P. Motylinski, C. White, and B. R. Webber, *Single-top hadroproduction in association with a W boson*, **JHEP** **07** (2008) 029, arXiv: [0805.3067](#) [[hep-ph](#)].
- [129] Y. Zhang et al., *QCD NLO and EW NLO corrections to $t\bar{t}H$ production with top quark decays at hadron collider*, **Phys. Lett. B** **738** (2014) 1, arXiv: [1407.1110](#) [[hep-ph](#)].
- [130] J. M. Campbell et al., *$t\bar{t}W^{+-}$ production and decay at NLO*, **JHEP** **07** (2012) 052, arXiv: [1204.5678](#) [[hep-ph](#)].
- [131] R. Frederix, D. Pagani and M. Zaro, *Large NLO corrections in $t\bar{t}W^{\pm}$ and $t\bar{t}\bar{t}$ hadroproduction from supposedly subleading EW contributions*, **JHEP** **02** (2018) 031, arXiv: [1711.02116](#) [[hep-ph](#)].
- [132] R. Frederix and S. Frixione, *Merging meets matching in MC@NLO*, **JHEP** **12** (2012) 061, arXiv: [1209.6215](#) [[hep-ph](#)].
- [133] L. Moneta, K. Cranmer, G. Schott and W. Verkerke, *The RooStats project*, **PoS ACAT2010** (2011) 057, arXiv: [1009.1003](#) [[physics.data-an](#)].
- [134] W. Verkerke and D. Kirkby, *The RooFit toolkit for data modeling*, 2003, arXiv: [physics/0306116](#) [[physics.data-an](#)].
- [135] M. Baak et al., *HistFitter software framework for statistical data analysis*, **Eur. Phys. J. C** **75** (2015) 153, arXiv: [1410.1280](#) [[hep-ex](#)].
- [136] G. Cowan, K. Cranmer, E. Gross and O. Vitells, *Asymptotic formulae for likelihood-based tests of new physics*, **Eur. Phys. J. C** **71** (2011) 1554, arXiv: [1007.1727](#) [[physics.data-an](#)], Erratum: **Eur. Phys. J. C** **73** (2013) 2501.
- [137] A. L. Read, *Presentation of search results: the CL_S technique*, **J. Phys. G** **28** (2002) 2693.
- [138] ATLAS Collaboration, *ATLAS Computing Acknowledgements*, ATL-SOFT-PUB-2023-001, 2023, URL: <https://cds.cern.ch/record/2869272>.

The ATLAS Collaboration

G. Aad ¹⁰⁴, E. Aakvaag ¹⁷, B. Abbott ¹²³, S. Abdelhameed ^{119a}, K. Abeling ⁵⁶, N.J. Abicht ⁵⁰, S.H. Abidi ³⁰, M. Aboeela ⁴⁶, A. Aboulhorma ^{36e}, H. Abramowicz ¹⁵⁵, Y. Abulaiti ¹²⁰, B.S. Acharya ^{70a,70b,m}, A. Ackermann ^{64a}, C. Adam Bourdarios ⁴, L. Adamczyk ^{87a}, S.V. Addepalli ¹⁴⁷, M.J. Addison ¹⁰³, J. Adelman ¹¹⁸, A. Adiguzel ^{22c}, T. Adye ¹³⁷, A.A. Affolder ¹³⁹, Y. Afik ⁴¹, M.N. Agaras ¹³, A. Aggarwal ¹⁰², C. Agheorghiesei ^{28c}, F. Ahmadov ^{40,ab}, S. Ahuja ⁹⁷, X. Ai ^{63e}, G. Aielli ^{77a,77b}, A. Aikot ¹⁶⁸, M. Ait Tamliah ^{36e}, B. Aitbenkikh ^{36a}, M. Akbiyik ¹⁰², T.P.A. Åkesson ¹⁰⁰, A.V. Akimov ¹⁴⁹, D. Akiyama ¹⁷³, N.N. Akolkar ²⁵, S. Aktas ^{22a}, G.L. Alberghi ^{24b}, J. Albert ¹⁷⁰, P. Albicocco ⁵⁴, G.L. Albouy ⁶¹, S. Alderweireldt ⁵³, Z.L. Alegria ¹²⁴, M. Aleksa ³⁷, I.N. Aleksandrov ⁴⁰, C. Alexa ^{28b}, T. Alexopoulos ¹⁰, F. Alfonsi ^{24b}, M. Algren ⁵⁷, M. Alhroob ¹⁷², B. Ali ¹³⁵, H.M.J. Ali ^{93,v}, S. Ali ³², S.W. Alibocus ⁹⁴, M. Aliev ^{34c}, G. Alimonti ^{72a}, W. Alkahi ⁵⁶, C. Allaire ⁶⁷, B.M.M. Allbrooke ¹⁵⁰, J.S. Allen ¹⁰³, J.F. Allen ⁵³, P.P. Allport ²¹, A. Aloisio ^{73a,73b}, F. Alonso ⁹², C. Alpigiani ¹⁴², Z.M.K. Alsolami ⁹³, A. Alvarez Fernandez ¹⁰², M. Alves Cardoso ⁵⁷, M.G. Alviggi ^{73a,73b}, M. Aly ¹⁰³, Y. Amaral Coutinho ^{84b}, A. Ambler ¹⁰⁶, C. Amelung ³⁷, M. Amerl ¹⁰³, C.G. Ames ¹¹¹, D. Amidei ¹⁰⁸, B. Amini ⁵⁵, K.J. Amirie ¹⁵⁹, A. Amirkhanov ⁴⁰, S.P. Amor Dos Santos ^{133a}, K.R. Amos ¹⁶⁸, D. Amperiadou ¹⁵⁶, S. An ⁸⁵, V. Ananiev ¹²⁸, C. Anastopoulos ¹⁴³, T. Andeen ¹¹, J.K. Anders ⁹⁴, A.C. Anderson ⁶⁰, A. Andreazza ^{72a,72b}, S. Angelidakis ⁹, A. Angerami ⁴³, A.V. Anisenkov ³⁹, A. Annovi ^{75a}, C. Antel ⁵⁷, E. Antipov ¹⁴⁹, M. Antonelli ⁵⁴, F. Anulli ^{76a}, M. Aoki ⁸⁵, T. Aoki ¹⁵⁷, M.A. Aparo ¹⁵⁰, L. Aperio Bella ⁴⁹, C. Appelt ¹⁵⁵, A. Apyan ²⁷, S.J. Arbiol Val ⁸⁸, C. Arcangeletti ⁵⁴, A.T.H. Arce ⁵², J-F. Arguin ¹¹⁰, S. Argyropoulos ¹⁵⁶, J.-H. Arling ⁴⁹, O. Arnaez ⁴, H. Arnold ¹⁴⁹, G. Artoni ^{76a,76b}, H. Asada ¹¹³, K. Asai ¹²¹, S. Asai ¹⁵⁷, N.A. Asbah ³⁷, R.A. Ashby Pickering ¹⁷², A.M. Aslam ⁹⁷, K. Assamagan ³⁰, R. Astalos ^{29a}, K.S.V. Astrand ¹⁰⁰, S. Atashi ¹⁶³, R.J. Atkin ^{34a}, H. Atmani ^{36f}, P.A. Atmasiddha ¹³¹, K. Augsten ¹³⁵, A.D. Auriol ⁴², V.A. Austrup ¹⁰³, G. Avolio ³⁷, K. Axiotis ⁵⁷, G. Azuelos ^{110,af}, D. Babal ^{29b}, H. Bachacou ¹³⁸, K. Bachas ^{156,q}, A. Bachiu ³⁵, E. Bachmann ⁵¹, M.J. Backes ^{64a}, A. Badea ⁴¹, T.M. Baer ¹⁰⁸, P. Bagnaia ^{76a,76b}, M. Bahmani ¹⁹, D. Bahner ⁵⁵, K. Bai ¹²⁶, J.T. Baines ¹³⁷, L. Baines ⁹⁶, O.K. Baker ¹⁷⁷, E. Bakos ¹⁶, D. Bakshi Gupta ⁸, L.E. Balabram Filho ^{84b}, V. Balakrishnan ¹²³, R. Balasubramanian ⁴, E.M. Baldin ³⁹, P. Balek ^{87a}, E. Ballabene ^{24b,24a}, F. Balli ¹³⁸, L.M. Baltes ^{64a}, W.K. Balunas ³³, J. Balz ¹⁰², I. Bamwidhi ^{119b}, E. Banas ⁸⁸, M. Bandieramonte ¹³², A. Bandyopadhyay ²⁵, S. Bansal ²⁵, L. Barak ¹⁵⁵, M. Barakat ⁴⁹, E.L. Barberio ¹⁰⁷, D. Barberis ^{58b,58a}, M. Barbero ¹⁰⁴, M.Z. Barel ¹¹⁷, T. Barillari ¹¹², M-S. Barisits ³⁷, T. Barklow ¹⁴⁷, P. Baron ¹²⁵, D.A. Baron Moreno ¹⁰³, A. Baroncelli ^{63a}, A.J. Barr ¹²⁹, J.D. Barr ⁹⁸, F. Barreiro ¹⁰¹, J. Barreiro Guimarães da Costa ¹⁴, M.G. Barros Teixeira ^{133a}, S. Barsov ³⁹, F. Bartels ^{64a}, R. Bartoldus ¹⁴⁷, A.E. Barton ⁹³, P. Bartos ^{29a}, A. Basan ¹⁰², M. Baselga ⁵⁰, S. Bashiri ⁸⁸, A. Bassalat ^{67,b}, M.J. Basso ^{160a}, S. Bataju ⁴⁶, R. Bate ¹⁶⁹, R.L. Bates ⁶⁰, S. Batlamous ¹⁰¹, M. Battaglia ¹³⁹, D. Battulga ¹⁹, M. Bauce ^{76a,76b}, M. Bauer ⁸⁰, P. Bauer ²⁵, L.T. Bayer ⁴⁹, L.T. Bazzano Hurrell ³¹, J.B. Beacham ¹¹², T. Beau ¹³⁰, J.Y. Beaucamp ⁹², P.H. Beauchemin ¹⁶², P. Bechtel ²⁵, H.P. Beck ^{20,p}, K. Becker ¹⁷², A.J. Beddall ⁸³, V.A. Bednyakov ⁴⁰, C.P. Bee ¹⁴⁹, L.J. Beemster ¹⁶, M. Begalli ^{84d}, M. Begel ³⁰, J.K. Behr ⁴⁹, J.F. Beirer ³⁷, F. Beisiegel ²⁵, M. Belfkir ^{119b}, G. Bella ¹⁵⁵, L. Bellagamba ^{24b}, A. Bellerive ³⁵, P. Bellos ²¹, K. Beloborodov ³⁹, D. Benchebroun ^{36a}, F. Bendebba ^{36a}, Y. Benhammou ¹⁵⁵, K.C. Benkendorfer ⁶², L. Beresford ⁴⁹, M. Beretta ⁵⁴, E. Bergeas Kuutmann ¹⁶⁶, N. Berger ⁴,

B. Bergmann ¹³⁵, J. Beringer ^{18a}, G. Bernardi ⁵, C. Bernius ¹⁴⁷, F.U. Bernlochner ²⁵,
 F. Bernon ³⁷, A. Berrocal Guardia ¹³, T. Berry ⁹⁷, P. Berta ¹³⁶, A. Berthold ⁵¹, S. Bethke ¹¹²,
 A. Betti ^{76a,76b}, A.J. Bevan ⁹⁶, N.K. Bhalla ⁵⁵, S. Bharthuar ¹¹², S. Bhatta ¹⁴⁹,
 D.S. Bhattacharya ¹⁷¹, P. Bhattarai ¹⁴⁷, Z.M. Bhatti ¹²⁰, K.D. Bhide ⁵⁵, V.S. Bhopatkar ¹²⁴,
 R.M. Bianchi ¹³², G. Bianco ^{24b,24a}, O. Biebel ¹¹¹, M. Biglietti ^{78a}, C.S. Billingsley ⁴⁶,
 Y. Bimgdi ^{36f}, M. Bindi ⁵⁶, A. Bingham ¹⁷⁶, A. Bingul ^{22b}, C. Bini ^{76a,76b}, G.A. Bird ³³,
 M. Birman ¹⁷⁴, M. Biros ¹³⁶, S. Biryukov ¹⁵⁰, T. Bisanz ⁵⁰, E. Bisceglie ^{45b,45a}, J.P. Biswal ¹³⁷,
 D. Biswas ¹⁴⁵, I. Bloch ⁴⁹, A. Blue ⁶⁰, U. Blumenschein ⁹⁶, J. Blumenthal ¹⁰²,
 V.S. Bobrovnikov ⁴⁰, M. Boehler ⁵⁵, B. Boehm ¹⁷¹, D. Bogavac ³⁷, A.G. Bogdanchikov ³⁹,
 L.S. Boggia ¹³⁰, V. Boisvert ⁹⁷, P. Bokan ³⁷, T. Bold ^{87a}, M. Bomben ⁵, M. Bona ⁹⁶,
 M. Boonekamp ¹³⁸, A.G. Borbély ⁶⁰, I.S. Bordulev ³⁹, G. Borissov ⁹³, D. Bortoletto ¹²⁹,
 D. Boscherini ^{24b}, M. Bosman ¹³, K. Bouaouda ^{36a}, N. Bouchhar ¹⁶⁸, L. Boudet ⁴,
 J. Boudreau ¹³², E.V. Bouhova-Thacker ⁹³, D. Boumediene ⁴², R. Bouquet ^{58b,58a}, A. Boveia ¹²²,
 J. Boyd ³⁷, D. Boye ³⁰, I.R. Boyko ⁴⁰, L. Bozianu ⁵⁷, J. Bracinek ²¹, N. Brahimi ⁴,
 G. Brandt ¹⁷⁶, O. Brandt ³³, B. Brau ¹⁰⁵, J.E. Brau ¹²⁶, R. Brenner ¹⁷⁴, L. Brenner ¹¹⁷,
 R. Brenner ¹⁶⁶, S. Bressler ¹⁷⁴, G. Brianti ^{79a,79b}, D. Britton ⁶⁰, D. Britzger ¹¹², I. Brock ²⁵,
 R. Brock ¹⁰⁹, G. Brooijmans ⁴³, A.J. Brooks ⁶⁹, E.M. Brooks ^{160b}, E. Brost ³⁰, L.M. Brown ¹⁷⁰,
 L.E. Bruce ⁶², T.L. Bruckler ¹²⁹, P.A. Bruckman de Renstrom ⁸⁸, B. Brüers ⁴⁹, A. Bruni ^{24b},
 G. Bruni ^{24b}, D. Brunner ^{48a,48b}, M. Bruschi ^{24b}, N. Bruscolo ^{76a,76b}, T. Buanes ¹⁷, Q. Buat ¹⁴²,
 D. Buchin ¹¹², A.G. Buckley ⁶⁰, O. Bulekov ³⁹, B.A. Bullard ¹⁴⁷, S. Burdin ⁹⁴, C.D. Burgard ⁵⁰,
 A.M. Burger ³⁷, B. Burghgrave ⁸, O. Burlayenko ⁵⁵, J. Burleson ¹⁶⁷, J.T.P. Burr ³³,
 J.C. Burzynski ¹⁴⁶, E.L. Busch ⁴³, V. Büscher ¹⁰², P.J. Bussey ⁶⁰, J.M. Butler ²⁶, C.M. Buttar ⁶⁰,
 J.M. Butterworth ⁹⁸, W. Buttinger ¹³⁷, C.J. Buxo Vazquez ¹⁰⁹, A.R. Buzykaev ⁴⁰,
 S. Cabrera Urbán ¹⁶⁸, L. Cadamuro ⁶⁷, D. Caforio ⁵⁹, H. Cai ¹³², Y. Cai ^{24b,114c,24a}, Y. Cai ^{114a},
 V.M.M. Cairo ³⁷, O. Cakir ^{3a}, N. Calace ³⁷, P. Calafiura ^{18a}, G. Calderini ¹³⁰, P. Calfayan ³⁵,
 G. Callea ⁶⁰, L.P. Caloba ^{84b}, D. Calvet ⁴², S. Calvet ⁴², R. Camacho Toro ¹³⁰, S. Camarda ³⁷,
 D. Camarero Munoz ²⁷, P. Camarri ^{77a,77b}, M.T. Camerlingo ^{73a,73b}, D. Cameron ³⁷,
 C. Camincher ¹⁷⁰, M. Campanelli ⁹⁸, A. Camplani ⁴⁴, V. Canale ^{73a,73b}, A.C. Canbay ^{3a},
 E. Canonero ⁹⁷, J. Cantero ¹⁶⁸, Y. Cao ¹⁶⁷, F. Capocasa ²⁷, M. Capua ^{45b,45a}, A. Carbone ^{72a,72b},
 R. Cardarelli ^{77a}, J.C.J. Cardenas ⁸, M.P. Cardiff ²⁷, G. Carducci ^{45b,45a}, T. Carli ³⁷,
 G. Carlino ^{73a}, J.I. Carlotto ¹³, B.T. Carlson ^{132,r}, E.M. Carlson ¹⁷⁰, J. Carmignani ⁹⁴,
 L. Carminati ^{72a,72b}, A. Carnelli ¹³⁸, M. Carnesale ³⁷, S. Caron ¹¹⁶, E. Carquin ^{140f},
 I.B. Carr ¹⁰⁷, S. Carrá ^{72a}, G. Carratta ^{24b,24a}, A.M. Carroll ¹²⁶, M.P. Casado ^{13,h}, M. Caspar ⁴⁹,
 F.L. Castillo ⁴, L. Castillo Garcia ¹³, V. Castillo Gimenez ¹⁶⁸, N.F. Castro ^{133a,133e},
 A. Catinaccio ³⁷, J.R. Catmore ¹²⁸, T. Cavaliere ⁴, V. Cavaliere ³⁰, L.J. Caviedes Betancourt ^{23b},
 Y.C. Cekmecelioglu ⁴⁹, E. Celebi ⁸³, S. Cella ³⁷, V. Cepaitis ⁵⁷, K. Cerny ¹²⁵,
 A.S. Cerqueira ^{84a}, A. Cerri ^{75a,75b}, L. Cerrito ^{77a,77b}, F. Cerutti ^{18a}, B. Cervato ¹⁴⁵,
 A. Cervelli ^{24b}, G. Cesarini ⁵⁴, S.A. Cetin ⁸³, P.M. Chabrilat ¹³⁰, J. Chan ^{18a}, W.Y. Chan ¹⁵⁷,
 J.D. Chapman ³³, E. Chapon ¹³⁸, B. Chargeishvili ^{153b}, D.G. Charlton ²¹, C. Chauhan ¹³⁶,
 Y. Che ^{114a}, S. Chekanov ⁶, S.V. Chekulaev ^{160a}, G.A. Chelkov ^{40,a}, B. Chen ¹⁵⁵, B. Chen ¹⁷⁰,
 H. Chen ^{114a}, H. Chen ³⁰, J. Chen ^{63c}, J. Chen ¹⁴⁶, M. Chen ¹²⁹, S. Chen ⁸⁹, S.J. Chen ^{114a},
 X. Chen ^{63c}, X. Chen ^{15,ae}, C.L. Cheng ¹⁷⁵, H.C. Cheng ^{65a}, S. Cheong ¹⁴⁷, A. Cheplakov ⁴⁰,
 E. Cheremushkina ⁴⁹, E. Cherepanova ¹¹⁷, R. Cherkaoui El Moursli ^{36e}, E. Cheu ⁷, K. Cheung ⁶⁶,
 L. Chevalier ¹³⁸, V. Chiarella ⁵⁴, G. Chiarelli ^{75a}, N. Chiedde ¹⁰⁴, G. Chiodini ^{71a},
 A.S. Chisholm ²¹, A. Chitan ^{28b}, M. Chitishvili ¹⁶⁸, M.V. Chizhov ^{40,s}, K. Choi ¹¹, Y. Chou ¹⁴²,
 E.Y.S. Chow ¹¹⁶, K.L. Chu ¹⁷⁴, M.C. Chu ^{65a}, X. Chu ^{14,114c}, Z. Chubinidze ⁵⁴, J. Chudoba ¹³⁴,
 J.J. Chwastowski ⁸⁸, D. Cieri ¹¹², K.M. Ciesla ^{87a}, V. Cindro ⁹⁵, A. Ciocio ^{18a}, F. Ciroto ^{73a,73b},

Z.H. Citron ¹⁷⁴, M. Citterio ^{72a}, D.A. Ciubotaru ^{28b}, A. Clark ⁵⁷, P.J. Clark ⁵³, N. Clarke Hall ⁹⁸, C. Clarry ¹⁵⁹, S.E. Clawson ⁴⁹, C. Clement ^{48a,48b}, Y. Coadou ¹⁰⁴, M. Cobal ^{70a,70c}, A. Coccaro ^{58b}, R.F. Coelho Barrue ^{133a}, R. Coelho Lopes De Sa ¹⁰⁵, S. Coelli ^{72a}, L.S. Colangeli ¹⁵⁹, B. Cole ⁴³, J. Collot ⁶¹, P. Conde Muiño ^{133a,133g}, M.P. Connell ^{34c}, S.H. Connell ^{34c}, E.I. Conroy ¹²⁹, F. Conventi ^{73a,ag}, H.G. Cooke ²¹, A.M. Cooper-Sarkar ¹²⁹, F.A. Corchia ^{24b,24a}, A. Cordeiro Oudot Choi ¹³⁰, L.D. Corpe ⁴², M. Corradi ^{76a,76b}, F. Corriveau ^{106,aa}, A. Cortes-Gonzalez ¹⁹, M.J. Costa ¹⁶⁸, F. Costanza ⁴, D. Costanzo ¹⁴³, B.M. Cote ¹²², J. Couthures ⁴, G. Cowan ⁹⁷, K. Cranmer ¹⁷⁵, L. Cremer ⁵⁰, D. Cremonini ^{24b,24a}, S. Crépe-Renaudin ⁶¹, F. Crescioli ¹³⁰, M. Cristinziani ¹⁴⁵, M. Cristoforetti ^{79a,79b}, V. Croft ¹¹⁷, J.E. Crosby ¹²⁴, G. Crosetti ^{45b,45a}, A. Cueto ¹⁰¹, H. Cui ⁹⁸, Z. Cui ⁷, W.R. Cunningham ⁶⁰, F. Curcio ¹⁶⁸, J.R. Curran ⁵³, P. Czodrowski ³⁷, M.J. Da Cunha Sargedas De Sousa ^{58b,58a}, J.V. Da Fonseca Pinto ^{84b}, C. Da Via ¹⁰³, W. Dabrowski ^{87a}, T. Dado ³⁷, S. Dahbi ¹⁵², T. Dai ¹⁰⁸, D. Dal Santo ²⁰, C. Dallapiccola ¹⁰⁵, M. Dam ⁴⁴, G. D'amen ³⁰, V. D'Amico ¹¹¹, J. Damp ¹⁰², J.R. Dandoy ³⁵, D. Dannheim ³⁷, M. Danninger ¹⁴⁶, V. Dao ¹⁴⁹, G. Darbo ^{58b}, S.J. Das ³⁰, F. Dattola ⁴⁹, S. D'Auria ^{72a,72b}, A. D'Avanzo ^{73a,73b}, T. Davidek ¹³⁶, I. Dawson ⁹⁶, H.A. Day-hall ¹³⁵, K. De ⁸, C. De Almeida Rossi ¹⁵⁹, R. De Asmundis ^{73a}, N. De Biase ⁴⁹, S. De Castro ^{24b,24a}, N. De Groot ¹¹⁶, P. de Jong ¹¹⁷, H. De la Torre ¹¹⁸, A. De Maria ^{114a}, A. De Salvo ^{76a}, U. De Sanctis ^{77a,77b}, F. De Santis ^{71a,71b}, A. De Santo ¹⁵⁰, J.B. De Vivie De Regie ⁶¹, J. Debevc ⁹⁵, D.V. Dedovich ⁴⁰, J. Degens ⁹⁴, A.M. Deiana ⁴⁶, J. Del Peso ¹⁰¹, L. Delagrangé ¹³⁰, F. Deliot ¹³⁸, C.M. Delitzsch ⁵⁰, M. Della Pietra ^{73a,73b}, D. Della Volpe ⁵⁷, A. Dell'Acqua ³⁷, L. Dell'Asta ^{72a,72b}, M. Delmastro ⁴, C.C. Delogu ¹⁰², P.A. Delsart ⁶¹, S. Demers ¹⁷⁷, M. Demichev ⁴⁰, S.P. Denisov ³⁹, H. Denizli ^{22a,k}, L. D'Eramo ⁴², D. Derendarz ⁸⁸, F. Derue ¹³⁰, P. Dervan ⁹⁴, K. Desch ²⁵, C. Deutsch ²⁵, F.A. Di Bello ^{58b,58a}, A. Di Ciaccio ^{77a,77b}, L. Di Ciaccio ⁴, A. Di Domenico ^{76a,76b}, C. Di Donato ^{73a,73b}, A. Di Girolamo ³⁷, G. Di Gregorio ³⁷, A. Di Luca ^{79a,79b}, B. Di Micco ^{78a,78b}, R. Di Nardo ^{78a,78b}, K.F. Di Petrillo ⁴¹, M. Diamantopoulou ³⁵, F.A. Dias ¹¹⁷, T. Dias Do Vale ¹⁴⁶, M.A. Diaz ^{140a,140b}, A.R. Didenko ⁴⁰, M. Didenko ¹⁶⁸, E.B. Diehl ¹⁰⁸, S. Díez Cornell ⁴⁹, C. Diez Pardos ¹⁴⁵, C. Dimitriadi ¹⁴⁸, A. Dimitrievska ²¹, A. Dimri ¹⁴⁹, J. Dingfelder ²⁵, T. Dingley ¹²⁹, I-M. Dinu ^{28b}, S.J. Dittmeier ^{64b}, F. Dittus ³⁷, M. Divisek ¹³⁶, B. Dixit ⁹⁴, F. Djama ¹⁰⁴, T. Djobava ^{153b}, C. Doglioni ^{103,100}, A. Dohnalova ^{29a}, Z. Dolezal ¹³⁶, K. Domijan ^{87a}, K.M. Dona ⁴¹, M. Donadelli ^{84d}, B. Dong ¹⁰⁹, J. Donini ⁴², A. D'Onofrio ^{73a,73b}, M. D'Onofrio ⁹⁴, J. Dopke ¹³⁷, A. Doria ^{73a}, N. Dos Santos Fernandes ^{133a}, P. Dougan ¹⁰³, M.T. Dova ⁹², A.T. Doyle ⁶⁰, M.A. Draguet ¹²⁹, M.P. Drescher ⁵⁶, E. Dreyer ¹⁷⁴, I. Drivas-koulouris ¹⁰, M. Drnevich ¹²⁰, M. Drozdova ⁵⁷, D. Du ^{63a}, T.A. du Pree ¹¹⁷, F. Dubinin ³⁹, M. Dubovsky ^{29a}, E. Duchovni ¹⁷⁴, G. Duckeck ¹¹¹, O.A. Ducu ^{28b}, D. Duda ⁵³, A. Dudarev ³⁷, E.R. Duden ²⁷, M. D'uffizi ¹⁰³, L. Duflot ⁶⁷, M. Dührssen ³⁷, I. Duminica ^{28g}, A.E. Dumitriu ^{28b}, M. Dunford ^{64a}, S. Dungs ⁵⁰, K. Dunne ^{48a,48b}, A. Duperrin ¹⁰⁴, H. Duran Yildiz ^{3a}, M. Düren ⁵⁹, A. Durglishvili ^{153b}, B.L. Dwyer ¹¹⁸, G.I. Dyckes ^{18a}, M. Dyndal ^{87a}, B.S. Dziedzic ³⁷, Z.O. Earnshaw ¹⁵⁰, G.H. Eberwein ¹²⁹, B. Eckerova ^{29a}, S. Eggebrecht ⁵⁶, E. Egidio Purcino De Souza ^{84e}, G. Eigen ¹⁷, K. Einsweiler ^{18a}, T. Ekelof ¹⁶⁶, P.A. Ekman ¹⁰⁰, S. El Farkh ^{36b}, Y. El Ghazali ^{63a}, H. El Jarrari ³⁷, A. El Moussaouy ^{36a}, V. Ellajosyula ¹⁶⁶, M. Ellert ¹⁶⁶, F. Ellinghaus ¹⁷⁶, N. Ellis ³⁷, J. Elmsheuser ³⁰, M. Elsayy ^{119a}, M. Elsing ³⁷, D. Emeliyanov ¹³⁷, Y. Enari ⁸⁵, I. Ene ^{18a}, S. Epari ¹³, D. Ernani Martins Neto ⁸⁸, M. Errenst ¹⁷⁶, M. Escalier ⁶⁷, C. Escobar ¹⁶⁸, E. Etzion ¹⁵⁵, G. Evans ^{133a}, H. Evans ⁶⁹, L.S. Evans ⁹⁷, A. Ezhilov ³⁹, S. Ezzarqtouni ^{36a}, F. Fabbri ^{24b,24a}, L. Fabbri ^{24b,24a}, G. Facini ⁹⁸, V. Fadeyev ¹³⁹, R.M. Fakhrutdinov ³⁹, D. Fakoudis ¹⁰², S. Falciano ^{76a},

L.F. Falda Ulhoa Coelho [ID133a](#), F. Fallavollita [ID112](#), G. Falsetti [ID45b,45a](#), J. Faltova [ID136](#), C. Fan [ID167](#),
 K.Y. Fan [ID65b](#), Y. Fan [ID14](#), Y. Fang [ID14,114c](#), M. Fanti [ID72a,72b](#), M. Faraj [ID70a,70b](#), Z. Farazpay [ID99](#),
 A. Farbin [ID8](#), A. Farilla [ID78a](#), T. Farooque [ID109](#), J.N. Farr [ID177](#), S.M. Farrington [ID137,53](#), F. Fassi [ID36e](#),
 D. Fassouliotis [ID9](#), L. Fayard [ID67](#), P. Federic [ID136](#), P. Federicova [ID134](#), O.L. Fedin [ID39,a](#), M. Feickert [ID175](#),
 L. Feligioni [ID104](#), D.E. Fellers [ID126](#), C. Feng [ID63b](#), Z. Feng [ID117](#), M.J. Fenton [ID163](#), L. Ferencz [ID49](#),
 R.A.M. Ferguson [ID93](#), P. Fernandez Martinez [ID68](#), M.J.V. Fernoux [ID104](#), J. Ferrando [ID93](#), A. Ferrari [ID166](#),
 P. Ferrari [ID117,116](#), R. Ferrari [ID74a](#), D. Ferrere [ID57](#), C. Ferretti [ID108](#), M.P. Fewell [ID1](#), D. Fiacco [ID76a,76b](#),
 F. Fiedler [ID102](#), P. Fiedler [ID135](#), S. Filimonov [ID39](#), A. Filipčič [ID95](#), E.K. Filmer [ID160a](#), F. Filthaut [ID116](#),
 M.C.N. Fiolhais [ID133a,133c,c](#), L. Fiorini [ID168](#), W.C. Fisher [ID109](#), T. Fitschen [ID103](#), P.M. Fitzhugh [ID138](#),
 I. Fleck [ID145](#), P. Fleischmann [ID108](#), T. Flick [ID176](#), M. Flores [ID34d,ac](#), L.R. Flores Castillo [ID65a](#),
 L. Flores Sanz De Acedo [ID37](#), F.M. Follega [ID79a,79b](#), N. Fomin [ID33](#), J.H. Foo [ID159](#), A. Formica [ID138](#),
 A.C. Forti [ID103](#), E. Fortin [ID37](#), A.W. Fortman [ID18a](#), L. Fountas [ID9,i](#), D. Fournier [ID67](#), H. Fox [ID93](#),
 P. Francavilla [ID75a,75b](#), S. Francescato [ID62](#), S. Franchellucci [ID57](#), M. Franchini [ID24b,24a](#),
 S. Franchino [ID64a](#), D. Francis [ID37](#), L. Franco [ID116](#), V. Franco Lima [ID37](#), L. Franconi [ID49](#), M. Franklin [ID62](#),
 G. Frattari [ID27](#), Y.Y. Frid [ID155](#), J. Friend [ID60](#), N. Fritzsche [ID37](#), A. Froch [ID57](#), D. Froidevaux [ID37](#),
 J.A. Frost [ID129](#), Y. Fu [ID109](#), S. Fuenzalida Garrido [ID140f](#), M. Fujimoto [ID104](#), K.Y. Fung [ID65a](#),
 E. Furtado De Simas Filho [ID84e](#), M. Furukawa [ID157](#), J. Fuster [ID168](#), A. Gaa [ID56](#), A. Gabrielli [ID24b,24a](#),
 A. Gabrielli [ID159](#), P. Gadow [ID37](#), G. Gagliardi [ID58b,58a](#), L.G. Gagnon [ID18a](#), S. Gaid [ID165](#),
 S. Galantzan [ID155](#), J. Gallagher [ID1](#), E.J. Gallas [ID129](#), A.L. Gallen [ID166](#), B.J. Gallop [ID137](#), K.K. Gan [ID122](#),
 S. Ganguly [ID157](#), Y. Gao [ID53](#), A. Garabaglu [ID142](#), F.M. Garay Walls [ID140a,140b](#), B. Garcia [ID30](#),
 C. García [ID168](#), A. Garcia Alonso [ID117](#), A.G. Garcia Caffaro [ID177](#), J.E. García Navarro [ID168](#),
 M. Garcia-Sciveres [ID18a](#), G.L. Gardner [ID131](#), R.W. Gardner [ID41](#), N. Garelli [ID162](#), R.B. Garg [ID147](#),
 J.M. Gargan [ID53](#), C.A. Garner [ID159](#), C.M. Garvey [ID34a](#), V.K. Gassmann [ID162](#), G. Gaudio [ID74a](#), V. Gautam [ID13](#),
 P. Gauzzi [ID76a,76b](#), J. Gavranovic [ID95](#), I.L. Gavrilenko [ID39](#), A. Gavrilyuk [ID39](#), C. Gay [ID169](#),
 G. Gaycken [ID126](#), E.N. Gazis [ID10](#), A. Gekow [ID122](#), C. Gemme [ID58b](#), M.H. Genest [ID61](#), A.D. Gentry [ID115](#),
 S. George [ID97](#), W.F. George [ID21](#), T. Geralis [ID47](#), A.A. Gerwin [ID123](#), P. Gessinger-Befurt [ID37](#),
 M.E. Geyik [ID176](#), M. Ghani [ID172](#), K. Ghorbanian [ID96](#), A. Ghosal [ID145](#), A. Ghosh [ID163](#), A. Ghosh [ID7](#),
 B. Giacobbe [ID24b](#), S. Giagu [ID76a,76b](#), T. Giani [ID117](#), A. Giannini [ID63a](#), S.M. Gibson [ID97](#), M. Gignac [ID139](#),
 D.T. Gil [ID87b](#), A.K. Gilbert [ID87a](#), B.J. Gilbert [ID43](#), D. Gillberg [ID35](#), G. Gilles [ID117](#), L. Ginabat [ID130](#),
 D.M. Gingrich [ID2,af](#), M.P. Giordani [ID70a,70c](#), P.F. Giraud [ID138](#), G. Giugliarelli [ID70a,70c](#), D. Giugni [ID72a](#),
 F. Giuli [ID77a,77b](#), I. Gkialas [ID9,i](#), L.K. Gladilin [ID39](#), C. Glasman [ID101](#), G. Glemža [ID49](#), M. Glisic [ID126](#),
 I. Gnesi [ID45b](#), Y. Go [ID30](#), M. Goblirsch-Kolb [ID37](#), B. Gocke [ID50](#), D. Godin [ID110](#), B. Gokturk [ID22a](#),
 S. Goldfarb [ID107](#), T. Golling [ID57](#), M.G.D. Gololo [ID34c](#), D. Golubkov [ID39](#), J.P. Gombas [ID109](#),
 A. Gomes [ID133a,133b](#), G. Gomes Da Silva [ID145](#), A.J. Gomez Delegido [ID168](#), R. Gonçalves [ID133a](#),
 L. Gonella [ID21](#), A. Gongadze [ID153c](#), F. Gonnella [ID21](#), J.L. Gonski [ID147](#), R.Y. González Andana [ID53](#),
 S. González de la Hoz [ID168](#), R. Gonzalez Lopez [ID94](#), C. Gonzalez Renteria [ID18a](#),
 M.V. Gonzalez Rodrigues [ID49](#), R. Gonzalez Suarez [ID166](#), S. Gonzalez-Sevilla [ID57](#), L. Goossens [ID37](#),
 B. Gorini [ID37](#), E. Gorini [ID71a,71b](#), A. Gorišek [ID95](#), T.C. Gosart [ID131](#), A.T. Goshaw [ID52](#), M.I. Gostkin [ID40](#),
 S. Goswami [ID124](#), C.A. Gottardo [ID37](#), S.A. Gotz [ID111](#), M. Gouighri [ID36b](#), A.G. Goussiou [ID142](#),
 N. Govender [ID34c](#), R.P. Grabarczyk [ID129](#), I. Grabowska-Bold [ID87a](#), K. Graham [ID35](#), E. Gramstad [ID128](#),
 S. Grancagnolo [ID71a,71b](#), C.M. Grant [ID1,138](#), P.M. Gravila [ID28f](#), F.G. Gravili [ID71a,71b](#), H.M. Gray [ID18a](#),
 M. Greco [ID112](#), M.J. Green [ID1](#), C. Grefe [ID25](#), A.S. Grefsrud [ID17](#), I.M. Gregor [ID49](#), K.T. Greif [ID163](#),
 P. Grenier [ID147](#), S.G. Grewe [ID112](#), A.A. Grillo [ID139](#), K. Grimm [ID32](#), S. Grinstein [ID13,w](#), J.-F. Grivaz [ID67](#),
 E. Gross [ID174](#), J. Grosse-Knetter [ID56](#), L. Guan [ID108](#), G. Guerrieri [ID37](#), R. Gugel [ID102](#), J.A.M. Guhit [ID108](#),
 A. Guida [ID19](#), E. Guilloton [ID172](#), S. Guindon [ID37](#), F. Guo [ID14,114c](#), J. Guo [ID63c](#), L. Guo [ID49](#),
 L. Guo [ID114b,u](#), Y. Guo [ID108](#), A. Gupta [ID50](#), R. Gupta [ID132](#), S. Gurbuz [ID25](#), S.S. Gurdasani [ID49](#),
 G. Gustavino [ID76a,76b](#), P. Gutierrez [ID123](#), L.F. Gutierrez Zagazeta [ID131](#), M. Gutsche [ID51](#),

C. Gutschow ¹⁹⁸, C. Gwenlan ¹²⁹, C.B. Gwilliam ⁹⁴, E.S. Haaland ¹²⁸, A. Haas ¹²⁰,
 M. Habedank ⁶⁰, C. Haber ^{18a}, H.K. Hadavand ⁸, A. Haddad ⁴², A. Hadeef ⁵¹, A.I. Hagan ⁹³,
 J.J. Hahn ¹⁴⁵, E.H. Haines ⁹⁸, M. Haleem ¹⁷¹, J. Haley ¹²⁴, G.D. Hallewell ¹⁰⁴, L. Halser ²⁰,
 K. Hamano ¹⁷⁰, M. Hamer ²⁵, E.J. Hampshire ⁹⁷, J. Han ^{63b}, L. Han ^{114a}, L. Han ^{63a},
 S. Han ^{18a}, K. Hanagaki ⁸⁵, M. Hance ¹³⁹, D.A. Hangal ⁴³, H. Hanif ¹⁴⁶, M.D. Hank ¹³¹,
 J.B. Hansen ⁴⁴, P.H. Hansen ⁴⁴, D. Harada ⁵⁷, T. Harenberg ¹⁷⁶, S. Harkusha ¹⁷⁸,
 M.L. Harris ¹⁰⁵, Y.T. Harris ²⁵, J. Harrison ¹³, N.M. Harrison ¹²², P.F. Harrison ¹⁷²,
 N.M. Hartman ¹¹², N.M. Hartmann ¹¹¹, R.Z. Hasan ^{97,137}, Y. Hasegawa ¹⁴⁴, F. Haslbeck ¹²⁹,
 S. Hassan ¹⁷, R. Hauser ¹⁰⁹, C.M. Hawkes ²¹, R.J. Hawkings ³⁷, Y. Hayashi ¹⁵⁷, D. Hayden ¹⁰⁹,
 C. Hayes ¹⁰⁸, R.L. Hayes ¹¹⁷, C.P. Hays ¹²⁹, J.M. Hays ⁹⁶, H.S. Hayward ⁹⁴, F. He ^{63a},
 M. He ^{14,114c}, Y. He ⁴⁹, Y. He ⁹⁸, N.B. Heatley ⁹⁶, V. Hedberg ¹⁰⁰, A.L. Heggelund ¹²⁸,
 C. Heidegger ⁵⁵, K.K. Heidegger ⁵⁵, J. Heilman ³⁵, S. Heim ⁴⁹, T. Heim ^{18a}, J.G. Heinlein ¹³¹,
 J.J. Heinrich ¹²⁶, L. Heinrich ^{112,ad}, J. Hejbal ¹³⁴, A. Held ¹⁷⁵, S. Hellesund ¹⁷,
 C.M. Helling ¹⁶⁹, S. Hellman ^{48a,48b}, L. Henkelmann ³³, A.M. Henriques Correia ³⁷, H. Herde ¹⁰⁰,
 Y. Hernández Jiménez ¹⁴⁹, L.M. Herrmann ²⁵, T. Herrmann ⁵¹, G. Herten ⁵⁵, R. Hertenberger ¹¹¹,
 L. Hervas ³⁷, M.E. Hesping ¹⁰², N.P. Hessey ^{160a}, J. Hessler ¹¹², M. Hidaoui ^{36b}, N. Hidic ¹³⁶,
 E. Hill ¹⁵⁹, S.J. Hillier ²¹, J.R. Hinds ¹⁰⁹, F. Hinterkeuser ²⁵, M. Hirose ¹²⁷, S. Hirose ¹⁶¹,
 D. Hirschbuehl ¹⁷⁶, T.G. Hitchings ¹⁰³, B. Hiti ⁹⁵, J. Hobbs ¹⁴⁹, R. Hobincu ^{28e}, N. Hod ¹⁷⁴,
 M.C. Hodgkinson ¹⁴³, B.H. Hodgkinson ¹²⁹, A. Hoecker ³⁷, D.D. Hofer ¹⁰⁸, J. Hofer ¹⁶⁸,
 M. Holzbock ³⁷, L.B.A.H. Hommels ³³, B.P. Honan ¹⁰³, J.J. Hong ⁶⁹, J. Hong ^{63c},
 T.M. Hong ¹³², B.H. Hooberman ¹⁶⁷, W.H. Hopkins ⁶, M.C. Hoppesch ¹⁶⁷, Y. Horii ¹¹³,
 M.E. Horstmann ¹¹², S. Hou ¹⁵², M.R. Housenga ¹⁶⁷, A.S. Howard ⁹⁵, J. Howarth ⁶⁰, J. Hoya ⁶,
 M. Hrabovsky ¹²⁵, T. Hryn'ova ⁴, P.J. Hsu ⁶⁶, S.-C. Hsu ¹⁴², T. Hsu ⁶⁷, M. Hu ^{18a}, Q. Hu ^{63a},
 S. Huang ³³, X. Huang ^{14,114c}, Y. Huang ¹³⁶, Y. Huang ^{114b}, Y. Huang ¹⁰², Y. Huang ¹⁴,
 Z. Huang ¹⁰³, Z. Hubacek ¹³⁵, M. Huebner ²⁵, F. Huegging ²⁵, T.B. Huffman ¹²⁹,
 M. Hufnagel Maranha De Faria ^{84a}, C.A. Hugli ⁴⁹, M. Huhtinen ³⁷, S.K. Huiberts ¹⁷,
 R. Hulsken ¹⁰⁶, C.E. Hultquist ^{18a}, N. Huseynov ^{12,f}, J. Huston ¹⁰⁹, J. Huth ⁶², R. Hyneman ⁷,
 G. Iacobucci ⁵⁷, G. Iakovidis ³⁰, L. Iconomidou-Fayard ⁶⁷, J.P. Iddon ³⁷, P. Iengo ^{73a,73b},
 R. Iguchi ¹⁵⁷, Y. Iiyama ¹⁵⁷, T. Iizawa ¹²⁹, Y. Ikegami ⁸⁵, D. Iliadis ¹⁵⁶, N. Ilic ¹⁵⁹,
 H. Imam ^{84c}, G. Inacio Goncalves ^{84d}, S.A. Infante Cabanas ^{140c}, T. Ingebretsen Carlson ^{48a,48b},
 J.M. Inglis ⁹⁶, G. Introzzi ^{74a,74b}, M. Iodice ^{78a}, V. Ippolito ^{76a,76b}, R.K. Irwin ⁹⁴, M. Ishino ¹⁵⁷,
 W. Islam ¹⁷⁵, C. Issever ¹⁹, S. Istin ^{22a,ak}, H. Ito ¹⁷³, R. Iuppa ^{79a,79b}, A. Ivina ¹⁷⁴, V. Izzo ^{73a},
 P. Jacka ¹³⁴, P. Jackson ¹, P. Jain ⁴⁹, K. Jakobs ⁵⁵, T. Jakoubek ¹⁷⁴, J. Jamieson ⁶⁰,
 W. Jang ¹⁵⁷, M. Javurkova ¹⁰⁵, P. Jawahar ¹⁰³, L. Jeanty ¹²⁶, J. Jejelava ^{153a}, P. Jenni ^{55,e},
 C.E. Jessiman ³⁵, C. Jia ^{63b}, H. Jia ¹⁶⁹, J. Jia ¹⁴⁹, X. Jia ^{14,114c}, Z. Jia ^{114a}, C. Jiang ⁵³,
 Q. Jiang ^{65b}, S. Jiggins ⁴⁹, J. Jimenez Pena ¹³, S. Jin ^{114a}, A. Jinaru ^{28b}, O. Jinnouchi ¹⁴¹,
 P. Johansson ¹⁴³, K.A. Johns ⁷, J.W. Johnson ¹³⁹, F.A. Jolly ⁴⁹, D.M. Jones ¹⁵⁰, E. Jones ⁴⁹,
 K.S. Jones ⁸, P. Jones ³³, R.W.L. Jones ⁹³, T.J. Jones ⁹⁴, H.L. Joos ^{56,37}, R. Joshi ¹²²,
 J. Jovicevic ¹⁶, X. Ju ^{18a}, J.J. Junggeburth ³⁷, T. Junkermann ^{64a}, A. Juste Rozas ^{13,w},
 M.K. Juzek ⁸⁸, S. Kabana ^{140e}, A. Kaczmarek ⁸⁸, M. Kado ¹¹², H. Kagan ¹²², M. Kagan ¹⁴⁷,
 A. Kahn ¹³¹, C. Kahra ¹⁰², T. Kaji ¹⁵⁷, E. Kajomovitz ¹⁵⁴, N. Kakati ¹⁷⁴, I. Kalaitzidou ⁵⁵,
 N.J. Kang ¹³⁹, D. Kar ^{34g}, K. Karava ¹²⁹, E. Karentzos ²⁵, O. Karkout ¹¹⁷, S.N. Karpov ⁴⁰,
 Z.M. Karpova ⁴⁰, V. Kartvelishvili ⁹³, A.N. Karyukhin ³⁹, E. Kasimi ¹⁵⁶, J. Katzy ⁴⁹,
 S. Kaur ³⁵, K. Kawade ¹⁴⁴, M.P. Kawale ¹²³, C. Kawamoto ⁸⁹, T. Kawamoto ^{63a}, E.F. Kay ³⁷,
 F.I. Kaya ¹⁶², S. Kazakos ¹⁰⁹, V.F. Kazanin ³⁹, Y. Ke ¹⁴⁹, J.M. Keaveney ^{34a}, R. Keeler ¹⁷⁰,
 G.V. Kehris ⁶², J.S. Keller ³⁵, J.J. Kempster ¹⁵⁰, O. Kepka ¹³⁴, J. Kerr ^{160b}, B.P. Kerridge ¹³⁷,
 B.P. Kerševan ⁹⁵, L. Keszeghova ^{29a}, R.A. Khan ¹³², A. Khanov ¹²⁴, A.G. Kharlamov ³⁹,

T. Kharlamova [ID³⁹](#), E.E. Khoda [ID¹⁴²](#), M. Kholodenko [ID^{133a}](#), T.J. Khoo [ID¹⁹](#), G. Khoraiuli [ID¹⁷¹](#), J. Khubua [ID^{153b,*}](#), Y.A.R. Khwaira [ID¹³⁰](#), B. Kibirige^{34g}, D. Kim [ID⁶](#), D.W. Kim [ID^{48a,48b}](#), Y.K. Kim [ID⁴¹](#), N. Kimura [ID⁹⁸](#), M.K. Kingston [ID⁵⁶](#), A. Kirchhoff [ID⁵⁶](#), C. Kirfel [ID²⁵](#), F. Kirfel [ID²⁵](#), J. Kirk [ID¹³⁷](#), A.E. Kiryunin [ID¹¹²](#), S. Kita [ID¹⁶¹](#), C. Kitsaki [ID¹⁰](#), O. Kivernyk [ID²⁵](#), M. Klassen [ID¹⁶²](#), C. Klein [ID³⁵](#), L. Klein [ID¹⁷¹](#), M.H. Klein [ID⁴⁶](#), S.B. Klein [ID⁵⁷](#), U. Klein [ID⁹⁴](#), A. Klimentov [ID³⁰](#), T. Klioutchnikova [ID³⁷](#), P. Kluit [ID¹¹⁷](#), S. Kluth [ID¹¹²](#), E. Kneringer [ID⁸⁰](#), T.M. Knight [ID¹⁵⁹](#), A. Knue [ID⁵⁰](#), D. Kobylanskii [ID¹⁷⁴](#), S.F. Koch [ID¹²⁹](#), M. Kocian [ID¹⁴⁷](#), P. Kodyš [ID¹³⁶](#), D.M. Koeck [ID¹²⁶](#), P.T. Koenig [ID²⁵](#), T. Koffas [ID³⁵](#), O. Kolay [ID⁵¹](#), I. Koletsou [ID⁴](#), T. Komarek [ID⁸⁸](#), K. Köneke [ID⁵⁶](#), A.X.Y. Kong [ID¹](#), T. Kono [ID¹²¹](#), N. Konstantinidis [ID⁹⁸](#), P. Kontaxakis [ID⁵⁷](#), B. Konya [ID¹⁰⁰](#), R. Kopeliansky [ID⁴³](#), S. Koperny [ID^{87a}](#), K. Korcyl [ID⁸⁸](#), K. Kordas [ID^{156,d}](#), A. Korn [ID⁹⁸](#), S. Korn [ID⁵⁶](#), I. Korolkov [ID¹³](#), N. Korotkova [ID³⁹](#), B. Kortman [ID¹¹⁷](#), O. Kortner [ID¹¹²](#), S. Kortner [ID¹¹²](#), W.H. Kostecka [ID¹¹⁸](#), V.V. Kostyukhin [ID¹⁴⁵](#), A. Kotsokechagia [ID³⁷](#), A. Kotwal [ID⁵²](#), A. Koulouris [ID³⁷](#), A. Kourkoumeli-Charalampidi [ID^{74a,74b}](#), C. Kourkoumelis [ID⁹](#), E. Kourlitis [ID^{112,ad}](#), O. Kovanda [ID¹²⁶](#), R. Kowalewski [ID¹⁷⁰](#), W. Kozanecki [ID¹²⁶](#), A.S. Kozhin [ID³⁹](#), V.A. Kramarenko [ID³⁹](#), G. Kramberger [ID⁹⁵](#), P. Kramer [ID²⁵](#), M.W. Krasny [ID¹³⁰](#), A. Krasznahorkay [ID¹⁰⁵](#), A.C. Kraus [ID¹¹⁸](#), J.W. Kraus [ID¹⁷⁶](#), J.A. Kremer [ID⁴⁹](#), T. Kresse [ID⁵¹](#), L. Kretschmann [ID¹⁷⁶](#), J. Kretschmar [ID⁹⁴](#), K. Kreul [ID¹⁹](#), P. Krieger [ID¹⁵⁹](#), K. Krizka [ID²¹](#), K. Kroeninger [ID⁵⁰](#), H. Kroha [ID¹¹²](#), J. Kroll [ID¹³⁴](#), J. Kroll [ID¹³¹](#), K.S. Krowpman [ID¹⁰⁹](#), U. Kruchonak [ID⁴⁰](#), H. Krüger [ID²⁵](#), N. Krumnack⁸², M.C. Kruse [ID⁵²](#), O. Kuchinskaia [ID³⁹](#), S. Kuday [ID^{3a}](#), S. Kuehn [ID³⁷](#), R. Kuesters [ID⁵⁵](#), T. Kuhl [ID⁴⁹](#), V. Kukhtin [ID⁴⁰](#), Y. Kulchitsky [ID⁴⁰](#), S. Kuleshov [ID^{140d,140b}](#), M. Kumar [ID^{34g}](#), N. Kumari [ID⁴⁹](#), P. Kumari [ID^{160b}](#), A. Kupco [ID¹³⁴](#), T. Kupfer⁵⁰, A. Kupich [ID³⁹](#), O. Kuprash [ID⁵⁵](#), H. Kurashige [ID⁸⁶](#), L.L. Kurchaninov [ID^{160a}](#), O. Kurdysh [ID⁴](#), Y.A. Kurochkin [ID³⁸](#), A. Kurova [ID³⁹](#), M. Kuze [ID¹⁴¹](#), A.K. Kvam [ID¹⁰⁵](#), J. Kvita [ID¹²⁵](#), N.G. Kyriacou [ID¹⁰⁸](#), L.A.O. Laatu [ID¹⁰⁴](#), C. Lacasta [ID¹⁶⁸](#), F. Lacava [ID^{76a,76b}](#), H. Lacker [ID¹⁹](#), D. Lacour [ID¹³⁰](#), N.N. Lad [ID⁹⁸](#), E. Ladygin [ID⁴⁰](#), A. Lafarge [ID⁴²](#), B. Laforge [ID¹³⁰](#), T. Lagouri [ID¹⁷⁷](#), F.Z. Lahbabi [ID^{36a}](#), S. Lai [ID⁵⁶](#), J.E. Lambert [ID¹⁷⁰](#), S. Lammers [ID⁶⁹](#), W. Lampl [ID⁷](#), C. Lampoudis [ID^{156,d}](#), G. Lamprinoudis [ID¹⁰²](#), A.N. Lancaster [ID¹¹⁸](#), E. Lançon [ID³⁰](#), U. Landgraf [ID⁵⁵](#), M.P.J. Landon [ID⁹⁶](#), V.S. Lang [ID⁵⁵](#), O.K.B. Langrekken [ID¹²⁸](#), A.J. Lankford [ID¹⁶³](#), F. Lanni [ID³⁷](#), K. Lantzsck [ID²⁵](#), A. Lanza [ID^{74a}](#), M. Lanzac Berrocal [ID¹⁶⁸](#), J.F. Laporte [ID¹³⁸](#), T. Lari [ID^{72a}](#), F. Lasagni Manghi [ID^{24b}](#), M. Lassnig [ID³⁷](#), V. Latonova [ID¹³⁴](#), S.D. Lawlor [ID¹⁴³](#), Z. Lawrence [ID¹⁰³](#), R. Lazaridou¹⁷², M. Lazzaroni [ID^{72a,72b}](#), H.D.M. Le [ID¹⁰⁹](#), E.M. Le Boulicaut [ID¹⁷⁷](#), L.T. Le Pottier [ID^{18a}](#), B. Leban [ID^{24b,24a}](#), M. LeBlanc [ID¹⁰³](#), F. Ledroit-Guillon [ID⁶¹](#), S.C. Lee [ID¹⁵²](#), T.F. Lee [ID⁹⁴](#), L.L. Leeuw [ID^{34c,ai}](#), M. Lefebvre [ID¹⁷⁰](#), C. Leggett [ID^{18a}](#), G. Lehmann Miotto [ID³⁷](#), M. Leigh [ID⁵⁷](#), W.A. Leight [ID¹⁰⁵](#), W. Leinonen [ID¹¹⁶](#), A. Leisos [ID^{156,t}](#), M.A.L. Leite [ID^{84c}](#), C.E. Leitgeb [ID¹⁹](#), R. Leitner [ID¹³⁶](#), K.J.C. Leney [ID⁴⁶](#), T. Lenz [ID²⁵](#), S. Leone [ID^{75a}](#), C. Leonidopoulos [ID⁵³](#), A. Leopold [ID¹⁴⁸](#), J.H. Lepage Bourbonnais [ID³⁵](#), R. Les [ID¹⁰⁹](#), C.G. Lester [ID³³](#), M. Levchenko [ID³⁹](#), J. Levêque [ID⁴](#), L.J. Levinson [ID¹⁷⁴](#), G. Levrini [ID^{24b,24a}](#), M.P. Lewicki [ID⁸⁸](#), C. Lewis [ID¹⁴²](#), D.J. Lewis [ID⁴](#), L. Lewitt [ID¹⁴³](#), A. Li [ID³⁰](#), B. Li [ID^{63b}](#), C. Li¹⁰⁸, C-Q. Li [ID¹¹²](#), H. Li [ID^{63a}](#), H. Li [ID^{63b}](#), H. Li [ID¹⁰³](#), H. Li [ID¹⁵](#), H. Li [ID^{63b}](#), J. Li [ID^{63c}](#), K. Li [ID¹⁴](#), L. Li [ID^{63c}](#), R. Li [ID¹⁷⁷](#), S. Li [ID^{14,114c}](#), S. Li [ID^{63d,63c}](#), T. Li [ID⁵](#), X. Li [ID¹⁰⁶](#), Z. Li [ID¹⁵⁷](#), Z. Li [ID^{14,114c}](#), Z. Li [ID^{63a}](#), S. Liang [ID^{14,114c}](#), Z. Liang [ID¹⁴](#), M. Liberatore [ID¹³⁸](#), B. Liberti [ID^{77a}](#), K. Lie [ID^{65c}](#), J. Lieber Marin [ID^{84e}](#), H. Lien [ID⁶⁹](#), H. Lin [ID¹⁰⁸](#), L. Linden [ID¹¹¹](#), R.E. Lindley [ID⁷](#), J.H. Lindon [ID²](#), J. Ling [ID⁶²](#), E. Lipeles [ID¹³¹](#), A. Lipniacka [ID¹⁷](#), A. Lister [ID¹⁶⁹](#), J.D. Little [ID⁶⁹](#), B. Liu [ID¹⁴](#), B.X. Liu [ID^{114b}](#), D. Liu [ID^{63d,63c}](#), E.H.L. Liu [ID²¹](#), J.K.K. Liu [ID³³](#), K. Liu [ID^{63d}](#), K. Liu [ID^{63d,63c}](#), M. Liu [ID^{63a}](#), M.Y. Liu [ID^{63a}](#), P. Liu [ID¹⁴](#), Q. Liu [ID^{63d,142,63c}](#), X. Liu [ID^{63a}](#), X. Liu [ID^{63b}](#), Y. Liu [ID^{114b,114c}](#), Y.L. Liu [ID^{63b}](#), Y.W. Liu [ID^{63a}](#), S.L. Lloyd [ID⁹⁶](#), E.M. Lobodzinska [ID⁴⁹](#), P. Loch [ID⁷](#), E. Lodhi [ID¹⁵⁹](#), T. Lohse [ID¹⁹](#), K. Lohwasser [ID¹⁴³](#), E. Loiacono [ID⁴⁹](#), J.D. Lomas [ID²¹](#), J.D. Long [ID⁴³](#), I. Longarini [ID¹⁶³](#), R. Longo [ID¹⁶⁷](#), A. Lopez Solis [ID⁴⁹](#), N.A. Lopez-canelas [ID⁷](#), N. Lorenzo Martinez [ID⁴](#), A.M. Lory [ID¹¹¹](#), M. Losada [ID^{119a}](#), G. Lösckce Centeno [ID¹⁵⁰](#), O. Loseva [ID³⁹](#), X. Lou [ID^{48a,48b}](#), X. Lou [ID^{14,114c}](#), A. Lounis [ID⁶⁷](#), P.A. Love [ID⁹³](#), G. Lu [ID^{14,114c}](#), M. Lu [ID⁶⁷](#), S. Lu [ID¹³¹](#), Y.J. Lu [ID¹⁵²](#), H.J. Lubatti [ID¹⁴²](#),

C. Luci ^{76a,76b}, F.L. Lucio Alves ^{114a}, F. Luehring ⁶⁹, B.S. Lunday ¹³¹, O. Lundberg ¹⁴⁸,
 B. Lund-Jensen ^{148,*}, N.A. Luongo ⁶, M.S. Lutz ³⁷, A.B. Lux ²⁶, D. Lynn ³⁰, R. Lysak ¹³⁴,
 E. Lytken ¹⁰⁰, V. Lyubushkin ⁴⁰, T. Lyubushkina ⁴⁰, M.M. Lyukova ¹⁴⁹, M.Firdaus M. Soberi ⁵³,
 H. Ma ³⁰, K. Ma ^{63a}, L.L. Ma ^{63b}, W. Ma ^{63a}, Y. Ma ¹²⁴, J.C. MacDonald ¹⁰²,
 P.C. Machado De Abreu Farias ^{84e}, R. Madar ⁴², T. Madula ⁹⁸, J. Maeda ⁸⁶, T. Maeno ³⁰,
 P.T. Mafa ^{34c,j}, H. Maguire ¹⁴³, V. Maiboroda ¹³⁸, A. Maio ^{133a,133b,133d}, K. Maj ^{87a},
 O. Majersky ⁴⁹, S. Majewski ¹²⁶, R. Makhmanazarov ³⁹, N. Makovec ⁶⁷, V. Maksimovic ¹⁶,
 B. Malaescu ¹³⁰, Pa. Malecki ⁸⁸, V.P. Maleev ³⁹, F. Malek ^{61,o}, M. Mali ⁹⁵, D. Malito ⁹⁷,
 U. Mallik ^{81,*}, S. Maltezos ¹⁰, S. Malyukov ⁴⁰, J. Mamuzic ¹³, G. Mancini ⁵⁴, M.N. Mancini ²⁷,
 G. Manco ^{74a,74b}, J.P. Mandalia ⁹⁶, S.S. Mandarry ¹⁵⁰, I. Mandić ⁹⁵,
 L. Manhaes de Andrade Filho ^{84a}, I.M. Maniatis ¹⁷⁴, J. Manjarres Ramos ⁹¹, D.C. Mankad ¹⁷⁴,
 A. Mann ¹¹¹, S. Manzoni ³⁷, L. Mao ^{63c}, X. Mapekula ^{34c}, A. Marantis ^{156,t}, G. Marchiori ⁵,
 M. Marcisovsky ¹³⁴, C. Marcon ^{72a}, M. Marinescu ²¹, S. Marium ⁴⁹, M. Marjanovic ¹²³,
 A. Markhoos ⁵⁵, M. Markovitch ⁶⁷, M.K. Maroun ¹⁰⁵, E.J. Marshall ⁹³, Z. Marshall ^{18a},
 S. Marti-Garcia ¹⁶⁸, J. Martin ⁹⁸, T.A. Martin ¹³⁷, V.J. Martin ⁵³, B. Martin dit Latour ¹⁷,
 L. Martinelli ^{76a,76b}, M. Martinez ^{13,w}, P. Martinez Agullo ¹⁶⁸, V.I. Martinez Outschoorn ¹⁰⁵,
 P. Martinez Suarez ¹³, S. Martin-Haugh ¹³⁷, G. Martinovicova ¹³⁶, V.S. Martoiu ^{28b},
 A.C. Martyniuk ⁹⁸, A. Marzin ³⁷, D. Mascione ^{79a,79b}, L. Masetti ¹⁰², J. Masik ¹⁰³,
 A.L. Maslennikov ⁴⁰, S.L. Mason ⁴³, P. Massarotti ^{73a,73b}, P. Mastrandrea ^{75a,75b},
 A. Mastroberardino ^{45b,45a}, T. Masubuchi ¹²⁷, T.T. Mathew ¹²⁶, J. Matousek ¹³⁶, D.M. Mattern ⁵⁰,
 J. Maurer ^{28b}, T. Maurin ⁶⁰, A.J. Maury ⁶⁷, B. Maček ⁹⁵, D.A. Maximov ³⁹, A.E. May ¹⁰³,
 R. Mazini ^{34g}, I. Maznas ¹¹⁸, M. Mazza ¹⁰⁹, S.M. Mazza ¹³⁹, E. Mazzeo ^{72a,72b},
 J.P. Mc Gowan ¹⁷⁰, S.P. Mc Kee ¹⁰⁸, C.A. Mc Lean ⁶, C.C. McCracken ¹⁶⁹, E.F. McDonald ¹⁰⁷,
 A.E. McDougall ¹¹⁷, L.F. Mcelhinney ⁹³, J.A. Mcfayden ¹⁵⁰, R.P. McGovern ¹³¹,
 R.P. Mckenzie ^{34g}, T.C. Mclachlan ⁴⁹, D.J. Mclaughlin ⁹⁸, S.J. McMahon ¹³⁷,
 C.M. Mcpartland ⁹⁴, R.A. McPherson ^{170,aa}, S. Mehlhase ¹¹¹, A. Mehta ⁹⁴, D. Melini ¹⁶⁸,
 B.R. Mellado Garcia ^{34g}, A.H. Melo ⁵⁶, F. Meloni ⁴⁹, A.M. Mendes Jacques Da Costa ¹⁰³,
 H.Y. Meng ¹⁵⁹, L. Meng ⁹³, S. Menke ¹¹², M. Mentink ³⁷, E. Meoni ^{45b,45a}, G. Mercado ¹¹⁸,
 S. Merianos ¹⁵⁶, C. Merlassino ^{70a,70c}, C. Meroni ^{72a,72b}, J. Metcalfe ⁶, A.S. Mete ⁶,
 E. Meuser ¹⁰², C. Meyer ⁶⁹, J-P. Meyer ¹³⁸, R.P. Middleton ¹³⁷, L. Mijović ⁵³,
 G. Mikenberg ¹⁷⁴, M. Mikeskikova ¹³⁴, M. Mikuž ⁹⁵, H. Mildner ¹⁰², A. Milic ³⁷,
 D.W. Miller ⁴¹, E.H. Miller ¹⁴⁷, L.S. Miller ³⁵, A. Milov ¹⁷⁴, D.A. Milstead ^{48a,48b}, T. Min ^{114a},
 A.A. Minaenko ³⁹, I.A. Minashvili ^{153b}, A.I. Mincer ¹²⁰, B. Mindur ^{87a}, M. Mineev ⁴⁰,
 Y. Mino ⁸⁹, L.M. Mir ¹³, M. Miralles Lopez ⁶⁰, M. Mironova ^{18a}, M.C. Missio ¹¹⁶, A. Mitra ¹⁷²,
 V.A. Mitsou ¹⁶⁸, Y. Mitsumori ¹¹³, O. Miu ¹⁵⁹, P.S. Miyagawa ⁹⁶, T. Mkrtchyan ^{64a},
 M. Mlinarevic ⁹⁸, T. Mlinarevic ⁹⁸, M. Mlynarikova ³⁷, S. Mobius ²⁰, P. Mogg ¹¹¹,
 M.H. Mohamed Farook ¹¹⁵, A.F. Mohammed ^{14,114c}, S. Mohapatra ⁴³, S. Mohiuddin ¹²⁴,
 G. Mokgatitwane ^{34g}, L. Moleri ¹⁷⁴, B. Mondal ¹⁴⁵, S. Mondal ¹³⁵, K. Mönig ⁴⁹,
 E. Monnier ¹⁰⁴, L. Monsonis Romero ¹⁶⁸, J. Montejo Berlingen ¹³, A. Montella ^{48a,48b},
 M. Montella ¹²², F. Montereali ^{78a,78b}, F. Monticelli ⁹², S. Monzani ^{70a,70c}, A. Morancho Tarda ⁴⁴,
 N. Morange ⁶⁷, A.L. Moreira De Carvalho ⁴⁹, M. Moreno Llácer ¹⁶⁸, C. Moreno Martinez ⁵⁷,
 J.M. Moreno Perez ^{23b}, P. Morettini ^{58b}, S. Morgenstern ³⁷, M. Morii ⁶², M. Morinaga ¹⁵⁷,
 M. Moritsu ⁹⁰, F. Morodei ^{76a,76b}, P. Moschovakos ³⁷, B. Moser ¹²⁹, M. Mosidze ^{153b},
 T. Moskalets ⁴⁶, P. Moskvitina ¹¹⁶, J. Moss ^{32,1}, P. Moszkowicz ^{87a}, A. Moussa ^{36d},
 Y. Moyal ¹⁷⁴, E.J.W. Moyse ¹⁰⁵, O. Mtintsilana ^{34g}, S. Muanza ¹⁰⁴, J. Mueller ¹³², R. Müller ³⁷,
 G.A. Mullier ¹⁶⁶, A.J. Mullin ³³, J.J. Mullin ¹³¹, A.E. Mulski ⁶², D.P. Mungo ¹⁵⁹,
 D. Munoz Perez ¹⁶⁸, F.J. Munoz Sanchez ¹⁰³, M. Murin ¹⁰³, W.J. Murray ^{172,137}, M. Muškinja ⁹⁵,

C. Mwewa ³⁰, A.G. Myagkov ^{39,a}, A.J. Myers ⁸, G. Myers ¹⁰⁸, M. Myska ¹³⁵,
 B.P. Nachman ^{18a}, K. Nagai ¹²⁹, K. Nagano ⁸⁵, R. Nagasaka ¹⁵⁷, J.L. Nagle ^{30,ah}, E. Nagy ¹⁰⁴,
 A.M. Nairz ³⁷, Y. Nakahama ⁸⁵, K. Nakamura ⁸⁵, K. Nakkalil ⁵, H. Nanjo ¹²⁷,
 E.A. Narayanan ⁴⁶, Y. Narukawa ¹⁵⁷, I. Naryshkin ³⁹, L. Nasella ^{72a,72b}, S. Nasri ^{119b},
 C. Nass ²⁵, G. Navarro ^{23a}, J. Navarro-Gonzalez ¹⁶⁸, A. Nayaz ¹⁹, P.Y. Nechaeva ³⁹,
 S. Nechaeva ^{24b,24a}, F. Nechansky ¹³⁴, L. Nedic ¹²⁹, T.J. Neep ²¹, A. Negri ^{74a,74b},
 M. Negrini ^{24b}, C. Nellist ¹¹⁷, C. Nelson ¹⁰⁶, K. Nelson ¹⁰⁸, S. Nemecek ¹³⁴, M. Nessi ^{37,g},
 M.S. Neubauer ¹⁶⁷, F. Neuhaus ¹⁰², J. Newell ⁹⁴, P.R. Newman ²¹, Y.W.Y. Ng ¹⁶⁷, B. Ngair ^{119a},
 H.D.N. Nguyen ¹¹⁰, R.B. Nickerson ¹²⁹, R. Nicolaidou ¹³⁸, J. Nielsen ¹³⁹, M. Niemeyer ⁵⁶,
 J. Niermann ³⁷, N. Nikiforou ³⁷, V. Nikolaenko ^{39,a}, I. Nikolic-Audit ¹³⁰, P. Nilsson ³⁰,
 I. Ninca ⁴⁹, G. Ninio ¹⁵⁵, A. Nisati ^{76a}, N. Nishu ², R. Nisius ¹¹², N. Nitika ^{70a,70c},
 J-E. Nitschke ⁵¹, E.K. Nkadimeng ^{34g}, T. Nobe ¹⁵⁷, T. Nommensen ¹⁵¹, M.B. Norfolk ¹⁴³,
 B.J. Norman ³⁵, M. Noury ^{36a}, J. Novak ⁹⁵, T. Novak ⁹⁵, R. Novotny ¹¹⁵, L. Nozka ¹²⁵,
 K. Ntekas ¹⁶³, N.M.J. Nunes De Moura Junior ^{84b}, J. Ocariz ¹³⁰, A. Ochi ⁸⁶, I. Ochoa ^{133a},
 S. Oerdek ^{49,x}, J.T. Offermann ⁴¹, A. Ogrodnik ¹³⁶, A. Oh ¹⁰³, C.C. Ohm ¹⁴⁸, H. Oide ⁸⁵,
 R. Oishi ¹⁵⁷, M.L. Ojeda ³⁷, Y. Okumura ¹⁵⁷, L.F. Oleiro Seabra ^{133a}, I. Oleksiyuk ⁵⁷,
 S.A. Olivares Pino ^{140d}, G. Oliveira Correa ¹³, D. Oliveira Damazio ³⁰, J.L. Oliver ¹⁶³,
 Ö.O. Öncel ⁵⁵, A.P. O'Neill ²⁰, A. Onofre ^{133a,133e}, P.U.E. Onyisi ¹¹, M.J. Oreglia ⁴¹,
 D. Orestano ^{78a,78b}, R.S. Orr ¹⁵⁹, L.M. Osojnak ¹³¹, Y. Osumi ¹¹³, G. Otero y Garzon ³¹,
 H. Otono ⁹⁰, G.J. Ottino ^{18a}, M. Ouchrif ^{36d}, F. Ould-Saada ¹²⁸, T. Ovsianikova ¹⁴²,
 M. Owen ⁶⁰, R.E. Owen ¹³⁷, V.E. Ozcan ^{22a}, F. Ozturk ⁸⁸, N. Ozturk ⁸, S. Ozturk ⁸³,
 H.A. Pacey ¹²⁹, K. Pachal ^{160a}, A. Pacheco Pages ¹³, C. Padilla Aranda ¹³, G. Padovano ^{76a,76b},
 S. Pagan Griso ^{18a}, G. Palacino ⁶⁹, A. Palazzo ^{71a,71b}, J. Pampel ²⁵, J. Pan ¹⁷⁷, T. Pan ^{65a},
 D.K. Panchal ¹¹, C.E. Pandini ¹¹⁷, J.G. Panduro Vazquez ¹³⁷, H.D. Pandya ¹, H. Pang ¹³⁸,
 P. Pani ⁴⁹, G. Panizzo ^{70a,70c}, L. Panwar ¹³⁰, L. Paolozzi ⁵⁷, S. Parajuli ¹⁶⁷, A. Paramonov ⁶,
 C. Paraskevopoulos ⁵⁴, D. Paredes Hernandez ^{65b}, A. Pareti ^{74a,74b}, K.R. Park ⁴³, T.H. Park ¹¹²,
 F. Parodi ^{58b,58a}, J.A. Parsons ⁴³, U. Parzefall ⁵⁵, B. Pascual Dias ¹¹⁰, L. Pascual Dominguez ¹⁰¹,
 E. Pasqualucci ^{76a}, S. Passaggio ^{58b}, F. Pastore ⁹⁷, P. Patel ⁸⁸, U.M. Patel ⁵², J.R. Pater ¹⁰³,
 T. Pauly ³⁷, F. Pauwels ¹³⁶, C.I. Pazos ¹⁶², M. Pedersen ¹²⁸, R. Pedro ^{133a}, S.V. Peleganchuk ³⁹,
 O. Penc ³⁷, E.A. Pender ⁵³, S. Peng ¹⁵, G.D. Penn ¹⁷⁷, K.E. Pensi ¹¹¹, M. Penzin ³⁹,
 B.S. Peralva ^{84d}, A.P. Pereira Peixoto ¹⁴², L. Pereira Sanchez ¹⁴⁷, D.V. Perepelitsa ^{30,ah},
 G. Perera ¹⁰⁵, E. Perez Codina ^{160a}, M. Perganti ¹⁰, H. Pernegger ³⁷, S. Perrella ^{76a,76b},
 O. Perrin ⁴², K. Peters ⁴⁹, R.F.Y. Peters ¹⁰³, B.A. Petersen ³⁷, T.C. Petersen ⁴⁴, E. Petit ¹⁰⁴,
 V. Petousis ¹³⁵, C. Petridou ^{156,d}, T. Petru ¹³⁶, A. Petrukhin ¹⁴⁵, M. Pettee ^{18a}, A. Petukhov ⁸³,
 K. Petukhova ³⁷, R. Pezoa ^{140f}, L. Pezzotti ^{24b,24a}, G. Pezzullo ¹⁷⁷, L. Pfaffenbichler ³⁷,
 A.J. Pflieger ³⁷, T.M. Pham ¹⁷⁵, T. Pham ¹⁰⁷, P.W. Phillips ¹³⁷, G. Piacquadio ¹⁴⁹, E. Pianori ^{18a},
 F. Piazza ¹²⁶, R. Piegai ³¹, D. Pietreanu ^{28b}, A.D. Pilkington ¹⁰³, M. Pinamonti ^{70a,70c},
 J.L. Pinfeld ², B.C. Pinheiro Pereira ^{133a}, J. Pinol Bel ¹³, A.E. Pinto Pinoargote ¹³⁸,
 L. Pintucci ^{70a,70c}, K.M. Piper ¹⁵⁰, A. Pirttikoski ⁵⁷, D.A. Pizzi ³⁵, L. Pizzimento ^{65b},
 M.-A. Pleier ³⁰, V. Pleskot ¹³⁶, E. Plotnikova ⁴⁰, G. Poddar ⁹⁶, R. Poettgen ¹⁰⁰, L. Poggioli ¹³⁰,
 S. Polacek ¹³⁶, G. Polesello ^{74a}, A. Poley ^{146,160a}, A. Polini ^{24b}, C.S. Pollard ¹⁷²,
 Z.B. Pollock ¹²², E. Pompa Pacchi ¹²³, N.I. Pond ⁹⁸, D. Ponomarenko ⁶⁹, L. Pontecorvo ³⁷,
 S. Popa ^{28a}, G.A. Popeneciu ^{28d}, A. Poreba ³⁷, D.M. Portillo Quintero ^{160a}, S. Pospisil ¹³⁵,
 M.A. Postill ¹⁴³, P. Postolache ^{28c}, K. Potamianos ¹⁷², P.A. Potepa ^{87a}, I.N. Potrap ⁴⁰,
 C.J. Potter ³³, H. Potti ¹⁵¹, J. Poveda ¹⁶⁸, M.E. Pozo Astigarraga ³⁷, A. Prades Ibanez ^{77a,77b},
 J. Pretel ¹⁷⁰, D. Price ¹⁰³, M. Primavera ^{71a}, L. Primomo ^{70a,70c}, M.A. Principe Martin ¹⁰¹,
 R. Privara ¹²⁵, T. Procter ⁶⁰, M.L. Proffitt ¹⁴², N. Proklova ¹³¹, K. Prokofiev ^{65c}, G. Proto ¹¹²,

J. Proudfoot ⁶, M. Przybycien ^{87a}, W.W. Przygoda ^{87b}, A. Psallidas ⁴⁷, J.E. Puddefoot ¹⁴³,
 D. Pudzha ⁵⁵, D. Pyatiizbyantseva ¹¹⁶, J. Qian ¹⁰⁸, R. Qian ¹⁰⁹, D. Qichen ¹⁰³, Y. Qin ¹³,
 T. Qiu ⁵³, A. Quadt ⁵⁶, M. Queitsch-Maitland ¹⁰³, G. Quetant ⁵⁷, R.P. Quinn ¹⁶⁹,
 G. Rabanal Bolanos ⁶², D. Rafanoharana ⁵⁵, F. Raffaelli ^{77a,77b}, F. Ragusa ^{72a,72b}, J.L. Rainbolt ⁴¹,
 J.A. Raine ⁵⁷, S. Rajagopalan ³⁰, E. Ramakoti ³⁹, L. Rambelli ^{58b,58a}, I.A. Ramirez-Berend ³⁵,
 K. Ran ^{49,114c}, D.S. Rankin ¹³¹, N.P. Rapheeha ^{34g}, H. Rasheed ^{28b}, V. Raskina ¹³⁰,
 D.F. Rassloff ^{64a}, A. Rastogi ^{18a}, S. Rave ¹⁰², S. Ravera ^{58b,58a}, B. Ravina ³⁷, I. Ravinovich ¹⁷⁴,
 M. Raymond ³⁷, A.L. Read ¹²⁸, N.P. Readioff ¹⁴³, D.M. Rebuzzi ^{74a,74b}, A.S. Reed ¹¹²,
 K. Reeves ²⁷, J.A. Reidelsturz ¹⁷⁶, D. Reikher ¹²⁶, A. Rej ⁵⁰, C. Rembser ³⁷, H. Ren ^{63a},
 M. Renda ^{28b}, F. Renner ⁴⁹, A.G. Rennie ¹⁶³, A.L. Rescia ⁴⁹, S. Resconi ^{72a},
 M. Ressegotti ^{58b,58a}, S. Rettie ³⁷, W.F. Rettie ³⁵, J.G. Reyes Rivera ¹⁰⁹, E. Reynolds ^{18a},
 O.L. Rezanova ⁴⁰, P. Reznicek ¹³⁶, H. Riani ^{36d}, N. Ribaric ⁵², E. Ricci ^{79a,79b}, R. Richter ¹¹²,
 S. Richter ^{48a,48b}, E. Richter-Was ^{87b}, M. Ridel ¹³⁰, S. Ridouani ^{36d}, P. Rieck ¹²⁰, P. Riedler ³⁷,
 E.M. Riefel ^{48a,48b}, J.O. Rieger ¹¹⁷, M. Rijssenbeek ¹⁴⁹, M. Rimoldi ³⁷, L. Rinaldi ^{24b,24a},
 P. Rincke ^{56,166}, G. Ripellino ¹⁶⁶, I. Riu ¹³, J.C. Rivera Vergara ¹⁷⁰, F. Rizatdinova ¹²⁴,
 E. Rizvi ⁹⁶, B.R. Roberts ^{18a}, S.S. Roberts ¹³⁹, D. Robinson ³³, M. Robles Manzano ¹⁰²,
 A. Robson ⁶⁰, A. Rocchi ^{77a,77b}, C. Roda ^{75a,75b}, S. Rodriguez Bosca ³⁷, Y. Rodriguez Garcia ^{23a},
 A.M. Rodríguez Vera ¹¹⁸, S. Roe ³⁷, J.T. Roemer ³⁷, O. Røhne ¹²⁸, C.P.A. Roland ¹³⁰, J. Roloff ³⁰,
 A. Romaniouk ⁸⁰, E. Romano ^{74a,74b}, M. Romano ^{24b}, A.C. Romero Hernandez ¹⁶⁷,
 N. Rompotis ⁹⁴, L. Roos ¹³⁰, S. Rosati ^{76a}, B.J. Rosser ⁴¹, E. Rossi ¹²⁹, E. Rossi ^{73a,73b},
 L.P. Rossi ⁶², L. Rossini ⁵⁵, R. Rosten ¹²², M. Rotaru ^{28b}, B. Rottler ⁵⁵, D. Rousseau ⁶⁷,
 D. Rousso ⁴⁹, S. Roy-Garand ¹⁵⁹, A. Rozanov ¹⁰⁴, Z.M.A. Rozario ⁶⁰, Y. Rozen ¹⁵⁴,
 A. Rubio Jimenez ¹⁶⁸, V.H. Ruelas Rivera ¹⁹, T.A. Ruggeri ¹, A. Ruggiero ¹²⁹,
 A. Ruiz-Martinez ¹⁶⁸, A. Rummler ³⁷, Z. Rurikova ⁵⁵, N.A. Rusakovich ⁴⁰, H.L. Russell ¹⁷⁰,
 G. Russo ^{76a,76b}, J.P. Rutherford ⁷, S. Rutherford Colmenares ³³, M. Rybar ¹³⁶, E.B. Rye ¹²⁸,
 A. Ryzhov ⁴⁶, J.A. Sabater Iglesias ⁵⁷, H.F.W. Sadrozinski ¹³⁹, F. Safai Tehrani ^{76a}, S. Saha ¹,
 M. Sahinsoy ⁸³, A. Saibel ¹⁶⁸, B.T. Saifuddin ¹²³, M. Saimpert ¹³⁸, M. Saito ¹⁵⁷, T. Saito ¹⁵⁷,
 A. Sala ^{72a,72b}, D. Salamani ³⁷, A. Salnikov ¹⁴⁷, J. Salt ¹⁶⁸, A. Salvador Salas ¹⁵⁵,
 D. Salvatore ^{45b,45a}, F. Salvatore ¹⁵⁰, A. Salzburger ³⁷, D. Sammel ⁵⁵, E. Sampson ⁹³,
 D. Sampsonidis ^{156,d}, D. Sampsonidou ¹²⁶, J. Sánchez ¹⁶⁸, V. Sanchez Sebastian ¹⁶⁸,
 H. Sandaker ¹²⁸, C.O. Sander ⁴⁹, J.A. Sandesara ¹⁰⁵, M. Sandhoff ¹⁷⁶, C. Sandoval ^{23b},
 L. Sanfilippo ^{64a}, D.P.C. Sankey ¹³⁷, T. Sano ⁸⁹, A. Sansoni ⁵⁴, L. Santi ³⁷, C. Santoni ⁴²,
 H. Santos ^{133a,133b}, A. Santra ¹⁷⁴, E. Sanzani ^{24b,24a}, K.A. Saoucha ¹⁶⁵, J.G. Saraiva ^{133a,133d},
 J. Sardain ⁷, O. Sasaki ⁸⁵, K. Sato ¹⁶¹, C. Sauer ³⁷, E. Sauvan ⁴, P. Savard ^{159,af}, R. Sawada ¹⁵⁷,
 C. Sawyer ¹³⁷, L. Sawyer ⁹⁹, C. Sbarra ^{24b}, A. Sbrizzi ^{24b,24a}, T. Scanlon ⁹⁸,
 J. Schaarschmidt ¹⁴², U. Schäfer ¹⁰², A.C. Schaffer ^{67,46}, D. Schaile ¹¹¹, R.D. Schamberger ¹⁴⁹,
 C. Scharf ¹⁹, M.M. Schefer ²⁰, V.A. Schegelsky ³⁹, D. Scheirich ¹³⁶, M. Schernau ^{140e},
 C. Scheulen ⁵⁷, C. Schiavi ^{58b,58a}, M. Schioppa ^{45b,45a}, B. Schlag ¹⁴⁷, S. Schlenker ³⁷,
 J. Schmeing ¹⁷⁶, M.A. Schmidt ¹⁷⁶, K. Schmieden ¹⁰², C. Schmitt ¹⁰², N. Schmitt ¹⁰²,
 S. Schmitt ⁴⁹, L. Schoeffel ¹³⁸, A. Schoening ^{64b}, P.G. Scholer ³⁵, E. Schopf ¹⁴⁵, M. Schott ²⁵,
 S. Schramm ⁵⁷, T. Schroer ⁵⁷, H-C. Schultz-Coulon ^{64a}, M. Schumacher ⁵⁵, B.A. Schumm ¹³⁹,
 Ph. Schune ¹³⁸, H.R. Schwartz ¹³⁹, A. Schwartzman ¹⁴⁷, T.A. Schwarz ¹⁰⁸, Ph. Schwemling ¹³⁸,
 R. Schwienhorst ¹⁰⁹, F.G. Sciacca ²⁰, A. Sciandra ³⁰, G. Sciolla ²⁷, F. Scuri ^{75a},
 C.D. Sebastiani ³⁷, K. Sedlaczek ¹¹⁸, S.C. Seidel ¹¹⁵, A. Seiden ¹³⁹, B.D. Seidlitz ⁴³,
 C. Seitz ⁴⁹, J.M. Seixas ^{84b}, G. Sekhniaidze ^{73a}, L. Selem ⁶¹, N. Semprini-Cesari ^{24b,24a},
 A. Semushin ^{178,39}, D. Sengupta ⁵⁷, V. Senthilkumar ¹⁶⁸, L. Serin ⁶⁷, M. Sessa ^{77a,77b},
 H. Severini ¹²³, F. Sforza ^{58b,58a}, A. Sfyrly ⁵⁷, Q. Sha ¹⁴, E. Shabalina ⁵⁶, H. Shaddix ¹¹⁸,

A.H. Shah ³³, R. Shaheen ¹⁴⁸, J.D. Shahinian ¹³¹, D. Shaked Renous ¹⁷⁴, M. Shamim ³⁷,
 L.Y. Shan ¹⁴, M. Shapiro ^{18a}, A. Sharma ³⁷, A.S. Sharma ¹⁶⁹, P. Sharma ³⁰, P.B. Shatalov ³⁹,
 K. Shaw ¹⁵⁰, S.M. Shaw ¹⁰³, Q. Shen ^{63c}, D.J. Sheppard ¹⁴⁶, P. Sherwood ⁹⁸, L. Shi ⁹⁸,
 X. Shi ¹⁴, S. Shimizu ⁸⁵, C.O. Shimmin ¹⁷⁷, I.P.J. Shipsey ^{129,*}, S. Shirabe ⁹⁰,
 M. Shiyakova ^{40,y}, M.J. Shochet ⁴¹, D.R. Shope ¹²⁸, B. Shrestha ¹²³, S. Shrestha ^{122,aj},
 I. Shreyber ³⁹, M.J. Shroff ¹⁷⁰, P. Sicho ¹³⁴, A.M. Sickles ¹⁶⁷, E. Sideras Haddad ^{34g,164},
 A.C. Sidley ¹¹⁷, A. Sidoti ^{24b}, F. Siegert ⁵¹, Dj. Sijacki ¹⁶, F. Sili ⁹², J.M. Silva ⁵³,
 I. Silva Ferreira ^{84b}, M.V. Silva Oliveira ³⁰, S.B. Silverstein ^{48a}, S. Simion ⁶⁷, R. Simoniello ³⁷,
 E.L. Simpson ¹⁰³, H. Simpson ¹⁵⁰, L.R. Simpson ¹⁰⁸, S. Simsek ⁸³, S. Sindhu ⁵⁶, P. Sinervo ¹⁵⁹,
 S.N. Singh ²⁷, S. Singh ³⁰, S. Sinha ⁴⁹, S. Sinha ¹⁰³, M. Sioli ^{24b,24a}, K. Sioulas ⁹, I. Siral ³⁷,
 E. Sitnikova ⁴⁹, J. Sjölin ^{48a,48b}, A. Skaf ⁵⁶, E. Skorda ²¹, P. Skubic ¹²³, M. Slawinska ⁸⁸,
 I. Slazyk ¹⁷, V. Smakhtin ¹⁷⁴, B.H. Smart ¹³⁷, S.Yu. Smirnov ^{140b}, Y. Smirnov ³⁹,
 L.N. Smirnova ^{39,a}, O. Smirnova ¹⁰⁰, A.C. Smith ⁴³, D.R. Smith ¹⁶³, E.A. Smith ⁴¹, J.L. Smith ¹⁰³,
 M.B. Smith ³⁵, R. Smith ¹⁴⁷, H. Smitmanns ¹⁰², M. Smizanska ⁹³, K. Smolek ¹³⁵, A.A. Snesarev ⁴⁰,
 H.L. Snoek ¹¹⁷, S. Snyder ³⁰, R. Sobie ^{170,aa}, A. Soffer ¹⁵⁵, C.A. Solans Sanchez ³⁷,
 E.Yu. Soldatov ³⁹, U. Soldevila ¹⁶⁸, A.A. Solodkov ^{34g}, S. Solomon ²⁷, A. Soloshenko ⁴⁰,
 K. Solovieva ⁵⁵, O.V. Solovyanov ⁴², P. Sommer ⁵¹, A. Sonay ¹³, W.Y. Song ^{160b},
 A. Sopczak ¹³⁵, A.L. Soppio ⁵³, F. Sopkova ^{29b}, J.D. Sorenson ¹¹⁵, I.R. Sotarriva Alvarez ¹⁴¹,
 V. Sothilingam ^{64a}, O.J. Soto Sandoval ^{140c,140b}, S. Sottocornola ⁶⁹, R. Soualah ¹⁶⁵,
 Z. Soumami ^{36e}, D. South ⁴⁹, N. Soybelman ¹⁷⁴, S. Spagnolo ^{71a,71b}, M. Spalla ¹¹²,
 D. Sperlich ⁵⁵, B. Spisso ^{73a,73b}, D.P. Spiteri ⁶⁰, M. Spousta ¹³⁶, E.J. Staats ³⁵, R. Stamen ^{64a},
 E. Stanecka ⁸⁸, W. Stanek-Maslouska ⁴⁹, M.V. Stange ⁵¹, B. Stanislaus ^{18a}, M.M. Stanitzki ⁴⁹,
 B. Stapf ⁴⁹, E.A. Starchenko ³⁹, G.H. Stark ¹³⁹, J. Stark ⁹¹, P. Staroba ¹³⁴, P. Starovoitov ¹⁶⁵,
 R. Staszewski ⁸⁸, G. Stavropoulos ⁴⁷, A. Steff ³⁷, P. Steinberg ³⁰, B. Stelzer ^{146,160a},
 H.J. Stelzer ¹³², O. Stelzer-Chilton ^{160a}, H. Stenzel ⁵⁹, T.J. Stevenson ¹⁵⁰, G.A. Stewart ³⁷,
 J.R. Stewart ¹²⁴, M.C. Stockton ³⁷, G. Stoicea ^{28b}, M. Stolarski ^{133a}, S. Stonjek ¹¹²,
 A. Straessner ⁵¹, J. Strandberg ¹⁴⁸, S. Strandberg ^{48a,48b}, M. Stratmann ¹⁷⁶, M. Strauss ¹²³,
 T. Streblor ¹⁰⁴, P. Strizenec ^{29b}, R. Ströhmer ¹⁷¹, D.M. Strom ¹²⁶, R. Stroynowski ⁴⁶,
 A. Strubig ^{48a,48b}, S.A. Stucci ³⁰, B. Stugu ¹⁷, J. Stupak ¹²³, N.A. Styles ⁴⁹, D. Su ¹⁴⁷,
 S. Su ^{63a}, W. Su ^{63d}, X. Su ^{63a}, D. Suchy ^{29a}, K. Sugizaki ¹³¹, V.V. Sulin ³⁹, M.J. Sullivan ⁹⁴,
 D.M.S. Sultan ¹²⁹, L. Sultanaliyeva ³⁹, S. Sultansoy ^{3b}, S. Sun ¹⁷⁵, W. Sun ¹⁴,
 O. Sunneborn Gudnadottir ¹⁶⁶, N. Sur ¹⁰⁴, M.R. Sutton ¹⁵⁰, H. Suzuki ¹⁶¹, M. Svatos ¹³⁴,
 M. Swiatlowski ^{160a}, T. Swirski ¹⁷¹, I. Sykora ^{29a}, M. Sykora ¹³⁶, T. Sykora ¹³⁶, D. Ta ¹⁰²,
 K. Tackmann ^{49,x}, A. Taffard ¹⁶³, R. Tafirout ^{160a}, J.S. Tafuya Vargas ⁵⁷, Y. Takubo ⁸⁵,
 M. Talby ¹⁰⁴, A.A. Talyshev ³⁹, K.C. Tam ^{65b}, N.M. Tamir ¹⁵⁵, A. Tanaka ¹⁵⁷, J. Tanaka ¹⁵⁷,
 R. Tanaka ⁶⁷, M. Tanasini ¹⁴⁹, Z. Tao ¹⁶⁹, S. Tapia Araya ^{140f}, S. Tapprogge ¹⁰²,
 A. Tarek Abouelfadl Mohamed ¹⁰⁹, S. Tarem ¹⁵⁴, K. Tariq ¹⁴, G. Tarna ^{28b}, G.F. Tartarelli ^{72a},
 M.J. Tartarin ⁹¹, P. Tas ¹³⁶, M. Tasevsky ¹³⁴, E. Tassi ^{45b,45a}, A.C. Tate ¹⁶⁷, G. Tateno ¹⁵⁷,
 Y. Tayalati ^{36e,z}, G.N. Taylor ¹⁰⁷, W. Taylor ^{160b}, A.S. Tegetmeier ⁹¹, P. Teixeira-Dias ⁹⁷,
 J.J. Teoh ¹⁵⁹, K. Terashi ¹⁵⁷, J. Terron ¹⁰¹, S. Terzo ¹³, M. Testa ⁵⁴, R.J. Teuscher ^{159,aa},
 A. Thaler ⁸⁰, O. Theiner ⁵⁷, T. Thevenaux-Pelzer ¹⁰⁴, O. Thielmann ¹⁷⁶, D.W. Thomas ⁹⁷,
 J.P. Thomas ²¹, E.A. Thompson ^{18a}, P.D. Thompson ²¹, E. Thomson ¹³¹, R.E. Thornberry ⁴⁶,
 C. Tian ^{63a}, Y. Tian ⁵⁷, V. Tikhomirov ^{39,a}, Yu.A. Tikhonov ³⁹, S. Timoshenko ³⁹,
 D. Timoshyn ¹³⁶, E.X.L. Ting ¹, P. Tipton ¹⁷⁷, A. Tishelman-Charny ³⁰, S.H. Tlou ^{34g},
 K. Todome ¹⁴¹, S. Todorova-Nova ¹³⁶, S. Todt ⁵¹, L. Toffolin ^{70a,70c}, M. Togawa ⁸⁵, J. Tojo ⁹⁰,
 S. Tokár ^{29a}, O. Toldaiev ⁶⁹, G. Tolkachev ¹⁰⁴, M. Tomoto ^{85,113}, L. Tompkins ^{147,n},
 E. Torrence ¹²⁶, H. Torres ⁹¹, E. Torró Pastor ¹⁶⁸, M. Toscani ³¹, C. Toscirri ⁴¹, M. Tost ¹¹,

D.R. Tovey ¹⁴³, T. Trefzger ¹⁷¹, A. Tricoli ³⁰, I.M. Trigger ^{160a}, S. Trincaz-Duvoid ¹³⁰,
D.A. Trischuk ²⁷, A. Tropina ⁴⁰, L. Truong ^{34c}, M. Trzebinski ⁸⁸, A. Trzupke ⁸⁸, F. Tsai ¹⁴⁹,
M. Tsai ¹⁰⁸, A. Tsiamis ¹⁵⁶, P.V. Tsiarehka ⁴⁰, S. Tsigaridas ^{160a}, A. Tsigotis ^{156,t},
V. Tsiskaridze ¹⁵⁹, E.G. Tskhadadze ^{153a}, M. Tsopoulou ¹⁵⁶, Y. Tsujikawa ⁸⁹, I.I. Tsukerman ³⁹,
V. Tsulaia ^{18a}, S. Tsuno ⁸⁵, K. Tsuru ¹²¹, D. Tsybychev ¹⁴⁹, Y. Tu ^{65b}, A. Tudorache ^{28b},
V. Tudorache ^{28b}, S. Turchikhin ^{58b,58a}, I. Turk Cakir ^{3a}, R. Turra ^{72a}, T. Turtuvshin ⁴⁰,
P.M. Tuts ⁴³, S. Tzamarias ^{156,d}, E. Tzovara ¹⁰², F. Ukegawa ¹⁶¹, P.A. Ulloa Poblete ^{140c,140b},
E.N. Umaka ³⁰, G. Unal ³⁷, A. Undrus ³⁰, G. Unel ¹⁶³, J. Urban ^{29b}, P. Urrejola ^{140a},
G. Usai ⁸, R. Ushioda ¹⁵⁸, M. Usman ¹¹⁰, F. Ustuner ⁵³, Z. Uysal ⁸³, V. Vacek ¹³⁵,
B. Vachon ¹⁰⁶, T. Vafeiadis ³⁷, A. Vaitkus ⁹⁸, C. Valderanis ¹¹¹, E. Valdes Santurio ^{48a,48b},
M. Valente ^{160a}, S. Valentinetti ^{24b,24a}, A. Valero ¹⁶⁸, E. Valiente Moreno ¹⁶⁸, A. Vallier ⁹¹,
J.A. Valls Ferrer ¹⁶⁸, D.R. Van Arneman ¹¹⁷, T.R. Van Daalen ¹⁴², A. Van Der Graaf ⁵⁰,
P. Van Gemmeren ⁶, M. Van Rijnbach ³⁷, S. Van Stroud ⁹⁸, I. Van Vulpen ¹¹⁷, P. Vana ¹³⁶,
M. Vanadia ^{77a,77b}, U.M. Vande Voorde ¹⁴⁸, W. Vandelli ³⁷, E.R. Vandewall ¹²⁴, D. Vannicola ¹⁵⁵,
L. Vannoli ⁵⁴, R. Vari ^{76a}, E.W. Varnes ⁷, C. Varni ^{18b}, D. Varouchas ⁶⁷, L. Varriale ¹⁶⁸,
K.E. Varvell ¹⁵¹, M.E. Vasile ^{28b}, L. Vaslin ⁸⁵, A. Vasyukov ⁴⁰, L.M. Vaughan ¹²⁴, R. Vavricka ¹³⁶,
T. Vazquez Schroeder ¹³, J. Veatch ³², V. Vecchio ¹⁰³, M.J. Veen ¹⁰⁵, I. Veliscek ³⁰,
L.M. Veloce ¹⁵⁹, F. Veloso ^{133a,133c}, S. Veneziano ^{76a}, A. Ventura ^{71a,71b},
S. Ventura Gonzalez ¹³⁸, A. Verbytskyi ¹¹², M. Verducci ^{75a,75b}, C. Vergis ⁹⁶,
M. Verissimo De Araujo ^{84b}, W. Verkerke ¹¹⁷, J.C. Vermeulen ¹¹⁷, C. Vernieri ¹⁴⁷,
M. Vessella ¹⁶³, M.C. Vetterli ^{146,af}, A. Vgenopoulos ¹⁰², N. Viaux Maira ^{140f}, T. Vickey ¹⁴³,
O.E. Vickey Boeriu ¹⁴³, G.H.A. Viehhauser ¹²⁹, L. Vigani ^{64b}, M. Vigl ¹¹², M. Villa ^{24b,24a},
M. Villaplana Perez ¹⁶⁸, E.M. Villhauer ⁵³, E. Vilucchi ⁵⁴, M.G. Vinciter ³⁵, A. Visibile ¹¹⁷,
C. Vittori ³⁷, I. Vivarelli ^{24b,24a}, E. Voevodina ¹¹², F. Vogel ¹¹¹, J.C. Voigt ⁵¹, P. Vokac ¹³⁵,
Yu. Volkotrub ^{87b}, E. Von Toerne ²⁵, B. Vormwald ³⁷, K. Vorobev ³⁹, M. Vos ¹⁶⁸, K. Voss ¹⁴⁵,
M. Vozak ³⁷, L. Vozdecky ¹²³, N. Vranjes ¹⁶, M. Vranjes Milosavljevic ¹⁶, M. Vreeswijk ¹¹⁷,
N.K. Vu ^{63d}, R. Vuillermet ³⁷, O. Vujanovic ¹⁰², I. Vukotic ⁴¹, I.K. Vyas ³⁵, S. Wada ¹⁶¹,
C. Wagner ¹⁴⁷, J.M. Wagner ^{18a}, W. Wagner ¹⁷⁶, S. Wahdan ¹⁷⁶, H. Wahlberg ⁹², C.H. Waits ¹²³,
J. Walder ¹³⁷, R. Walker ¹¹¹, W. Walkowiak ¹⁴⁵, A. Wall ¹³¹, E.J. Wallin ¹⁰⁰, T. Wamorkar ^{18a},
A.Z. Wang ¹³⁹, C. Wang ¹⁰², C. Wang ¹¹, H. Wang ^{18a}, J. Wang ^{65c}, P. Wang ¹⁰³, P. Wang ⁹⁸,
R. Wang ⁶², R. Wang ⁶, S.M. Wang ¹⁵², S. Wang ¹⁴, T. Wang ^{63a}, W.T. Wang ⁸¹, W. Wang ¹⁴,
X. Wang ¹⁶⁷, X. Wang ^{63c}, Y. Wang ^{114a}, Y. Wang ^{63a}, Z. Wang ¹⁰⁸, Z. Wang ^{63d,52,63c},
Z. Wang ¹⁰⁸, C. Wanotayaroj ⁸⁵, A. Warburton ¹⁰⁶, R.J. Ward ²¹, A.L. Warnerbring ¹⁴⁵,
N. Warrack ⁶⁰, S. Waterhouse ⁹⁷, A.T. Watson ²¹, H. Watson ⁵³, M.F. Watson ²¹, E. Watton ⁶⁰,
G. Watts ¹⁴², B.M. Waugh ⁹⁸, J.M. Webb ⁵⁵, C. Weber ³⁰, H.A. Weber ¹⁹, M.S. Weber ²⁰,
S.M. Weber ^{64a}, C. Wei ^{63a}, Y. Wei ⁵⁵, A.R. Weidberg ¹²⁹, E.J. Weik ¹²⁰, J. Weingarten ⁵⁰,
C. Weiser ⁵⁵, C.J. Wells ⁴⁹, T. Wenaus ³⁰, B. Wendland ⁵⁰, T. Wengler ³⁷, N.S. Wenke ¹¹²,
N. Wermes ²⁵, M. Wessels ^{64a}, A.M. Wharton ⁹³, A.S. White ⁶², A. White ⁸, M.J. White ¹,
D. Whiteson ¹⁶³, L. Wickremasinghe ¹²⁷, W. Wiedenmann ¹⁷⁵, M. Wielers ¹³⁷,
C. Wiglesworth ⁴⁴, D.J. Wilbern ¹²³, H.G. Wilkens ³⁷, J.J.H. Wilkinson ³³, D.M. Williams ⁴³,
H.H. Williams ¹³¹, S. Williams ³³, S. Willocq ¹⁰⁵, B.J. Wilson ¹⁰³, D.J. Wilson ¹⁰³,
P.J. Windischhofer ⁴¹, F.I. Winkel ³¹, F. Winklmeier ¹²⁶, B.T. Winter ⁵⁵, M. Wittgen ¹⁴⁷,
M. Wobisch ⁹⁹, T. Wojtkowski ⁶¹, Z. Wolffs ¹¹⁷, J. Wollrath ³⁷, M.W. Wolter ⁸⁸, H. Wolters ^{133a,133c},
M.C. Wong ¹³⁹, E.L. Woodward ⁴³, S.D. Worm ⁴⁹, B.K. Wosiek ⁸⁸, K.W. Woźniak ⁸⁸,
S. Wozniowski ⁵⁶, K. Wraight ⁶⁰, C. Wu ²¹, M. Wu ^{114b}, M. Wu ¹¹⁶, S.L. Wu ¹⁷⁵, X. Wu ⁵⁷,
X. Wu ^{63a}, Y. Wu ^{63a}, Z. Wu ⁴, J. Wuerzinger ^{112,ad}, T.R. Wyatt ¹⁰³, B.M. Wynne ⁵³,
S. Xella ⁴⁴, L. Xia ^{114a}, M. Xia ¹⁵, M. Xie ^{63a}, A. Xiong ¹²⁶, J. Xiong ^{18a}, D. Xu ¹⁴,

H. Xu ¹, L. Xu ², R. Xu ³, T. Xu ⁴, Y. Xu ⁵, Z. Xu ⁶, Z. Xu ⁷, B. Yabsley ⁸, S. Yacoob ⁹, Y. Yamaguchi ¹⁰, E. Yamashita ¹¹, H. Yamauchi ¹², T. Yamazaki ¹³, Y. Yamazaki ¹⁴, S. Yan ¹⁵, Z. Yan ¹⁶, H.J. Yang ¹⁷, H.T. Yang ¹⁸, S. Yang ¹⁹, T. Yang ²⁰, X. Yang ²¹, X. Yang ²², Y. Yang ²³, Y. Yang ²⁴, W-M. Yao ²⁵, H. Ye ²⁶, J. Ye ²⁷, S. Ye ²⁸, X. Ye ²⁹, Y. Yeh ³⁰, I. Yeletsikh ³¹, B. Yeo ³², M.R. Yexley ³³, T.P. Yildirim ³⁴, P. Yin ³⁵, K. Yorita ³⁶, S. Younas ³⁷, C.J.S. Young ³⁸, C. Young ³⁹, N.D. Young ⁴⁰, Y. Yu ⁴¹, J. Yuan ⁴², M. Yuan ⁴³, R. Yuan ⁴⁴, L. Yue ⁴⁵, M. Zaazoua ⁴⁶, B. Zabinski ⁴⁷, I. Zahir ⁴⁸, Z.K. Zak ⁴⁹, T. Zakareishvili ⁵⁰, S. Zambito ⁵¹, J.A. Zamora Saa ⁵², J. Zang ⁵³, D. Zanzi ⁵⁴, R. Zanzottera ⁵⁵, O. Zaplatilek ⁵⁶, C. Zeitnitz ⁵⁷, H. Zeng ⁵⁸, J.C. Zeng ⁵⁹, D.T. Zenger Jr ⁶⁰, O. Zenin ⁶¹, T. Ženiš ⁶², S. Zenz ⁶³, S. Zerradi ⁶⁴, D. Zerwas ⁶⁵, M. Zhai ⁶⁶, D.F. Zhang ⁶⁷, J. Zhang ⁶⁸, J. Zhang ⁶⁹, K. Zhang ⁷⁰, L. Zhang ⁷¹, L. Zhang ⁷², P. Zhang ⁷³, R. Zhang ⁷⁴, S. Zhang ⁷⁵, T. Zhang ⁷⁶, X. Zhang ⁷⁷, Y. Zhang ⁷⁸, Y. Zhang ⁷⁹, Y. Zhang ⁸⁰, Y. Zhang ⁸¹, Z. Zhang ⁸², Z. Zhang ⁸³, H. Zhao ⁸⁴, T. Zhao ⁸⁵, Y. Zhao ⁸⁶, Z. Zhao ⁸⁷, A. Zhemchugov ⁸⁸, J. Zheng ⁸⁹, K. Zheng ⁹⁰, X. Zheng ⁹¹, Z. Zheng ⁹², D. Zhong ⁹³, B. Zhou ⁹⁴, H. Zhou ⁹⁵, N. Zhou ⁹⁶, Y. Zhou ⁹⁷, Y. Zhou ⁹⁸, Y. Zhou ⁹⁹, C.G. Zhu ¹⁰⁰, J. Zhu ¹⁰¹, X. Zhu ¹⁰², Y. Zhu ¹⁰³, Y. Zhu ¹⁰⁴, X. Zhuang ¹⁰⁵, K. Zhukov ¹⁰⁶, N.I. Zimine ¹⁰⁷, J. Zinsser ¹⁰⁸, M. Ziolkowski ¹⁰⁹, L. Živković ¹¹⁰, A. Zoccoli ¹¹¹, K. Zoch ¹¹², T.G. Zorbas ¹¹³, O. Zormpa ¹¹⁴, W. Zou ¹¹⁵, L. Zwalinski ¹¹⁶.

¹Department of Physics, University of Adelaide, Adelaide; Australia.

²Department of Physics, University of Alberta, Edmonton AB; Canada.

³(^a)Department of Physics, Ankara University, Ankara; (^b)Division of Physics, TOBB University of Economics and Technology, Ankara; Türkiye.

⁴LAPP, Université Savoie Mont Blanc, CNRS/IN2P3, Annecy; France.

⁵APC, Université Paris Cité, CNRS/IN2P3, Paris; France.

⁶High Energy Physics Division, Argonne National Laboratory, Argonne IL; United States of America.

⁷Department of Physics, University of Arizona, Tucson AZ; United States of America.

⁸Department of Physics, University of Texas at Arlington, Arlington TX; United States of America.

⁹Physics Department, National and Kapodistrian University of Athens, Athens; Greece.

¹⁰Physics Department, National Technical University of Athens, Zografou; Greece.

¹¹Department of Physics, University of Texas at Austin, Austin TX; United States of America.

¹²Institute of Physics, Azerbaijan Academy of Sciences, Baku; Azerbaijan.

¹³Institut de Física d'Altes Energies (IFAE), Barcelona Institute of Science and Technology, Barcelona; Spain.

¹⁴Institute of High Energy Physics, Chinese Academy of Sciences, Beijing; China.

¹⁵Physics Department, Tsinghua University, Beijing; China.

¹⁶Institute of Physics, University of Belgrade, Belgrade; Serbia.

¹⁷Department for Physics and Technology, University of Bergen, Bergen; Norway.

¹⁸(^a)Physics Division, Lawrence Berkeley National Laboratory, Berkeley CA; (^b)University of California, Berkeley CA; United States of America.

¹⁹Institut für Physik, Humboldt Universität zu Berlin, Berlin; Germany.

²⁰Albert Einstein Center for Fundamental Physics and Laboratory for High Energy Physics, University of Bern, Bern; Switzerland.

²¹School of Physics and Astronomy, University of Birmingham, Birmingham; United Kingdom.

²²(^a)Department of Physics, Bogazici University, Istanbul; (^b)Department of Physics Engineering, Gaziantep University, Gaziantep; (^c)Department of Physics, Istanbul University, Istanbul; Türkiye.

- ^{23(a)}Facultad de Ciencias y Centro de Investigaciones, Universidad Antonio Nariño, Bogotá;^(b)Departamento de Física, Universidad Nacional de Colombia, Bogotá; Colombia.
- ^{24(a)}Dipartimento di Fisica e Astronomia A. Righi, Università di Bologna, Bologna;^(b)INFN Sezione di Bologna; Italy.
- ²⁵Physikalisches Institut, Universität Bonn, Bonn; Germany.
- ²⁶Department of Physics, Boston University, Boston MA; United States of America.
- ²⁷Department of Physics, Brandeis University, Waltham MA; United States of America.
- ^{28(a)}Transilvania University of Brasov, Brasov;^(b)Horia Hulubei National Institute of Physics and Nuclear Engineering, Bucharest;^(c)Department of Physics, Alexandru Ioan Cuza University of Iasi, Iasi;^(d)National Institute for Research and Development of Isotopic and Molecular Technologies, Physics Department, Cluj-Napoca;^(e)National University of Science and Technology Politehnica, Bucharest;^(f)West University in Timisoara, Timisoara;^(g)Faculty of Physics, University of Bucharest, Bucharest; Romania.
- ^{29(a)}Faculty of Mathematics, Physics and Informatics, Comenius University, Bratislava;^(b)Department of Subnuclear Physics, Institute of Experimental Physics of the Slovak Academy of Sciences, Kosice; Slovak Republic.
- ³⁰Physics Department, Brookhaven National Laboratory, Upton NY; United States of America.
- ³¹Universidad de Buenos Aires, Facultad de Ciencias Exactas y Naturales, Departamento de Física, y CONICET, Instituto de Física de Buenos Aires (IFIBA), Buenos Aires; Argentina.
- ³²California State University, CA; United States of America.
- ³³Cavendish Laboratory, University of Cambridge, Cambridge; United Kingdom.
- ^{34(a)}Department of Physics, University of Cape Town, Cape Town;^(b)iThemba Labs, Western Cape;^(c)Department of Mechanical Engineering Science, University of Johannesburg, Johannesburg;^(d)National Institute of Physics, University of the Philippines Diliman (Philippines);^(e)University of South Africa, Department of Physics, Pretoria;^(f)University of Zululand, KwaDlangezwa;^(g)School of Physics, University of the Witwatersrand, Johannesburg; South Africa.
- ³⁵Department of Physics, Carleton University, Ottawa ON; Canada.
- ^{36(a)}Faculté des Sciences Ain Chock, Université Hassan II de Casablanca;^(b)Faculté des Sciences, Université Ibn-Tofail, Kénitra;^(c)Faculté des Sciences Semlalia, Université Cadi Ayyad, LPHEA-Marrakech;^(d)LPMR, Faculté des Sciences, Université Mohamed Premier, Oujda;^(e)Faculté des sciences, Université Mohammed V, Rabat;^(f)Institute of Applied Physics, Mohammed VI Polytechnic University, Ben Guerir; Morocco.
- ³⁷CERN, Geneva; Switzerland.
- ³⁸Affiliated with an institute formerly covered by a cooperation agreement with CERN.
- ³⁹Affiliated with an institute covered by a cooperation agreement with CERN.
- ⁴⁰Affiliated with an international laboratory covered by a cooperation agreement with CERN.
- ⁴¹Enrico Fermi Institute, University of Chicago, Chicago IL; United States of America.
- ⁴²LPC, Université Clermont Auvergne, CNRS/IN2P3, Clermont-Ferrand; France.
- ⁴³Nevis Laboratory, Columbia University, Irvington NY; United States of America.
- ⁴⁴Niels Bohr Institute, University of Copenhagen, Copenhagen; Denmark.
- ^{45(a)}Dipartimento di Fisica, Università della Calabria, Rende;^(b)INFN Gruppo Collegato di Cosenza, Laboratori Nazionali di Frascati; Italy.
- ⁴⁶Physics Department, Southern Methodist University, Dallas TX; United States of America.
- ⁴⁷National Centre for Scientific Research "Demokritos", Agia Paraskevi; Greece.
- ^{48(a)}Department of Physics, Stockholm University;^(b)Oskar Klein Centre, Stockholm; Sweden.
- ⁴⁹Deutsches Elektronen-Synchrotron DESY, Hamburg and Zeuthen; Germany.
- ⁵⁰Fakultät Physik, Technische Universität Dortmund, Dortmund; Germany.
- ⁵¹Institut für Kern- und Teilchenphysik, Technische Universität Dresden, Dresden; Germany.

- ⁵²Department of Physics, Duke University, Durham NC; United States of America.
- ⁵³SUPA - School of Physics and Astronomy, University of Edinburgh, Edinburgh; United Kingdom.
- ⁵⁴INFN e Laboratori Nazionali di Frascati, Frascati; Italy.
- ⁵⁵Physikalisches Institut, Albert-Ludwigs-Universität Freiburg, Freiburg; Germany.
- ⁵⁶II. Physikalisches Institut, Georg-August-Universität Göttingen, Göttingen; Germany.
- ⁵⁷Département de Physique Nucléaire et Corpusculaire, Université de Genève, Genève; Switzerland.
- ⁵⁸(^a) Dipartimento di Fisica, Università di Genova, Genova; (^b) INFN Sezione di Genova; Italy.
- ⁵⁹II. Physikalisches Institut, Justus-Liebig-Universität Giessen, Giessen; Germany.
- ⁶⁰SUPA - School of Physics and Astronomy, University of Glasgow, Glasgow; United Kingdom.
- ⁶¹LPSC, Université Grenoble Alpes, CNRS/IN2P3, Grenoble INP, Grenoble; France.
- ⁶²Laboratory for Particle Physics and Cosmology, Harvard University, Cambridge MA; United States of America.
- ⁶³(^a) Department of Modern Physics and State Key Laboratory of Particle Detection and Electronics, University of Science and Technology of China, Hefei; (^b) Institute of Frontier and Interdisciplinary Science and Key Laboratory of Particle Physics and Particle Irradiation (MOE), Shandong University, Qingdao; (^c) School of Physics and Astronomy, Shanghai Jiao Tong University, Key Laboratory for Particle Astrophysics and Cosmology (MOE), SKLPPC, Shanghai; (^d) Tsung-Dao Lee Institute, Shanghai; (^e) School of Physics, Zhengzhou University; China.
- ⁶⁴(^a) Kirchhoff-Institut für Physik, Ruprecht-Karls-Universität Heidelberg, Heidelberg; (^b) Physikalisches Institut, Ruprecht-Karls-Universität Heidelberg, Heidelberg; Germany.
- ⁶⁵(^a) Department of Physics, Chinese University of Hong Kong, Shatin, N.T., Hong Kong; (^b) Department of Physics, University of Hong Kong, Hong Kong; (^c) Department of Physics and Institute for Advanced Study, Hong Kong University of Science and Technology, Clear Water Bay, Kowloon, Hong Kong; China.
- ⁶⁶Department of Physics, National Tsing Hua University, Hsinchu; Taiwan.
- ⁶⁷IJCLab, Université Paris-Saclay, CNRS/IN2P3, 91405, Orsay; France.
- ⁶⁸Centro Nacional de Microelectrónica (IMB-CNM-CSIC), Barcelona; Spain.
- ⁶⁹Department of Physics, Indiana University, Bloomington IN; United States of America.
- ⁷⁰(^a) INFN Gruppo Collegato di Udine, Sezione di Trieste, Udine; (^b) ICTP, Trieste; (^c) Dipartimento Politecnico di Ingegneria e Architettura, Università di Udine, Udine; Italy.
- ⁷¹(^a) INFN Sezione di Lecce; (^b) Dipartimento di Matematica e Fisica, Università del Salento, Lecce; Italy.
- ⁷²(^a) INFN Sezione di Milano; (^b) Dipartimento di Fisica, Università di Milano, Milano; Italy.
- ⁷³(^a) INFN Sezione di Napoli; (^b) Dipartimento di Fisica, Università di Napoli, Napoli; Italy.
- ⁷⁴(^a) INFN Sezione di Pavia; (^b) Dipartimento di Fisica, Università di Pavia, Pavia; Italy.
- ⁷⁵(^a) INFN Sezione di Pisa; (^b) Dipartimento di Fisica E. Fermi, Università di Pisa, Pisa; Italy.
- ⁷⁶(^a) INFN Sezione di Roma; (^b) Dipartimento di Fisica, Sapienza Università di Roma, Roma; Italy.
- ⁷⁷(^a) INFN Sezione di Roma Tor Vergata; (^b) Dipartimento di Fisica, Università di Roma Tor Vergata, Roma; Italy.
- ⁷⁸(^a) INFN Sezione di Roma Tre; (^b) Dipartimento di Matematica e Fisica, Università Roma Tre, Roma; Italy.
- ⁷⁹(^a) INFN-TIFPA; (^b) Università degli Studi di Trento, Trento; Italy.
- ⁸⁰Universität Innsbruck, Department of Astro and Particle Physics, Innsbruck; Austria.
- ⁸¹University of Iowa, Iowa City IA; United States of America.
- ⁸²Department of Physics and Astronomy, Iowa State University, Ames IA; United States of America.
- ⁸³Istinye University, Sariyer, Istanbul; Türkiye.
- ⁸⁴(^a) Departamento de Engenharia Elétrica, Universidade Federal de Juiz de Fora (UFJF), Juiz de Fora; (^b) Universidade Federal do Rio De Janeiro COPPE/EE/IF, Rio de Janeiro; (^c) Instituto de Física, Universidade de São Paulo, São Paulo; (^d) Rio de Janeiro State University, Rio de Janeiro; (^e) Federal

University of Bahia, Bahia; Brazil.

⁸⁵KEK, High Energy Accelerator Research Organization, Tsukuba; Japan.

⁸⁶Graduate School of Science, Kobe University, Kobe; Japan.

⁸⁷(^a) AGH University of Krakow, Faculty of Physics and Applied Computer Science, Krakow; (^b) Marian Smoluchowski Institute of Physics, Jagiellonian University, Krakow; Poland.

⁸⁸Institute of Nuclear Physics Polish Academy of Sciences, Krakow; Poland.

⁸⁹Faculty of Science, Kyoto University, Kyoto; Japan.

⁹⁰Research Center for Advanced Particle Physics and Department of Physics, Kyushu University, Fukuoka ; Japan.

⁹¹L2IT, Université de Toulouse, CNRS/IN2P3, UPS, Toulouse; France.

⁹²Instituto de Física La Plata, Universidad Nacional de La Plata and CONICET, La Plata; Argentina.

⁹³Physics Department, Lancaster University, Lancaster; United Kingdom.

⁹⁴Oliver Lodge Laboratory, University of Liverpool, Liverpool; United Kingdom.

⁹⁵Department of Experimental Particle Physics, Jožef Stefan Institute and Department of Physics, University of Ljubljana, Ljubljana; Slovenia.

⁹⁶School of Physics and Astronomy, Queen Mary University of London, London; United Kingdom.

⁹⁷Department of Physics, Royal Holloway University of London, Egham; United Kingdom.

⁹⁸Department of Physics and Astronomy, University College London, London; United Kingdom.

⁹⁹Louisiana Tech University, Ruston LA; United States of America.

¹⁰⁰Fysiska institutionen, Lunds universitet, Lund; Sweden.

¹⁰¹Departamento de Física Teórica C-15 and CIAFF, Universidad Autónoma de Madrid, Madrid; Spain.

¹⁰²Institut für Physik, Universität Mainz, Mainz; Germany.

¹⁰³School of Physics and Astronomy, University of Manchester, Manchester; United Kingdom.

¹⁰⁴CPPM, Aix-Marseille Université, CNRS/IN2P3, Marseille; France.

¹⁰⁵Department of Physics, University of Massachusetts, Amherst MA; United States of America.

¹⁰⁶Department of Physics, McGill University, Montreal QC; Canada.

¹⁰⁷School of Physics, University of Melbourne, Victoria; Australia.

¹⁰⁸Department of Physics, University of Michigan, Ann Arbor MI; United States of America.

¹⁰⁹Department of Physics and Astronomy, Michigan State University, East Lansing MI; United States of America.

¹¹⁰Group of Particle Physics, University of Montreal, Montreal QC; Canada.

¹¹¹Fakultät für Physik, Ludwig-Maximilians-Universität München, München; Germany.

¹¹²Max-Planck-Institut für Physik (Werner-Heisenberg-Institut), München; Germany.

¹¹³Graduate School of Science and Kobayashi-Maskawa Institute, Nagoya University, Nagoya; Japan.

¹¹⁴(^a) Department of Physics, Nanjing University, Nanjing; (^b) School of Science, Shenzhen Campus of Sun Yat-sen University; (^c) University of Chinese Academy of Science (UCAS), Beijing; China.

¹¹⁵Department of Physics and Astronomy, University of New Mexico, Albuquerque NM; United States of America.

¹¹⁶Institute for Mathematics, Astrophysics and Particle Physics, Radboud University/Nikhef, Nijmegen; Netherlands.

¹¹⁷Nikhef National Institute for Subatomic Physics and University of Amsterdam, Amsterdam; Netherlands.

¹¹⁸Department of Physics, Northern Illinois University, DeKalb IL; United States of America.

¹¹⁹(^a) New York University Abu Dhabi, Abu Dhabi; (^b) United Arab Emirates University, Al Ain; United Arab Emirates.

¹²⁰Department of Physics, New York University, New York NY; United States of America.

¹²¹Ochanomizu University, Otsuka, Bunkyo-ku, Tokyo; Japan.

- ¹²²Ohio State University, Columbus OH; United States of America.
- ¹²³Homer L. Dodge Department of Physics and Astronomy, University of Oklahoma, Norman OK; United States of America.
- ¹²⁴Department of Physics, Oklahoma State University, Stillwater OK; United States of America.
- ¹²⁵Palacký University, Joint Laboratory of Optics, Olomouc; Czech Republic.
- ¹²⁶Institute for Fundamental Science, University of Oregon, Eugene, OR; United States of America.
- ¹²⁷Graduate School of Science, Osaka University, Osaka; Japan.
- ¹²⁸Department of Physics, University of Oslo, Oslo; Norway.
- ¹²⁹Department of Physics, Oxford University, Oxford; United Kingdom.
- ¹³⁰LPNHE, Sorbonne Université, Université Paris Cité, CNRS/IN2P3, Paris; France.
- ¹³¹Department of Physics, University of Pennsylvania, Philadelphia PA; United States of America.
- ¹³²Department of Physics and Astronomy, University of Pittsburgh, Pittsburgh PA; United States of America.
- ¹³³^(a)Laboratório de Instrumentação e Física Experimental de Partículas - LIP, Lisboa; ^(b)Departamento de Física, Faculdade de Ciências, Universidade de Lisboa, Lisboa; ^(c)Departamento de Física, Universidade de Coimbra, Coimbra; ^(d)Centro de Física Nuclear da Universidade de Lisboa, Lisboa; ^(e)Departamento de Física, Universidade do Minho, Braga; ^(f)Departamento de Física Teórica y del Cosmos, Universidad de Granada, Granada (Spain); ^(g)Departamento de Física, Instituto Superior Técnico, Universidade de Lisboa, Lisboa; Portugal.
- ¹³⁴Institute of Physics of the Czech Academy of Sciences, Prague; Czech Republic.
- ¹³⁵Czech Technical University in Prague, Prague; Czech Republic.
- ¹³⁶Charles University, Faculty of Mathematics and Physics, Prague; Czech Republic.
- ¹³⁷Particle Physics Department, Rutherford Appleton Laboratory, Didcot; United Kingdom.
- ¹³⁸IRFU, CEA, Université Paris-Saclay, Gif-sur-Yvette; France.
- ¹³⁹Santa Cruz Institute for Particle Physics, University of California Santa Cruz, Santa Cruz CA; United States of America.
- ¹⁴⁰^(a)Departamento de Física, Pontificia Universidad Católica de Chile, Santiago; ^(b)Millennium Institute for Subatomic physics at high energy frontier (SAPHIR), Santiago; ^(c)Instituto de Investigación Multidisciplinario en Ciencia y Tecnología, y Departamento de Física, Universidad de La Serena; ^(d)Universidad Andres Bello, Department of Physics, Santiago; ^(e)Instituto de Alta Investigación, Universidad de Tarapacá, Arica; ^(f)Departamento de Física, Universidad Técnica Federico Santa María, Valparaíso; Chile.
- ¹⁴¹Department of Physics, Institute of Science, Tokyo; Japan.
- ¹⁴²Department of Physics, University of Washington, Seattle WA; United States of America.
- ¹⁴³Department of Physics and Astronomy, University of Sheffield, Sheffield; United Kingdom.
- ¹⁴⁴Department of Physics, Shinshu University, Nagano; Japan.
- ¹⁴⁵Department Physik, Universität Siegen, Siegen; Germany.
- ¹⁴⁶Department of Physics, Simon Fraser University, Burnaby BC; Canada.
- ¹⁴⁷SLAC National Accelerator Laboratory, Stanford CA; United States of America.
- ¹⁴⁸Department of Physics, Royal Institute of Technology, Stockholm; Sweden.
- ¹⁴⁹Departments of Physics and Astronomy, Stony Brook University, Stony Brook NY; United States of America.
- ¹⁵⁰Department of Physics and Astronomy, University of Sussex, Brighton; United Kingdom.
- ¹⁵¹School of Physics, University of Sydney, Sydney; Australia.
- ¹⁵²Institute of Physics, Academia Sinica, Taipei; Taiwan.
- ¹⁵³^(a)E. Andronikashvili Institute of Physics, Iv. Javakhishvili Tbilisi State University, Tbilisi; ^(b)High Energy Physics Institute, Tbilisi State University, Tbilisi; ^(c)University of Georgia, Tbilisi; Georgia.

- ¹⁵⁴Department of Physics, Technion, Israel Institute of Technology, Haifa; Israel.
- ¹⁵⁵Raymond and Beverly Sackler School of Physics and Astronomy, Tel Aviv University, Tel Aviv; Israel.
- ¹⁵⁶Department of Physics, Aristotle University of Thessaloniki, Thessaloniki; Greece.
- ¹⁵⁷International Center for Elementary Particle Physics and Department of Physics, University of Tokyo, Tokyo; Japan.
- ¹⁵⁸Graduate School of Science and Technology, Tokyo Metropolitan University, Tokyo; Japan.
- ¹⁵⁹Department of Physics, University of Toronto, Toronto ON; Canada.
- ¹⁶⁰(^a) TRIUMF, Vancouver BC; (^b) Department of Physics and Astronomy, York University, Toronto ON; Canada.
- ¹⁶¹Division of Physics and Tomonaga Center for the History of the Universe, Faculty of Pure and Applied Sciences, University of Tsukuba, Tsukuba; Japan.
- ¹⁶²Department of Physics and Astronomy, Tufts University, Medford MA; United States of America.
- ¹⁶³Department of Physics and Astronomy, University of California Irvine, Irvine CA; United States of America.
- ¹⁶⁴University of West Attica, Athens; Greece.
- ¹⁶⁵University of Sharjah, Sharjah; United Arab Emirates.
- ¹⁶⁶Department of Physics and Astronomy, University of Uppsala, Uppsala; Sweden.
- ¹⁶⁷Department of Physics, University of Illinois, Urbana IL; United States of America.
- ¹⁶⁸Instituto de Física Corpuscular (IFIC), Centro Mixto Universidad de Valencia - CSIC, Valencia; Spain.
- ¹⁶⁹Department of Physics, University of British Columbia, Vancouver BC; Canada.
- ¹⁷⁰Department of Physics and Astronomy, University of Victoria, Victoria BC; Canada.
- ¹⁷¹Fakultät für Physik und Astronomie, Julius-Maximilians-Universität Würzburg, Würzburg; Germany.
- ¹⁷²Department of Physics, University of Warwick, Coventry; United Kingdom.
- ¹⁷³Waseda University, Tokyo; Japan.
- ¹⁷⁴Department of Particle Physics and Astrophysics, Weizmann Institute of Science, Rehovot; Israel.
- ¹⁷⁵Department of Physics, University of Wisconsin, Madison WI; United States of America.
- ¹⁷⁶Fakultät für Mathematik und Naturwissenschaften, Fachgruppe Physik, Bergische Universität Wuppertal, Wuppertal; Germany.
- ¹⁷⁷Department of Physics, Yale University, New Haven CT; United States of America.
- ¹⁷⁸Yerevan Physics Institute, Yerevan; Armenia.
- ^a Also Affiliated with an institute covered by a cooperation agreement with CERN.
- ^b Also at An-Najah National University, Nablus; Palestine.
- ^c Also at Borough of Manhattan Community College, City University of New York, New York NY; United States of America.
- ^d Also at Center for Interdisciplinary Research and Innovation (CIRI-AUTH), Thessaloniki; Greece.
- ^e Also at CERN, Geneva; Switzerland.
- ^f Also at CMD-AC UNEC Research Center, Azerbaijan State University of Economics (UNEC); Azerbaijan.
- ^g Also at Département de Physique Nucléaire et Corpusculaire, Université de Genève, Genève; Switzerland.
- ^h Also at Departament de Física de la Universitat Autònoma de Barcelona, Barcelona; Spain.
- ⁱ Also at Department of Financial and Management Engineering, University of the Aegean, Chios; Greece.
- ^j Also at Department of Mathematical Sciences, University of South Africa, Johannesburg; South Africa.
- ^k Also at Department of Physics, Bolu Abant İzzet Baysal University, Bolu; Türkiye.
- ^l Also at Department of Physics, California State University, Sacramento; United States of America.
- ^m Also at Department of Physics, King's College London, London; United Kingdom.
- ⁿ Also at Department of Physics, Stanford University, Stanford CA; United States of America.

- o* Also at Department of Physics, Stellenbosch University; South Africa.
- p* Also at Department of Physics, University of Fribourg, Fribourg; Switzerland.
- q* Also at Department of Physics, University of Thessaly; Greece.
- r* Also at Department of Physics, Westmont College, Santa Barbara; United States of America.
- s* Also at Faculty of Physics, Sofia University, 'St. Kliment Ohridski', Sofia; Bulgaria.
- t* Also at Hellenic Open University, Patras; Greece.
- u* Also at Henan University; China.
- v* Also at Imam Mohammad Ibn Saud Islamic University; Saudi Arabia.
- w* Also at Institutio Catalana de Recerca i Estudis Avancats, ICREA, Barcelona; Spain.
- x* Also at Institut für Experimentalphysik, Universität Hamburg, Hamburg; Germany.
- y* Also at Institute for Nuclear Research and Nuclear Energy (INRNE) of the Bulgarian Academy of Sciences, Sofia; Bulgaria.
- z* Also at Institute of Applied Physics, Mohammed VI Polytechnic University, Ben Guerir; Morocco.
- aa* Also at Institute of Particle Physics (IPP); Canada.
- ab* Also at Institute of Physics, Azerbaijan Academy of Sciences, Baku; Azerbaijan.
- ac* Also at National Institute of Physics, University of the Philippines Diliman (Philippines); Philippines.
- ad* Also at Technical University of Munich, Munich; Germany.
- ae* Also at The Collaborative Innovation Center of Quantum Matter (CICQM), Beijing; China.
- af* Also at TRIUMF, Vancouver BC; Canada.
- ag* Also at Università di Napoli Parthenope, Napoli; Italy.
- ah* Also at University of Colorado Boulder, Department of Physics, Colorado; United States of America.
- ai* Also at University of the Western Cape; South Africa.
- aj* Also at Washington College, Chestertown, MD; United States of America.
- ak* Also at Yeditepe University, Physics Department, Istanbul; Türkiye.
- * Deceased